Flexural Behaviour of Stay-in-Place PVC Encased Reinforced Concrete Walls with Various Panel Types

by

Benjamin Donald Scott

A thesis
presented to the University of Waterloo
in fulfillment of the
thesis requirement for the degree of
Masters of Applied Science
in
Civil Engineering

Waterloo, Ontario, Canada, 2014

AUTHOR'S DECLARATION

I hereby declare that I am the sole author of this thesis. This is a true copy of the thesis, including any required final revisions, as accepted by my examiners.

I understand that my thesis may be made electronically available to the public.

Abstract

The use of stay-in-place (SIP) formwork has become an increasingly popular tool for concrete structures, providing advantages in construction scheduling and labour reduction. Stay-in-place formwork made of strong materials such as fibre reinforced polymer (FRP) and steel have proven to supplement and even replace reinforcement in concrete elements. The use of polyvinyl chloride (PVC) SIP formwork has also been explored. Current research suggests that PVC provides an enhancement to reinforced concrete strength and ductility.

The research herein outlines tests on reinforced concrete walls with a compressive strength 25MPa, utilizing two types of PVC panels; flat or hollow, in order to further understand the polymer's contribution to flexural resistance. The PVC forming system consisted of panels on the tension and compression faces with evenly spaced connectors securing the faces of the wall. Variables studied included concrete core thickness (152 mm, 178 mm, and 203 mm), reinforcing ratio (3-10M bars or 3-15M bars), and panel type (hollow or flat). The walls were tested in four point bending. The concrete control walls failed due to steel yielding followed by concrete crushing. The failure of the flat panel encased walls was dependent on the reinforcing ratio. Wall reinforced with 10M bars and encased with flat panels failed due to steel yielding followed by concrete crushing, PVC buckling, and PVC rupture while walls with 15M bars did not experience PVC rupture. Finally the failure for walls encased in hollow panels was due to steel yielding, followed by concrete crushing and PVC buckling. The hollow panel encased specimens also experienced slip of the panels on the tensile face.

The PVC encasement enhanced the yield load, ultimate load, ductility, and toughness of the concrete walls. For flat panel encased walls, the average improvement at yield and ultimate loads were 21% and 27% respectively. Hollow panel encased walls recorded average yield and ultimate load improvements of 8% and 27% respectively. Flat panel encased walls improved ductility by an average of 71% and toughness by 122%. Hollow panel encased walls improved ductility by an average of 29% and toughness by 70%. Concrete cores were taken from the tested PVC encased specimens and compressive strength was found to be the same as the control walls.

An analytical model was developed to estimate the yield and ultimate load of PVC encased concrete walls. Calculated yield loads were in good agreement with the experimental data, with an average error of 8% for the control walls and 6% for the PVC encased walls. In addition, calculated ultimate (peak) loads showed good correlation with the experimental data. The average error for the control, flat panel and hollow panel encased walls were 3%, 3% and 8% respectively. Calculated and experimental PVC tensile strain values were in good correlation at ultimate load conditions. The average error for the calculated PVC tensile strain was 21%. With the proposed model providing results in good agreement with the test data, other PVC encased wall cross-sections were explored. An "optimized" panel layout was proposed that utilized flat panels on the compression side of the wall and hollow panels on the tension side. This configuration of panels resulted in the greatest estimated improvement at both yield and ultimate load levels.

Acknowledgements

First my deepest thanks to my late supervisor Dr. Khaled Soudki. His guidance, support, care, and experience provide a foundation on which I have learned much. I am honored to have known and worked with him and consider it a true honor to have been one of his students. It is a blessing to carry on his legacy.

My deepest gratitude to Dr. Noran Abdel Wahab, a constant ally both in my lab work and writing process. Her steadfast support, advice, and encouragement was a huge reason why the work came to completion. My thanks as well to Dr. Adil Al-Mayah, who graciously 'adopted' me as a student during my time at Waterloo. His enthusiasm towards my research and frequent availability made this unforeseen transition a smooth one. I am grateful for each of the three supervisors I was able to work with.

My thanks to the Civil and Environmental Engineering structures lab technicians; Michael Burgetz, Doug Hirst, Rob Sublan and Richard Morrison. Each of these men contributed to my time in the lab, and I would not have had the success there without their support and expertise.

To my peers in the department, thank you for friendship and support these past two (and in some cases seven) years. My time at the University would have been a shadow of what I had without your presence.

To my family, whose prayers and support in word and deed buoyed my spirit at all times. And lastly, to God, the Author and creator of all things. I am continually left in awe of His daily grace and love, may He receive glory in the work enclosed here.

Dedication

To: Dad, Mom, Thomas, Jessica, and Erin

Table of Contents

List of Figures

List of Tables

Chapter 1: Introduction

Stay-in-place formwork is a permanent system commonly used in construction projects throughout the world. Where traditional formwork is removed or 'stripped' when hardened concrete has achieved sufficient strength, stay-in-place forms become part of the finished structure. This type of formwork can be implemented with a variety of materials such as timber, galvanized steel, precast concrete, plastic, or fibre-reinforced polymers and offers a variety of benefits such as fast assembly, reducing or eliminating the need for supporting falsework, and allowing for increased standardization and repeatability of structural members (MacAdam, 1996). This particularly attractive for the construction of agricultural facilities, retaining walls and tanks; where the wall geometry remains consistent for the majority of the structure. In addition, the permanent layer offers the benefit of protecting the concrete from environmental exposure and attack. An example of stay-in-place formwork are provided in Figure 1.1

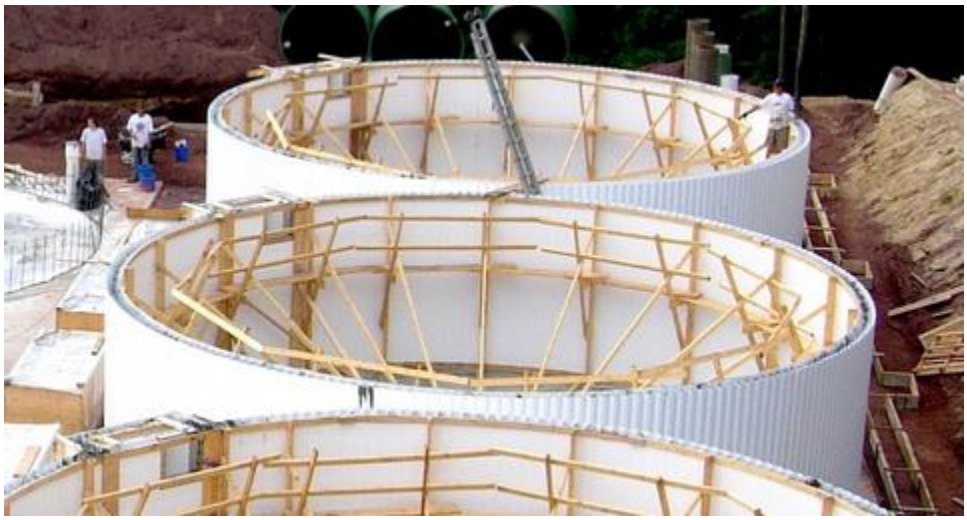

Figure 1.1 Example of tank construction using SIP formwork

Stay-in-place formwork can also play a role in providing additional structural capacity to an element. FRP and steel forms in particular are implemented as additional or even replacement reinforcement for concrete piles, slabs, and walls. In recent years, polyvinyl chloride (PVC) stay-in-place formwork has been developed as a solution for fast, secure and reliable concrete construction. It is proven to be an effective system to quickly erect walls for single and two storey structures. Tests on PVC encased concrete walls reveal an improvement in structural resistance to flexural forces and significant improvements to the ductility of the walls. Research is required to further investigate the flexural behaviour of the PVC encased wall system and develop an analytical model to estimate the ultimate capacity of these composite members. Depending on the amount of improvement, a reinforced concrete wall that is traditionally formed could have the same performance as a PVC encased wall with a thinner cross-section. This change in thickness, however small, applied to an entire structural system would have significant benefit for materials and cost savings.

1.1 Objectives and Scope

The purpose of this research is to determine the flexural behaviour of reinforced concrete (RC) walls that are encased in a PVC stay-in-place (SIP) forming system. Two types of PVC panels will be compared, as well as the effects of the concrete core thickness, and steel reinforcing ratio of the walls. An analytical model will be developed to estimate the yield and ultimate load capacities of the PVC encased concrete walls. Finally, experimental test results will be compared to the analytical model to verify the accuracy of the model results. The greatest motivation is to determine the contribution of the PVC to flexural stiffness, and strength, and if it is significant enough to allow for more slender walls. The slender wall is

of interest due to the potential materials savings if equivalent structural behaviour is achieved with the thinner PVC encased walls. This scenario has up to now been unexplored in this research area.

1.2 Thesis Outline

This thesis is organized into six chapters and an appendix as follows:

- Chapter 1: Introduction – This chapter describes the research motivation, the objectives of the research program, the scope of work, and the thesis outline.
- Chapter 2: Background and Literature Review – This chapter provides a summary of previous research work pertaining to permanent formwork and encased PVC walls.
- Chapter 3: Experimental Program – This chapter presents the test program, material properties, specimen fabrication, instrumentation, and testing set up.
- Chapter 4: Experimental Results – This chapter describes the failure modes of the test specimens. In addition, the experimental cracking, yield, and ultimate loads and deflections are presented. Finally, strain response to loading is discussed.
- Chapter 5: Analytical Model – This chapter discusses the development and validity of the analytical model for predicting yield and ultimate load levels for PVC encased walls.
- Chapter 6: Conclusions and Recommendations – This chapter presents the main conclusions from the study. Recommendations for future work are also provided.
- Appendix A: Experimental Results

Chapter 2: Background and Literature Review

In this chapter, a literature review of previous research on stay-in-place (SIP) structural formwork is conducted, with particular interest on FRP and PVC based systems. The behaviour of the FRP stay-in-place (SIP) formwork is presented, highlighting its effects on reinforced concrete's strength, stiffness, and ductility. Then, research investigating the influence of PVC SIP formwork on concrete behaviour is discussed. Finally, the development of analytical models to calculate the capacity of the PVC encased systems is reviewed.

2.1 FRP Stay-in-Place Formwork

2.1.1 FRP Material

Fibre-Reinforced Polymer (FRP) has recently emerged as a viable material in the construction industry. FRP is a composite material of fibres in a polymeric resin and can be manufactured into various shapes such as bars, sheets, or laminates. FRP material have high tensile strength, flexibility for application, light weight (compared to steel), and high corrosion resistance (ACI 440.R1-06, 2006).

Reinforced concrete structures exposed to severe environments can experience corrosion of reinforcing steel, leading to deterioration of the structure and loss of serviceability. Fibre-reinforced polymers have significantly better corrosion resistance compared to steel reinforcement, making FRP's an increasingly utilized structural material where moisture, chlorides, and temperature pose a threat to a reinforced concrete's durability (ACI 440.R1-06, 2006).

FRP has various applications for concrete structures in addition to acting as primary reinforcement. External application of FRP laminates or sheets to the surface of concrete members have proven to be an effective method of strengthening in service and deteriorated elements (Ritchie et al, 1991; Soudki et al, 2007). Other applications for the FRP's include the provision of confining effects for compression elements, and more recently stay in place formwork, primarily for walls and columns.

2.1.2 Behaviour of FRP-Formed Concrete Elements

One of the most popular applications of SIP FRP formwork has been in the construction of highway composite bridge decks. Two types of permanent formwork have been defined; structurally participating and structurally non-participating. Structural participating formwork is designed to resist both construction and in-service loads, while structurally non-participating forms are strictly intended for carrying construction loads (McClelland, 2007). In addition to providing structural support, permanent forms offer other benefits such as reducing or removing the need for falsework and stripping, while providing opportunity for standardization of construction and reduced labour. Finally, the intrinsic corrosion resistance and high tensile strength of FRP's effectively negate the effect of environmental exposure on bridge decks.

A variety of formwork geometries have been investigated, including concrete filled FRP tubes (CFFT). Rizkalla and Fam (2002) tested 20 CFFTs under four point bending to observe how these members would behave in flexure. The FRP tubes were filled with plain concrete within the tubes, providing both the flexural and shear reinforcement. Some tubes were cast with an inner longitudinal hole creating a wall thickness equal to the theoretical

compression block of a solid concrete cylinder. Different parameters were investigated including the specimen length, diameter, cross-section geometry, reinforcing ratio, and concrete strength. Tubes cast with an internal hole showed an increase in strength-to-weight ratio of 35% while reducing ultimate load capacity by 9%. In general, increasing the thickness (or cross-sectional area) of the FRP tube improved the moment capacity and the stiffness of the tubes.

It was concluded that as the FRP tube increased in stiffness, the benefit of filling the tube with concrete in order to further increase the stiffness was lessened. In other words, concrete contributes more to structures with weaker shells. In addition, placing fibers in the longitudinal direction to resist flexural forces caused a compression failure of the fibers and shear failure of the specimen.

Mohamed and Masmoudi (2012) continued exploring the use of FRP stay-in-place structural formwork for concrete beams. Seven cylindrical beams, 213 mm in diameter and 2000 mm long were tested in four-point bending. They were reinforced with either 6 steel bars 15 mm in diameter or 6 GFRP bars 16 mm in diameter. Test variables included concrete compressive strength (30 MPa and 45 MPa), FRP tube thickness (2.9 mm or 6.4 mm), internal reinforcement (FRP or steel), and fiber orientation. The fibers were oriented 60° and 90° to the longitudinal direction. The concrete filled GFRP tubes (CFFT's) all failed in shear. They failed at a higher deflection with increased stiffness and strength over the control beams. The combination of steel reinforcing bars and GFRP tube allowed for a higher ductility (86% average increase) and an increase in cracking loads ranging from 31% to 84% while improving the ultimate load of the element from 130% to 200% over the

control beams. Conversely, the CFFT specimens reinforced with GFRP bars were weaker than the equivalent specimens with steel internal reinforcing and failed suddenly due to rupture of the glass reinforcing bars. Finally, varying the concrete strength and FRP tube thickness did not significantly change the flexural performance of the specimens.

Dieter et al (2006) investigated the failure mechanisms and performance of a FRP formed bridge deck system by separately testing FRP reinforced slabs and beams. The slab specimens were 2745 mm square with a 200 mm thickness while the beams were 200 mm deep, 914 mm wide, and 2650 mm long. The FRP reinforced concrete specimens were composed of a FRP deck planks to resist positive bending and a top grid or mesh of FRP bars to resist negative bending. The FRP plank was a flat panel stiffened with corrugated box sections. The deck slab failed in punching shear. Ultimate strength results were significantly lower than predicted. They concluded that this reduction was due to the corrugation of the FRP plank, reducing the effective shear depth from 200mm to 127mm. In addition, the tests revealed that the FRP plank was not acting as a fully composite section with the concrete as the specimens held load through a higher than anticipated displacement. Further tests confirmed that the FRP formed concrete did not achieve full composite action.

An investigation of the flexural capacity of the pultruded FRP planks was completed by Bank et al. (2007). The planks were 305 mm wide. They formed the spans between the primary bridge girders, and acted as secondary reinforcement. Seven specimens were tested to compare the behaviour to the traditionally formed reinforced concrete beams and to examine the effect of the type of grit coating on the plank to achieve composite behaviour. Two planks, sand-coated and gravel-coated were tested in comparison to a control plank

without grit. The control specimen (smooth plank) failed in flexure and a slip was observed between the FRP and concrete. Specimens with coatings did not experience any slip and showed an increase in the ultimate capacity of the beams by 50% to 56%.

The control FRP planks were also compared with a steel reinforced concrete beam. The quantity of steel reinforcing reflected the AASHTO requirement for transverse reinforcement. At ultimate load the FRP specimens achieved 58% to 64% higher capacity than the steel reinforced concrete control specimen. It was concluded that the plank could effectively replace the steel as primary tensile reinforcement. The plank had to be coated with epoxy-adhered sand or gravel in order to develop composite action with the concrete. The smooth plank showed significant slip between the concrete and FRP, with a decreased load carrying capacity. (Bank & Oliva, 2007)

Other FRP stay-in-place structural forms have been investigated in recent years. Nelson and Fam (2014) concluded that structural response of the FRP SIP form system in terms of strength and flexural stiffness is similar to conventionally RC bridge decks. However, FRP's differ from steel in several aspects, most noteworthy is their stress-strain behaviour. The steel fails in a ductile manner, but the FRP's remain linear elastic until sudden failure at a decreased strain compared to the rupture strain of steel rebars (Fam & Nelson, 2014). This reduction in ductility is reflected in FRP formed elements where load capacity meets or exceeds RC elements but is less resilient.

A number of attempts have been made to improve the ductility of the FRP SIP systems. Gai et al(2013) developed an FRP stay-in-place formwork that confined concrete using

FRP's in order to increase the ductility of the concrete. Six slab specimens were tested in five-point bending and consisted of two 3000 mm long GFRP box sections (100 mm x 100 mm x 8 mm thick) adhered to a 300 mm wide, 3000 mm long moulded FRP grating. The box sections provided the tension flexural resistance while the concrete filled grating acted in compression. Transverse GFRP dowels between the concrete and GFRP box sections prevented brittle failure of the composite section, increasing the ductility of the system. The FRP grating confined the concrete, increasing the strain capacity and ductility of the concrete in the compression zone. Despite these improvements, the modified formwork required an increased amount of FRP to establish ductility, which is a costly solution. The use of other materials such as PVC for stay-in-place formwork, could increase ductility at a much lower cost.

2.2 PVC Stay-in-Place Formwork

Polyvinyl chloride (PVC) differs from fiber-reinforced polymers in several ways. The material is weaker than FRPs but offers distinct benefits such as lower cost and increased rupture strain when loaded. PVC stay-in-place formwork consists of a system of panels and connectors. The panels form the concrete wall faces, while the connectors secure the faces of the wall together. The connectors have hollow cells to allow for transverse reinforcement to be placed through the forms and for fresh concrete to flow into the entire wall (Figure 2.1).

a - Connector

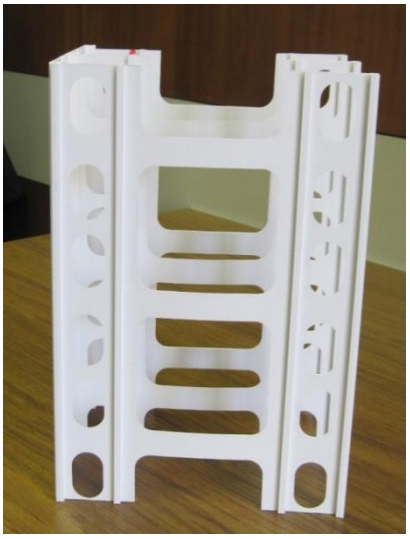

b – Side view of the wall cell

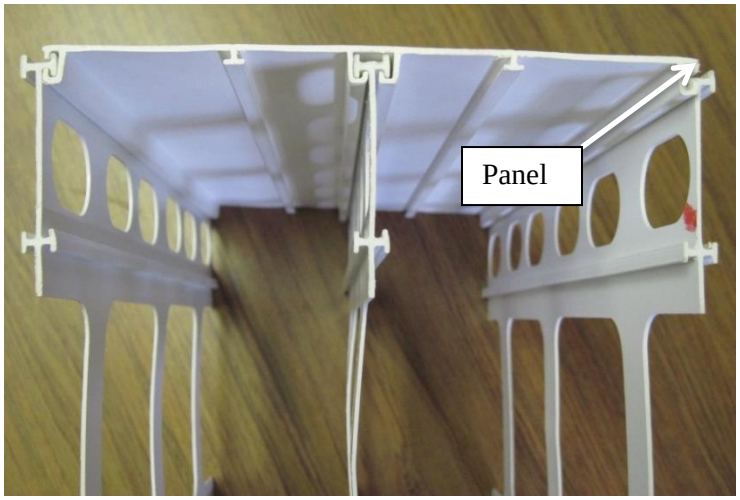

c – Top view of the wall cell

Figure 2.1: Element used in PVC SIP Formwork

The forms offer the advantage of a simplified construction process, especially in the construction of buildings with consistent and continuous geometries (i.e., retaining walls). While strength improvements have been most apparent in the use of fiber-reinforced polymers, the structural benefits of using PVC based formwork have not been explored in great detail.

Chahrour et al. (2005) investigated the flexural behavior of PVC stay-in-place formwork (Royal Building Systems) with and without steel reinforcement. They tested fifteen walls in four point bending. The specimens were 2000 mm long and 233 mm wide. Test variables included the thickness of the concrete core (100, 150 or 200 mm) and reinforcement ratio (un-reinforced, 1-10M rebar). Four PVC encased specimens (150 mm thick) without internal reinforcement developed 'saw tooth' load-deflection curves as shown in Figure 2.2. The load dropped at concrete cracking points and then increased or rebounded as the PVC panels resisted the tensile stresses at the cracked location. The specimens experienced several of these drops and rebounds as cracking continued and deflection increased until the load level began to drop. The specimen failed by rupture of the PVC on the tension side of the wall. The addition of steel reinforcement reduced the severity of the 'saw-tooth' jumps as shown in Figure 2.3.

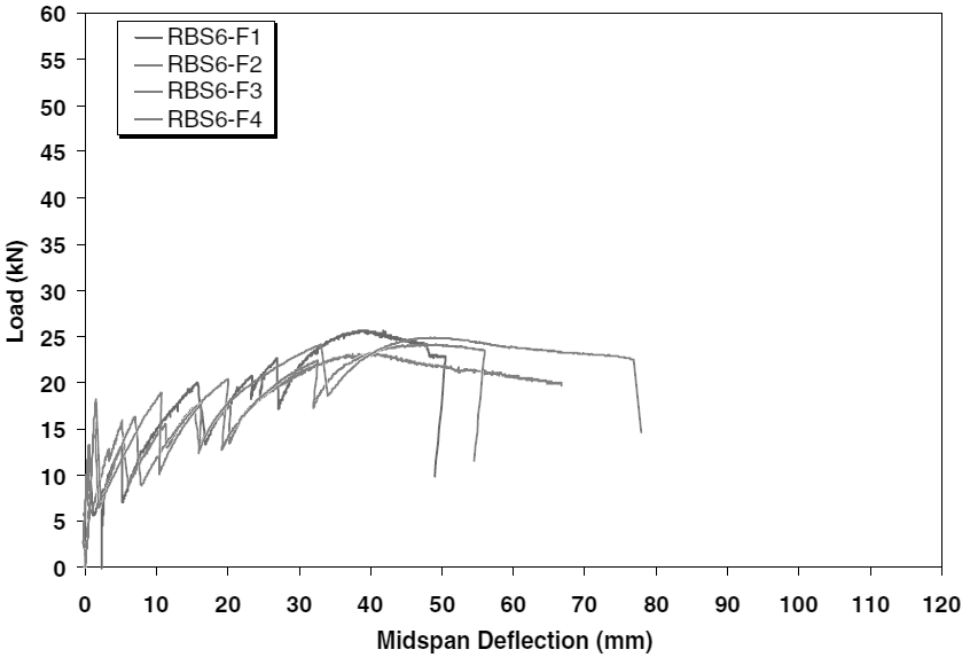

Figure 2.2: Load-deflection of PVC-encased plain concrete. (Chahrour et al. 2005)

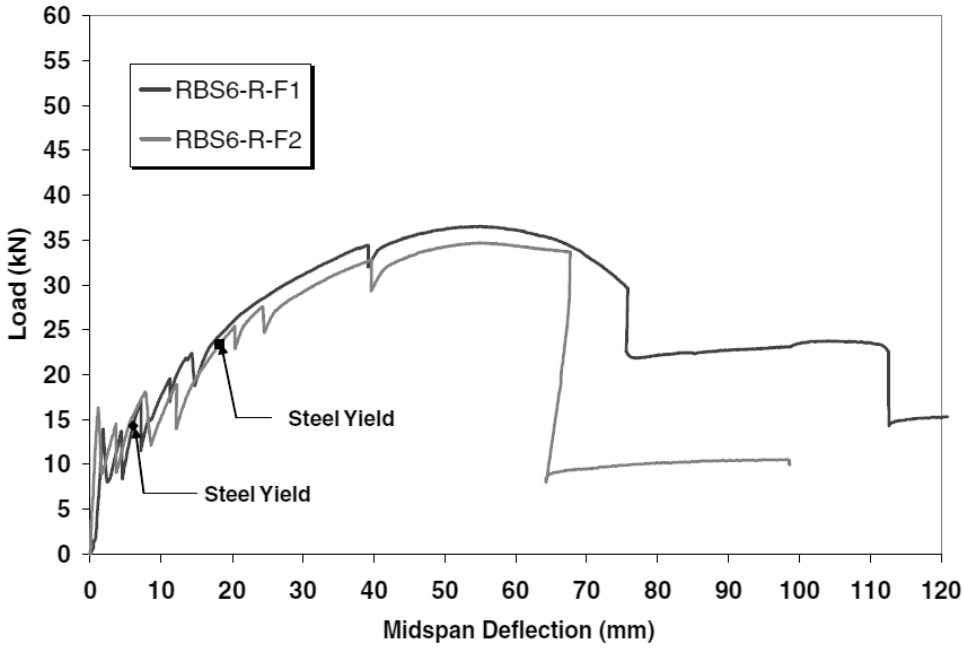

Figure 2.3: Load-deflection of steel reinforced PVC-encased concrete. (Chahrour et al. 2005)

All of the specimens experienced high ductility and ultimate load enhancement as the core thickness increased. It was concluded that the PVC form did not have sufficient strength to completely replace steel reinforcement in a concrete wall. Other materials would need to be incorporated (steel or FRP bars) as internal reinforcement in order to replicate a reinforced concrete wall.

Chahrour et al. (2005) incorporated reinforcing steel into only one of three concrete core thicknesses. Rteil et al. (2008) tested 20 PVC encased specimens (Octaform System) 305 mm wide and 2500 mm long under four-point bending. The test variables were concrete core thickness (150 mm or 200 mm), internal reinforcement (un-reinforced or 2-10M bars), and the configuration of the PVC connectors (middle or braced.) Plain PVC encased concrete walls (no steel reinforcement) showed increased ductility and ultimate load capacity over

plain concrete sections. This increase became more pronounced as the core thickness decreased. The PVC enhanced the ultimate load by 36% for 150 mm thick walls and 18% for 200 mm thick walls. They concluded that adding PVC SIP forms increased the cracking load and yield load of the reinforced specimens by 36% and 65% over their respective control walls. As reported earlier by Chahrour et al. (2005), they observed a change from the 'saw-tooth' behaviour load deflection curves in the unreinforced specimens to a continuous increase in load with deflection for the steel reinforced specimens. The forms increased the maximum deflection of the walls by 24% and 55% for 150 mm and 200 mm thick walls, respectively. The configuration of PVC connectors did not have a significant impact on steel reinforced specimens.

The effect of connector configuration on the mechanical performance of concrete was explored further by Kuder et al. (2009). Four 610 mm long PVC SIP concrete walls, using the Octaform system were cast. A square cross-section of 152.4 mm by 152.4 mm was reinforced with one 10M steel rebar. Each of the specimens was assembled with a different configuration of PVC connectors as shown in Figure 2.4.

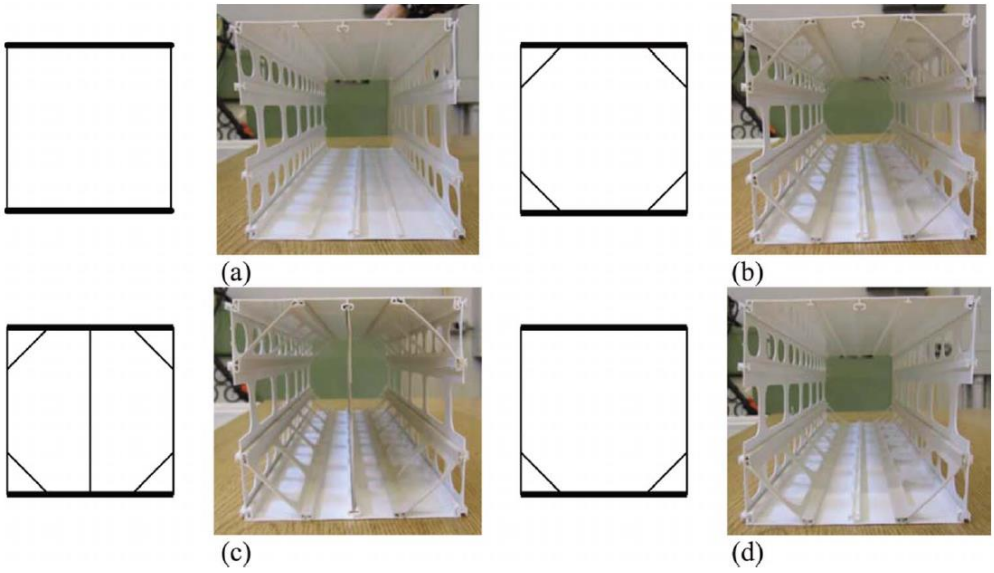

Figure 2.4: PVC connector arrangements (Kuder et al. 2009)

The walls were subjected to three-point bending with a shear span of 254 mm. They concluded that the encased specimens improved the flexural capacity and the toughness of the walls over the standard non-encased control specimens. The increases in flexural capacity and toughness varied from 39% to 66% and 41% to 60% respectively. The PVC configurations with the highest quantity of polymer in the cross-section (Figure 2.4 cross-section c) showed the highest increase in ultimate load.

Wahab and Soudki (2013) developed a large test program of 24 PVC encased concrete wall specimens (Octaform System). The walls were tested under four-point flexural bending. The walls were 457 mm wide and 3050 mm long, with a shear span of 1150 mm. Test variables were concrete core thickness (200 mm or 250 mm), steel reinforcing ratio (3-10M, 3-15M or 3-20M rebars), PVC connector configuration (middle or braced connectors), and

including insulating foam on the tension side of the walls. The test program was cast in two batches, with concrete strengths of 53 MPa and 43 MPa, respectively.

The PVC encased specimens showed an increase in cracking, yielding, and ultimate loads over the control wall specimens. Cracking load was the most significantly influenced, with a load increase of over 200% for both core depths. For yield and ultimate loads, lightly reinforced sections (10M) showed an average load increase in load of 22% versus 15% for heavily reinforced sections (15M and 20M). From the test data, it was concluded that the PVC contribution to flexural strength depended on the reinforcing ratio and section thickness. The configuration of the PVC connectors did not have any apparent effect on the resistance and thus could be ignored. The insulation did not have any effect on the contribution to flexural strength and was ignored. As the concrete core thickness and/or the internal reinforcement decreased, the enhancement of the PVC encasement to the wall's behaviour increased.

2.3 Analytical Modelling of PVC SIP Formwork

Several of the experimental programs completed on PVC SIP formwork were modeled through the development of an analytical model. These models were used to predict the ultimate load capacity of the PVC formed concrete elements. This section will examine four models in closer detail.

Chahrour et al. (2005) developed a strain compatibility model using linear strain analysis. Concrete in tension below the neutral axis was neglected in the analysis, with all tensile forces being resisted by the steel reinforcement (if present) and the polymer. The portion of

the polymer in compression was also neglected, with the concrete resisting all compressive forces. An equivalent rectangular concrete compression stress block and polymer tension block (acting on the polymer flanges and webs) were used to estimate the actual stresses within the cross-section. Finally, a summation of forces was used to determine the depth of the neutral axis 'c' to calculate the moment or flexural resistance of the wall (Equation 2-1)

$$c = \frac{A_{pt} f_{pu} + A_s f_y}{\alpha_1 f_c' \beta_1 b_c} \quad [2\text{-}1]$$

Where A_{pt} was the cross-sectional area of the polymer in tension, f_{pu} was the ultimate tensile stress of the polymer, A_s was the area of reinforcing steel in tension, f_y was the nominal yield stress of the reinforcement, α_1 is the stress factor for the concrete compression block, f'_c was the compression strength of concrete, and b_c is the width of the concrete compression block. Results from the model were within ±7% of the test results.

Kuder et al. (2009) identified that Chahrour did not examine the influence of various PVC SIP connectors' configurations. A model was developed following Euler-Bernoulli beam theory and linear strain distributions. Some assumptions from the previous model were adapted such as; ignoring the tensile strength of concrete, and using a rectangular concrete compressive stress block. Further modifications were made to modelling the PVC. Perfect composite action between the concrete and PVC was assumed, and the confining action of the PVC in the compression zone was neglected (Kuder et al., 2009). Finally, the PVC connector and panel were separated into individual forces, as seen in Equation [2-2].

$$a = \frac{(A_c + A_p)f_{pu} + A_s f_y}{0.85 f_c' b_c} \quad [2\text{-}2]$$

Where A_c is the PVC connector area in tension, A_p is the PVC panel area in tension, and f_{pu} is the ultimate stress in the PVC. The model results were conservative or underestimated by an average of 27% when compared to the experimental results. Despite this discrepancy, the results from the model indicated that the PVC forms increased the flexural capacity of the concrete wall due to an increased tensile capacity of the cross-section.

Rteil et al. (2008) developed a similar model to the one developed by Kuder et al. (2009). They assumed the wall failed when the concrete in compression crushed after the steel had yielded. However, the portions of the PVC connector acting in tension were ignored in the stress profile. In addition, the stress block factors α_1 and β_1, were calculated from linear strain distribution using the equations presented by Collins and Mitchell (Equations [2-3] and [2-4]).

$$\beta_1 = \frac{4 - \frac{\varepsilon_t}{\varepsilon_c'}}{6 - 2\frac{\varepsilon_t}{\varepsilon_c'}} \quad [2\text{-}3]$$

$$\alpha_1\beta_1 = \frac{\varepsilon_t}{\varepsilon'_c} - \frac{1}{3}\left(\frac{\varepsilon_t}{\varepsilon'_c}\right)^2 \quad [2\text{-}4]$$

Where; ε_t is the concrete strain at the top compression fibre and ε'_c is the concrete strain corresponding to the concrete compressive strength (f'_c) (Collins & Mitchell, 1997). Results from the model averaged 12% less than the experimental data. The authors suggested this was due to the effect of steel strain hardening not factored into the equation.

Wahab and Soudki (2013) used linear strain distribution in a model that accounted for the strain hardening of reinforcing steel in the walls. In addition, unlike previous models that had neglected the contribution of the compression panel, continuous portions of the PVC connectors acting in tension and the PVC panel acting in compression were considered in the analysis. Perfect bond or composite action was assumed between the concrete and PVC. Finally, the non-linear stress strain behaviour of the PVC was accounted for using Equation [2-5] as provided by the PVC manufacturer.

$$\sigma_{PVC} = -71518 * \varepsilon_{PVC}^2 + 3412.1 * \varepsilon_{PVC} \qquad [2\text{-}5]$$

Where; ε_{pvc} is the strain in the PVC, and σ_{pvc} is the corresponding stress at that strain level. Figure 2.5 shows the strain profile and stress distribution. Results from the analytical model showed good agreement with the test results, with an average error of 5%.

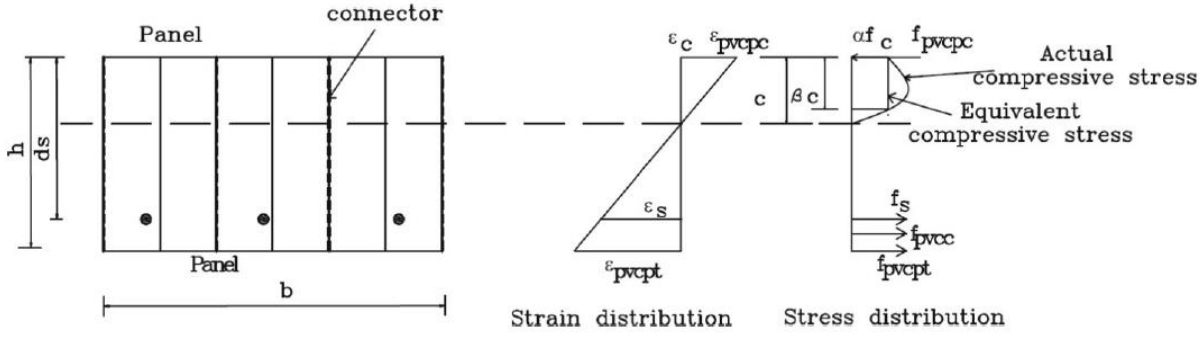

Figure 2.5: Stress and strain distribution of PVC SIP cross-section. (Wahab and Soudki 2013)

2.4 Research Needs

From the research presented, PVC SIP formwork does provide limited flexural strength enhancement to the reinforced concrete walls. While this enhancement is not as pronounced

as FRP structural formwork, there are significant improvements to the ductility of the walls. Previous research programs used concrete with high compressive strengths in excess of 40 MPa. The behavior of the PVC encased walls with low concrete strengths (25MPa to 30 MPa) reflective of typical wall designs needs more investigation. Finally, the majority of improvement retained from PVC forms has been due to the exterior panels and not the connectors. Other panel cross-sections have been developed featuring increased cross-sectional area.

The proposed research will produce a test program of PVC encased reinforced concrete walls that have a target strength of 25-30MPa. The program will focus on thin walls (150 mm 200 mm thick) that are lightly reinforced with steel. Thin-walled PVC encased sections with minimal steel reinforcement have showcased significant ultimate load and ductility improvement. This combination with lower concrete strength will provide further indication that PVC encased concrete walls may have the same ultimate load capacity as a thicker traditionally reinforced concrete wall. Finally, PVC panels with various cross-sections will be compared to allow for further understanding of how PVC encasement interacts with and improves the performance of reinforced concrete.

Chapter 3: Experimental Program

3.1 Test Program

Eighteen specimens were cast in the structures laboratory at the University of Waterloo. Six specimens were cast without PVC encasement to act as control walls. The remaining twelve specimens were cast using the PVC forming system. The test matrix is shown in Table 3.1. The variables studied were; concrete core thickness: 152, 178, and 203 mm (6, 7, or 8 inches, respectively), type of PVC forming panel: flat panel or hollow panel, and tension steel reinforcement: 3-10M or 3-15M rebars per specimen.

Table 3.1: Test matrix

Group	Panel	Thickness	Connector type	Reinforcement	Reinforcement ratio	Number of specimens
Panels with 6" thick wall						
C-6-10	None	152 mm (6")	None	3 – 10M	0.45%	1
C-6-15				3 – 15M	0.92%	1
PF-6-10	Flat		Middle	3 – 10M	0.45%	1
PF-6-15				3 – 15M	0.92%	1
PH-6-10	Hollow			3 – 10M	0.57%	1
PH-6-15				3 – 15M	1.17%	1
Panels with 7" thick wall						
C-7-10	None	178 mm (7")	None	3 – 10M	0.36%	1
C-7-15				3 – 15M	0.74%	1
PF-7-10	Flat		Middle	3 – 10M	0.36%	1
PF-7-15				3 – 15M	0.74%	1
PH-7-10	Hollow			3 – 10M	0.44%	1
PH-7-15				3 – 15M	0.90%	1
Panels with 8" thick wall						
C-8-10	None	203 mm (8")	None	3 – 10M	0.31%	1
C-8-15				3 – 15M	0.62%	1
PF-8-10	Flat		Middle	3 – 10M	0.31%	1
PF-8-15				3 – 15M	0.62%	1
PH-8-10	Hollow			3 – 10M	0.36%	1
PH-8-15				3 – 15M	0.73%	1

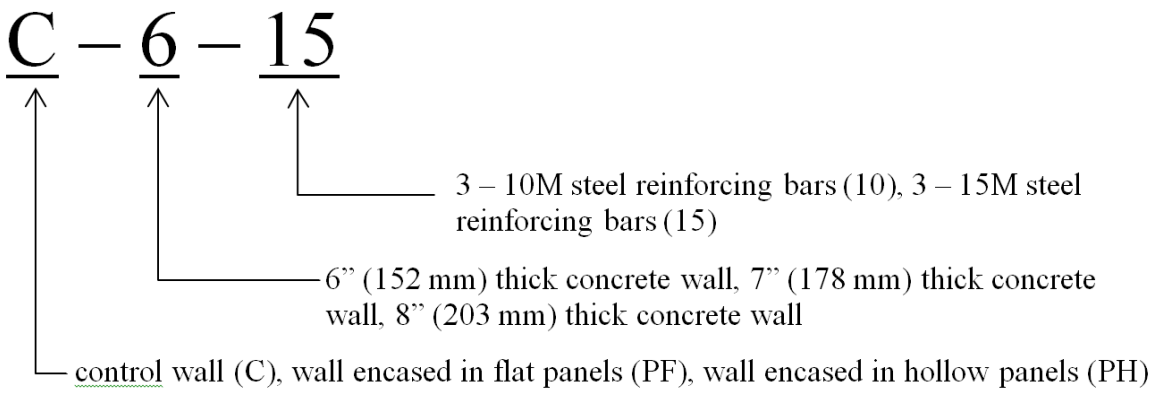

The specimen notation in Table 3.1 is as follows; the first letter designates the panel type; control (C), concrete wall encased with flat PVC panels (PF), or concrete wall encased with hollow PVC panels (PH). The following number reflects the concrete core size in inches. The final number designates the diameter of the reinforcement placed in the specimen; 3-10M or 3-15M rebar. For example; the specimen PF-8-15 denotes an 8 inch (203 mm) thick PVC encased wall specimen, formed with flat panels and reinforced with 3-15M rebars.

For walls of the same thickness, the corresponding reinforcement ratio for the hollow panel encased wall was higher. This increase is due to the thicker hollow panels reducing the depth of concrete to the reinforcement. When compared to the reinforcing ratios typically used with the SIP system, the wall sections tested would be considered as 'lightly' reinforced. With ratios of 0.31% to 0.36% for the 8" thick walls, some specimens are close to the CSA code minimum for reinforcing steel of 0.2% (Cement Association of Canada, 2006). Comparatively low reinforcing ratios were selected in order to best observe the effects of the SIP PVC system as testing occurred.

3.2 PVC Stay-in-Place components and wall

All specimens had a rectangular cross-section, with a constant length of 2440 mm (8 feet) and a width of 610 mm (2 feet). The core thickness of each specimen was 152, 178, or 203 mm (6, 7, or 8 inches, respectively). Each PVC encased specimen consisted of 4 bottom and 4 top panels. Walls with hollow panels had 5 middle connectors spaced at 152 mm, while walls with flat panels had 9 middle connectors spaced at 76 mm. Each specimen was reinforced in the longitudinal direction with 3 steel rebars (3-10M or 3-15M) with a clear cover of 38 mm on the tension side of the wall. The clear cover is measured from the PVC panel and concrete interface. Five transverse 10M rebars were added to the reinforcement (spaced at 450 mm) to simulate the transverse wall reinforcement used in practice and to secure the longitudinal rebars into place. The longitudinal and transverse steel rebars were tied together using spiral ties. Figure 3.1 presents typical cross-sections for each wall type; control, flat panel encased, and hollow panel encased. Figure 3.2 shows the two types of panels used in the fabrication of the walls; hollow panel (PH) and flat panel (PF). The thickness of the panels are 1 mm and 11 mm for flat and hollow panels, respectively.

The reinforcement was placed on only one side of the walls, creating singly reinforced sections. While many walls are doubly reinforced to combat applied forces on both loading directions, several of the wall types used in the SIP application have bending dominate in a single direction (i.e., retaining walls and chemical/water tanks).

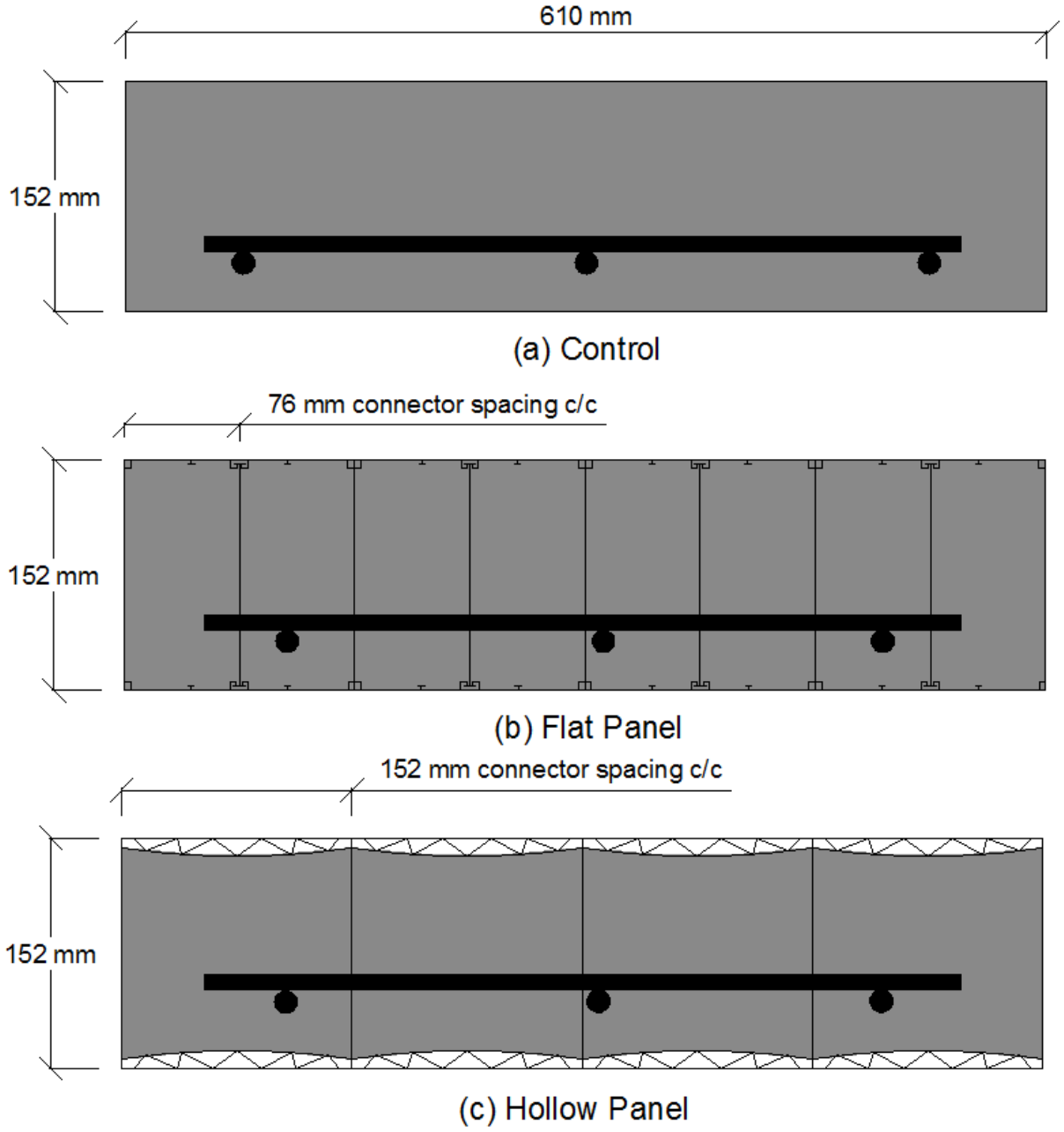

Figure 3.1: Cross-sections and dimensions for the (a) control, (b) flat panel encased, and (c) hollow panel encased wall specimens

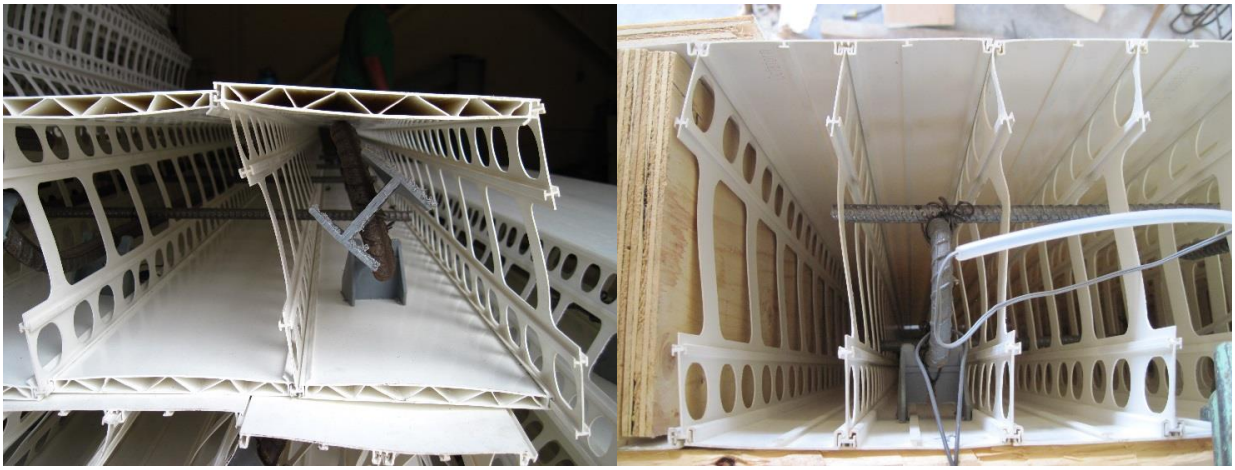

Figure 3.2: Examples of assembled hollow panel and flat panel walls

3.3 Specimen Fabrication

3.3.1 Control Specimens

Three double-layer plywood boxes were fabricated to form the control walls. Three sides of the box were assembled and then tilted into place. The reinforcing steel mats were then placed and secured inside the control boxes before attaching the final face of the form. The boxes were girdled using timber (2 X 4 inches) spaced at 300 mm to avoid any concrete blowouts during casting. Figure 3.3 shows one open-faced box with the steel cage in place and the final control box assembly.

Figure 3.3: Placing the reinforcing steel inside control box; final assembly of the three control boxes with timber girdling

3.3.2 PVC Encased Walls

All of the PVC encased specimens were assembled horizontally. Once the bottom panels and middle connectors were assembled, the longitudinal and transverse steel reinforcement were tied into place. Plastic chairs were used at the ends of the walls to ensure that the reinforcing mats would stay in place and maintain a consistent clear cover during construction and concrete pouring. The top panels were then slid into place. Finally, the walls were tilted vertically into their final casting position. Figure 3.4 shows a partial view of a row of walls being secured to the casting frame.

Figure 3.4: Wall specimens tilted into place

Due to space restrictions in the laboratory, the walls were placed in three parallel rows of 4 specimens per row. The rows of specimens were separated by timber spacer frames to provide enough space for each wall to expand freely during casting. Figure 3.5 shows the PVC encased walls arranged in place. Threaded rods were used to tie the entire assembly back to the casting frame as shown in Figure 3.6.

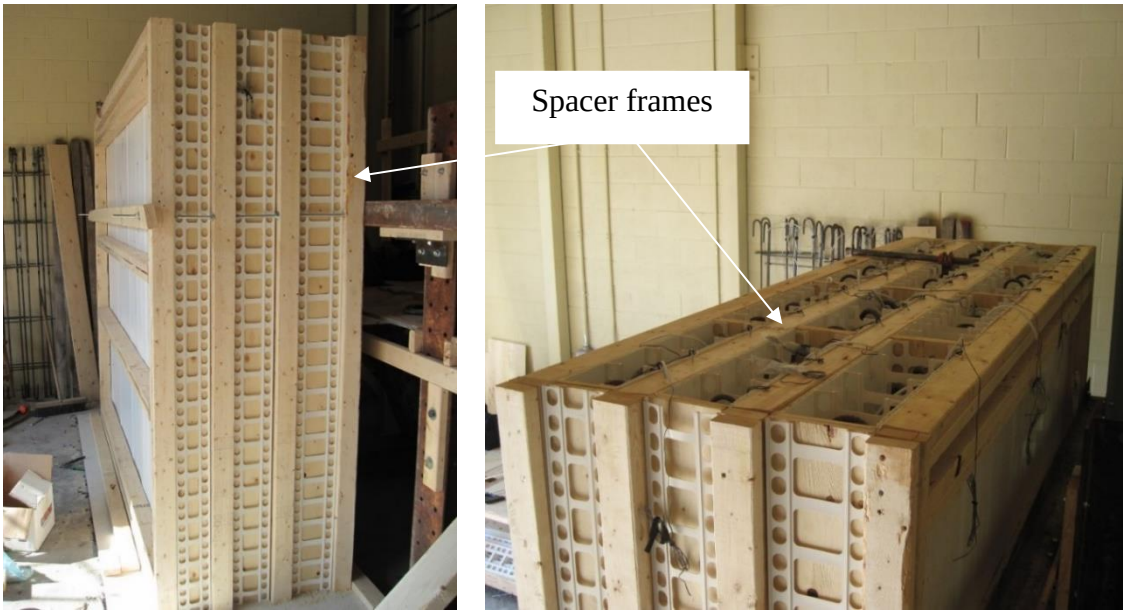

Figure 3.5: Selected views of the secured PVC encased specimens before concrete casting

Figure 3.6: Specimens in place before casting

3.3.3 Casting and Curing

Concrete was supplied by a local ready-mix plant. The properties of the concrete mix, as provided by the supplier, are shown in Table 3.2. Concrete was placed in three lifts using a conveyor belt until the walls were filled. After each lift the specimens were vibrated by using a 3 m long mechanical vibrator. Figure 3.7 shows the walls during casting. Forty cylinders were also cast alongside the specimens with concrete taken from the middle of the casting process. These cylinders were used to determine the compressive strength of the specimens at different ages.

Table 3.2: Concrete mix

Property	Value
Minimum strength	15 MPa
Target strength	26 MPa
w/c ratio	0.7
Slump	180 mm ± 20 mm

Figure 3.7: Casting using a chute and a conveyor belt

The walls were covered with wet burlap and plastic a few hours after casting. A wet curing routine was followed for 5 days, where the concrete was wetted with water daily and covered with wet burlap and plastic. Compressive strength tests on the cylinders were conducted at 4, 7, and 12 days. Upon achieving a concrete strength equal to 18 MPa, the wall specimens were stripped, rotated, and stacked horizontally in preparation for testing.

3.4 Material Properties

3.4.1 Concrete

The typical concrete strengths used in the PVC encased walls varied between 20 and 32 MPa. A mix was selected with a nominal compressive strength of 26 MPa. The concrete mix had a maximum aggregate size of 10 mm. Super plasticizers and retarders were used to provide a workable concrete. The actual slump for the mix was 210 mm.

Compressive strength tests were conducted on concrete cylinders cast from the mix. Table 3.3 shows the average compressive strength at different ages. The average compressive strength represents the average strength of 6 tested cylinders. The concrete strength was 21.8 MPa and 24.0 MPa at 28 and 56 days, respectively. The testing of the walls began at 56 days. Cylinders were tested after the wall testing was completed (116 days). The average strength of the concrete at this time was 27.6 ± 0.7 MPa.

Table 3.3: Average concrete strength

Day	Concrete compressive strength (MPa)
4	10.8 ± 0.2
7	14.3 ± 0.5
12	18.1 ± 0.6
21	20.7 ± 0.5
28	21.8 ± 0.7
56	24.0 ± 0.3
116	27.6 ± 0.7

As the control walls were being removed or stripped of their formwork, some small areas of segregation were observed on the surface of the walls. The most significant areas of segregation were seen in walls C-8-10 and C-8-15 (Figure 3.8). A cementiteous patch material (SikaDur 31) was applied to the control specimens to fill the cavities (Figure 3.9). The patch material could not be applied to the PVC encased walls. However, significant segregation was not observed when these walls were removed from the casting frame. Figure 3.10 shows the interior surface of a tested wall that has had the patch material applied to it. From the figure it can be seen that the patching material achieved good bond with the concrete substrate.

Figure 3.8: Segregation present on control wall specimens

Figure 3.9: Example of patch material applied to concrete wall with segregation.

Figure 3.10: Evidence of bond achieved between concrete and patch material.

3.4.2 Steel

Reinforcing steel rebars (10M and 15M) were used. Table 3.4 shows the mechanical properties of the rebars as provided by the manufacturer.

Table 3.4: Properties of reinforcing steel

Bar Size	Yield strength (MPa)	Ultimate strength (MPa)	Elongation (%)
10M	486	575	16.0
15M	478	580	18.0

3.4.3 Polyvinyl Chloride (PVC)

The properties of the polyvinyl chloride (PVC) as provided by the manufacturer are given in Table 3.5.

Table 3.5: Properties of PVC

Property	Value (MPa)
Tensile strength	45.9
Tensile modulus	2,896
Flexural strength	90
Flexural modulus	2,965

3.5 Instrumentation and Test Set-up

Strain gauges were supplied by Tokyo Sokki Kenkyujo Co. Ltd. The strain gauges had a resistance of 120±0.3 ohms with a thermal expansion of 11 PPM/°C. For each wall, two strain gauges were mounted at mid-span on two longitudinal rebars (outer and middle). Then, the gauge was waxed and protected with electrical tape to ensure protection of the gauge during handling and casting. (Figure 3.12)

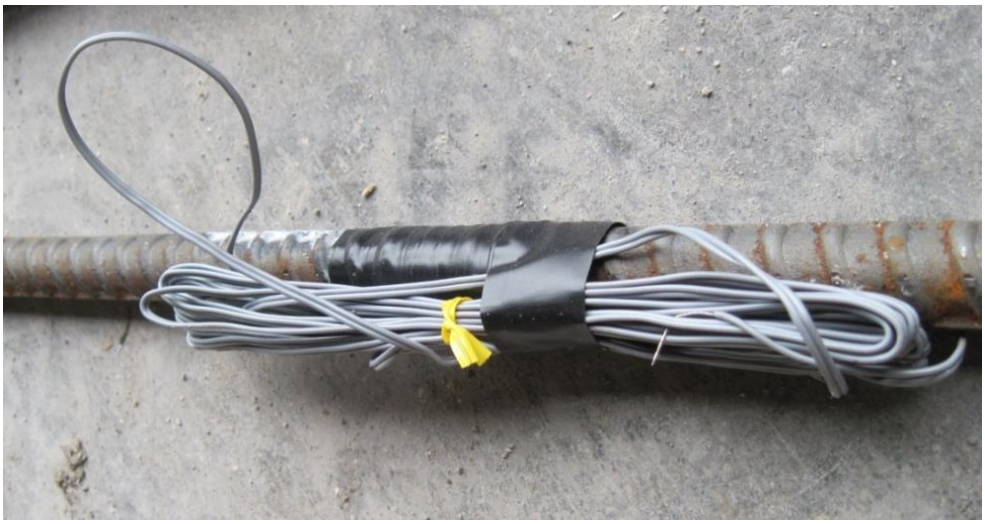

Figure 3.11: Protected strain gauge before assembly

Once the walls were cast, additional strain gauges were mounted on the compression side prior to testing. For the control specimens, two concrete strain gauges were placed on the compression face of the wall; one at the centerline of the cross section and another close to the edge of the cross section. For the PVC encased specimens, cuts were made through the PVC panel in the compression zone in order for a strain gauge (60 mm long) to be adhered to the concrete surface. Also, high elasticity strain gauges (5 mm long) were mounted on to the tension and compression faces of the PVC panels (Figure 3.13). Four PVC strain gauges were used to monitor the behaviour of each PVC encased specimen.

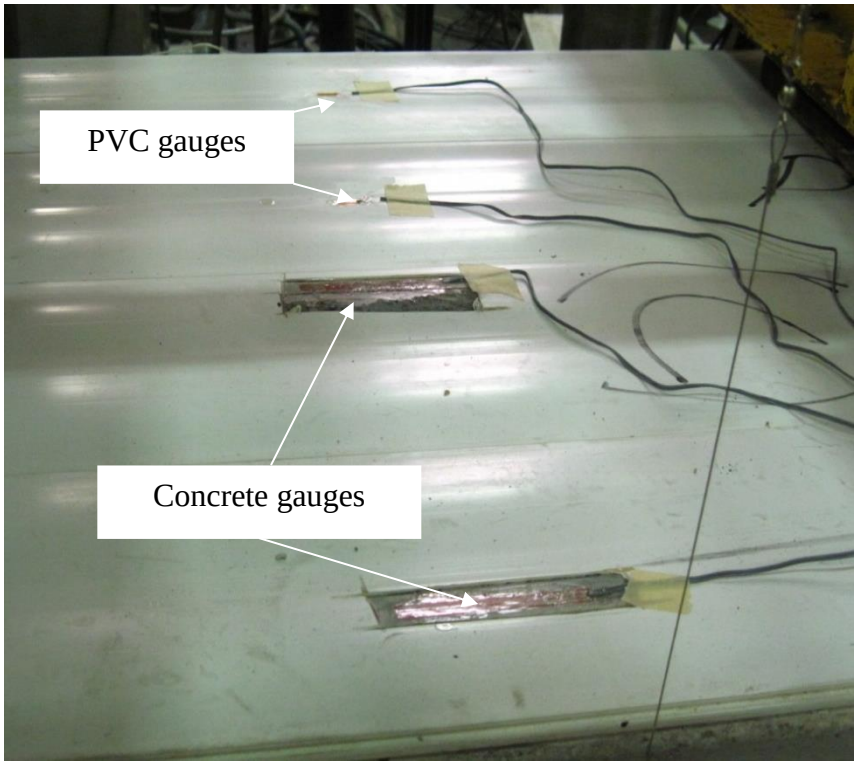

Figure 3.12: Concrete and PVC strain gauges on the compression face of the wall

The walls were tested in four-point bending using a servo-hydraulic actuator controlled by a MTS-Digital GT controller. The shear span was 760 mm and the constant moment region was 600 mm as shown in Figure 3.14. The load was applied at a rate of 2.5 mm/min. The duration of the tests varied between 60 and 120 minutes. The wall was supported on a hinge support at one end and a roller support at the other end. The hinge support was a cylindrical bar welded to a flat plate and the roller support was a steel cylinder between two curved plates. The load was measured using a 500 kN load cell. The deflection of the wall at mid span was measured using two external string pots attached to the sides of the specimen. The test was stopped when the load dropped by more than 20% of the peak load or if the

specimen shifted on the supports, resulting in a change in the loading conditions (encountered with one specimen only).

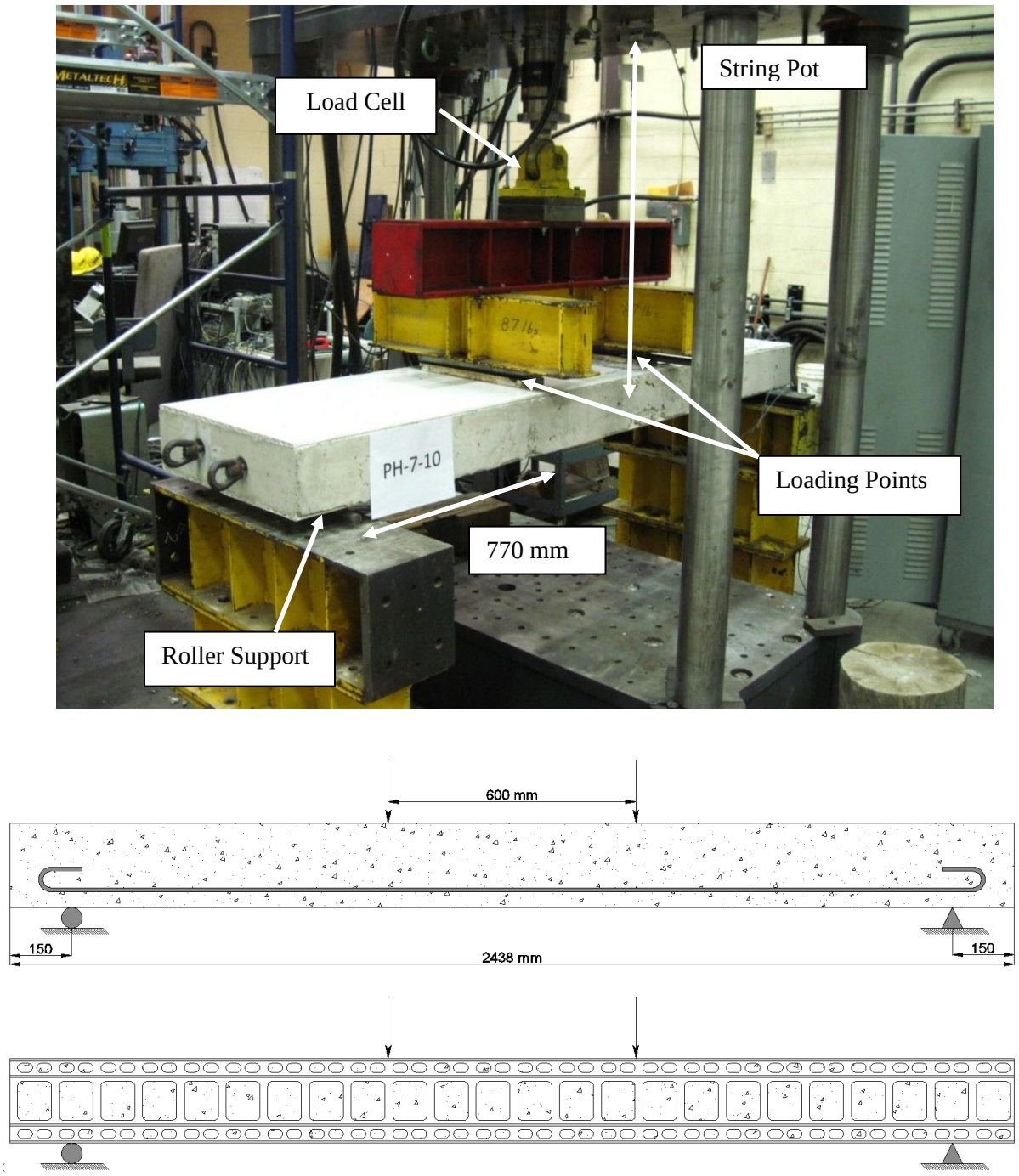

Figure 3.13: Test set-up

Chapter 4: Experimental Test Results

4.1 Introduction

In this chapter, the test results from the control specimens and PVC encased specimens are presented and compared. The results include the modes of failure observed, the load versus deflection behaviour, and the load versus strain behaviour of the different components of the walls.

4.2 Behaviour of the Control Specimens

4.2.1 Modes of Failure

Each of the six control specimens exhibited the same failure mechanism. The reinforcing steel yielded at mid span, followed by concrete crushing in the constant moment region. Most of the crushing failures occurred at mid span, as shown in Figure 4.1. However, for two specimens (C-7-15 and C-8-15) the crushing locations were close to the right loading point.

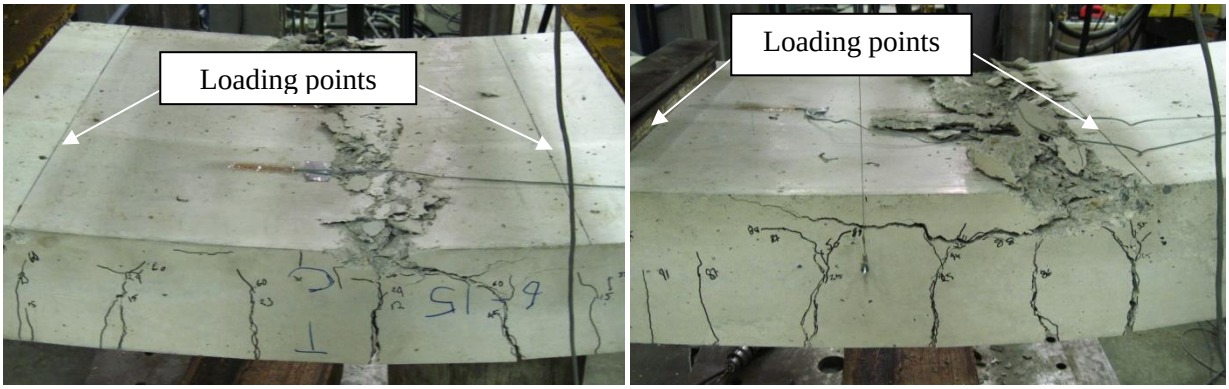

Specimen C-6-15 Specimen C-7-15

Figure 4.1: Failure modes for control walls

4.2.2 General Behaviour

Cracks first appeared at mid span in the constant moment region. As the load increased, cracks continued to form at a relatively even spacing between and just beyond the loading points. As the load increased further, the cracks propagated towards the compression face of the specimen. Once the steel yielded, the cracks in the constant moment region widened significantly as the curvature of the wall increased. At failure, the widest tension cracks were at the sections where the concrete crushed on the compression face.

4.2.3 Flexural Behaviour

4.2.3.1 Load-Deflection

The typical load versus deflection behaviour is presented in Figure 4.2. The vertical axis represents the applied load (kN) and the horizontal axis represents the mid span deflection (mm). The specimens showed the same load versus deflection behaviour, which can be described in three distinct phases; un-cracked, cracked, and post yield. The un-cracked phase refers to the rapid rise in load with minimal deflection (< 2 mm) until the cracking load is reached. The cracked phase occurs between the cracking and yield loads, where the load increases linearly with deflection. The stiffness in this phase is reduced compared to the un-cracked phase. At the yield load, the post yield phase starts where the deflection of the specimen increases rapidly in comparison to the load.

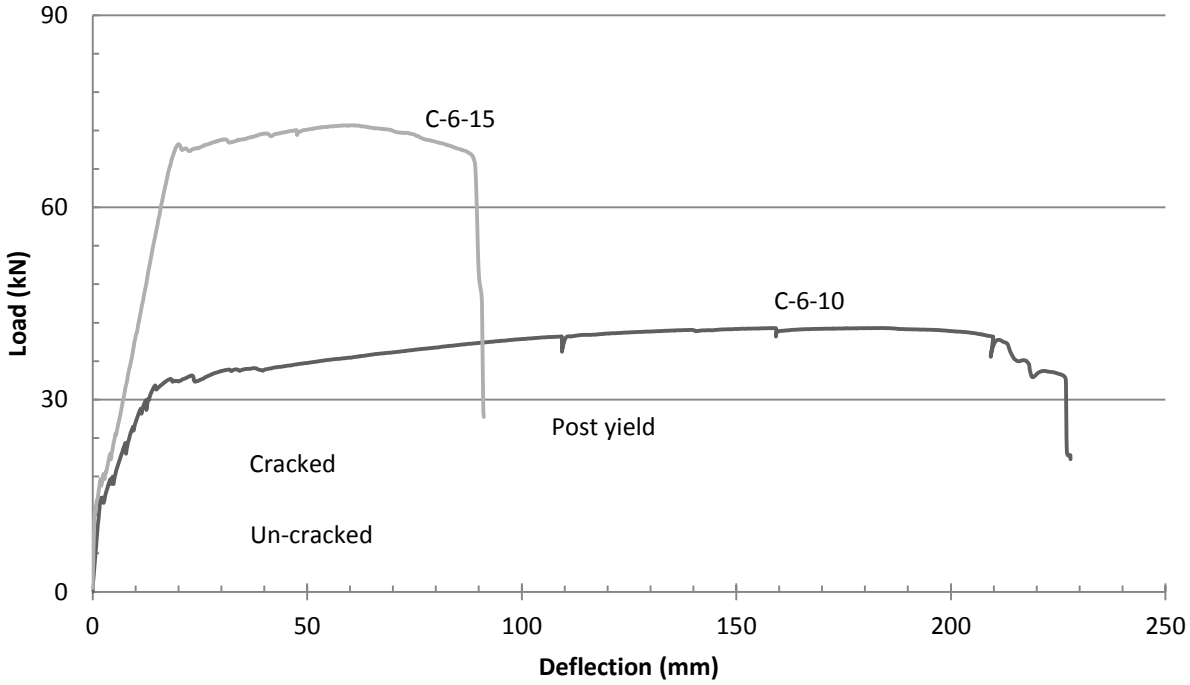

Control specimens 152 mm (6 inch) thick

Figure 4.2: Typical Load versus deflection for control specimens

Table 4.1 summarizes the cracking, yield, peak, and ultimate loads and their corresponding deflections for the control specimens. The cracking load depends on the thickness of the concrete section. As the thickness increased, the cracking load increased. The average cracking loads for the specimens with core thickness of 152 mm, 178 mm, and 203 mm were 15.8 kN, 18.8 kN, and 21.5 kN, respectively. At a constant core thickness, the yield load was a function of the quantity of tension steel reinforcement. As the diameter of the reinforcing bar increased, the yield load increased. For example, the specimen that was 152 mm thick and reinforced with 3-10M showed a yield load of 32 kN. When the reinforcement was increased to 3-15M, the yield load increased to 69 kN. This behaviour was seen for all wall thicknesses tested. For a given reinforcement (3-10M or 3-15M), as the concrete core

thickness increased the yield load increased. This is mainly due to the increased depth of the reinforcing steel in relation to the concrete compression block increased, thus improving the load resistance at yielding. For example, a 152 mm thick wall reinforced with 3-10M reinforcement yielded at 32 kN, while the equivalent beam with a 178 mm thickness yielded at 44.5 kN.

Similar to the yield loads, the peak loads of the specimens increased as the concrete core thickness and reinforcing steel increased. Specimens with a core thickness of 152 mm (6 inches) showed peak loads of 41 kN and 77.2 kN when reinforced with 3-10M and 3-15M rebars, respectively. When the concrete core thickness was increased to 178 mm (7 inches), the peak loads increased to 55.5 kN and 91 kN at a reinforcement equal to 3-10M and 3-15M rebars, respectively. The walls with a core thickness of 203 mm (8 inches) showed peak loads of 66 kN and 114 kN when reinforced with 3-10M and 3-15M, respectively.

The deflection at cracking load was less than 2 mm for each of the control specimens. For a given concrete core thickness, the deflection at the yield load increased as the reinforcement increased. For a given reinforcement, the deflection at the yield load decreased as the concrete core thickness increased. The ultimate deflections ranged from 90 mm to 226 mm for the 152 mm thick walls, 100 mm to 139 mm for the 178 mm thick specimens, and 136 mm to 158 mm for the 203 mm thick specimens, depending on the reinforcement. The ductility index is a ratio between the maximum (ultimate) deflection and yield deflection. A low ductility index indicates a brittle specimen while higher values indicate a more ductile wall. For a given core thickness, as the amount of reinforcing steel increased, the ductility index decreased. The ductility index of the 152 mm (6 inch) walls decreased from 15.7 to

4.6 as the diameter of the reinforcing rebar increased from 10M to 15M. Specimens with a thickness of 178 mm and 203 mm also reflected this trend, where the ductility index dropped from 12.2 to 5.6 and 13.5 to 12.0, respectively, as the reinforcing bar diameter increased from 10M to 15M.

Table 4.1: Test results for control walls

Steel	$P_{cracking}$ (kN)	P_{yield} (kN)	P_{peak} (kN)	$\Delta_{cracking}$* (mm)	Δ_{yield} (mm)	Δ_{ult} (mm)	Ductility index	Toughness (kN mm)
Thickness = 152 mm (6 inches)								
3-10M	14.6	32	41	1.9	14.4	226	15.7	8505
3-15M	17	69	77.2	1.3	19.6	90	4.6	5820
Thickness = 178 mm (7 inches)								
3-10M	17.5	44.5	55.5	1.6	11.4	139	12.2	7090
3-15M	20	84	91	2.1	17.4	99.9	5.7	8058
Thickness = 203 mm (8 inches)								
3-10M	22	53	66	1.2	10.1	136	13.5	8316
3-15M	21	102	114	1	13.2	158	12.0	16775

*: Δ stands for deflection

For walls with a 203 mm thick concrete core, the specimen reinforced with 3-10M (C-8-10) bars had a lower ultimate deflection than the wall reinforced with 3-15M bars (C-8-15) (138 mm vs 158 mm). At other thicknesses the wall specimens with 10M steel bars observed the greatest deflection capacity. The anticipated ultimate deflection for the 15M reinforced walls is less than the respective 10M reinforced walls. This is due to the increased ratio between the concrete crushing strain and the depth of the concrete compression block. As the quantity of reinforcing steel is lowered, the corresponding compression depth is also lowered. This ratio is also known as the curvature; the greater the curvature the greater the anticipated displacement or deflection of the concrete element.

This change in behaviour of the 203 mm core walls from the 152mm and 176mm control walls was attributed to the following reasons. First, the failure of C-8-15 occurred underneath one of the loading points. As such, the concrete at this location may be benefited from local confinement of the crushing zone, prolonging the ultimate failure and extending the deflection capacity of the wall. In addition, both wall specimens had experienced noticeable segregation of the concrete core at the mid span (test location). Figure 4.3 illustrates the extent of the weaker concrete paste observed on the surface of the control walls (right). The depth of the weaker paste into the core of the wall (left) was not significant. While the depth of this damage was not extensive enough to compromise the integrity of the walls, the resulting changes in section reduction influenced where the failure hinges formed.

Figure 4.3: Example of surface damage observed on C-8-15, with solid concrete underneath.

Table 4.1 presents toughness values for each of the control walls. Toughness is a measure of energy absorption and was calculated by determining the area underneath the load versus deflection curves. Generally, as the thickness of the control walls increased, the toughness of the 10M reinforced specimens decreased and the 15M reinforced specimens increased.

4.2.3.2 Load-Strain

All of the specimens showed similar load versus steel strain and load versus concrete strain behaviour. Figure 4.4 shows the test results for the 152 mm (6 inch) specimens. The vertical axis represents the applied load (kN) and the horizontal axis represents the concrete or steel strain. Positive values indicate tensile strains while negative values indicate compressive strains. Strain gauge readings are affected by the proximity to a crack location, yielding location, or failure location. From Figure 4.4a, the steel strain value was about 350με at the cracking load. Then, the strain gauge readings increased linearly with the applied load until reaching the yield load. After yielding, strain gauge readings increased rapidly with a small increase in the applied load until complete failure. Figure 4.4b shows the load versus the concrete strain behaviour. The strain gauge readings increased linearly with load from the beginning of the test until the yield point. Past the yield point, the strain gauge readings increased with load at a higher rate until failure (concrete crushing) was attained. The strain gauge readings when the concrete crushed varied from -3500 με to -5000 με.

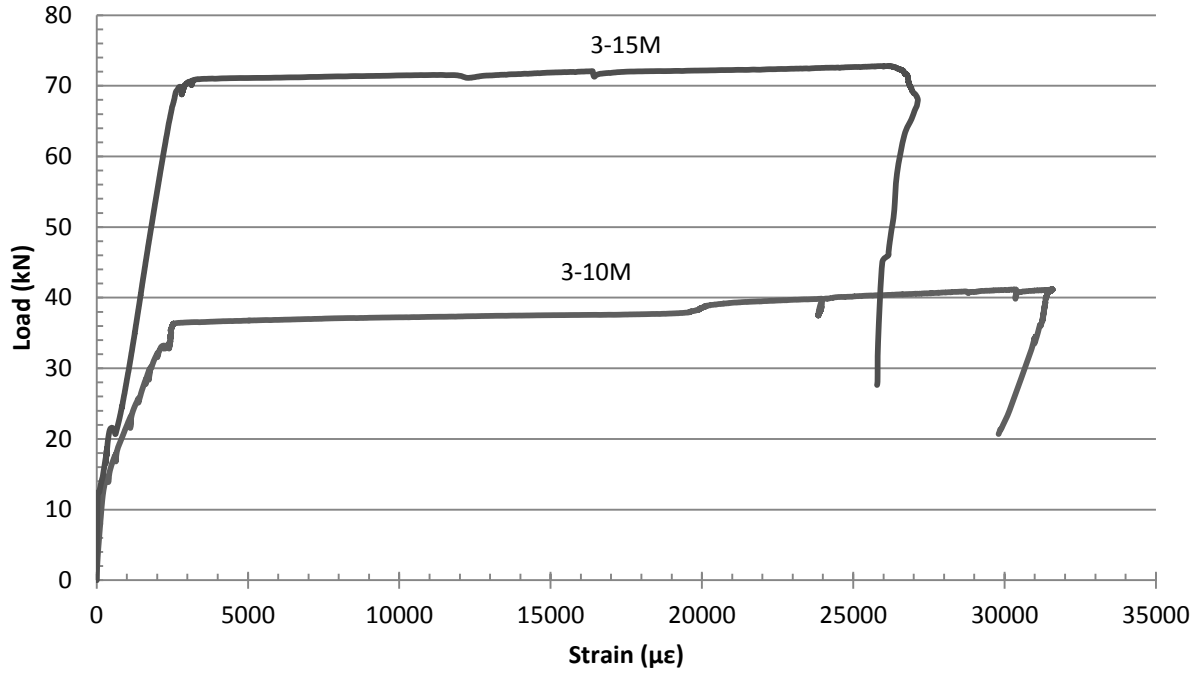

a – Load vs steel strain

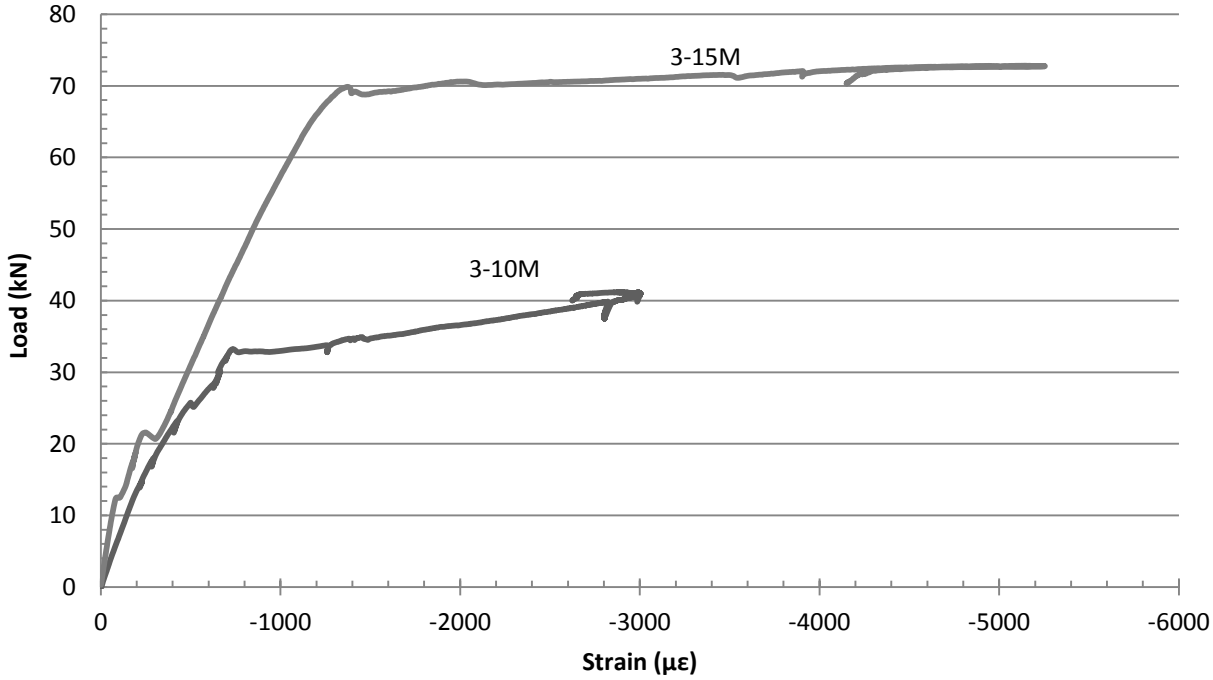

b – Load vs concrete strain

Figure 4.4: Load vs strain for C-6-10 and C-6-15

4.2.3.3 Strain Profile

Figure 4.5 provides a typical strain profile of a control wall. Two sets of strain data were used to create the profile, compression in the concrete on the top surface of the wall, and tension in the steel reinforcement. The strain distribution was plotted at different percentages of the peak load level as indicated in the figure. A line connects the two readings at each load level. It is clear that the neutral axis remained at the same location until reaching 80% of the peak load. Beyond this load level, strain gauge readings of both concrete and the steel increased and the depth of the concrete compression block decreased. This is understandable as at 80% load level the specimen had not yet yielded and the strains within the steel were relatively low.

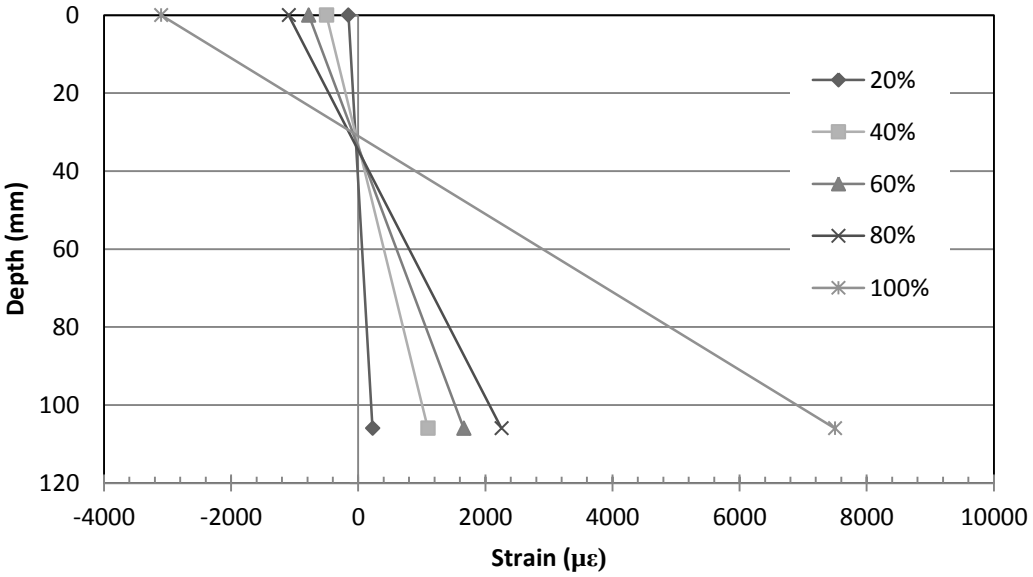

Figure 4.5: Strain profile for specimen C-6-15

4.3 Behaviour of PVC Encased Specimens with Flat Panels

4.3.1 Modes of Failure

For a given tension steel reinforcement quantity, all of the PVC encased walls with flat panels (PF) cracked in a similar manner and experienced the same failure mode. Specimens reinforced with 10M rebars failed first with steel yielding, followed by concrete crushing, then PVC bubbling or buckling and finally PVC rupture on the tension side of the wall. Specimens reinforced with 15M rebars failed in a similar manner but did not experience PVC rupture. Figure 4.6 shows the different modes of failure.

4.3.2 General Behaviour

The specimens showed similar behaviour when tested. The first concrete cracks appeared on the tension side at mid span in the constant moment region. As the load increased, several more cracks appeared just outside of the constant moment region. After the steel yield point was reached, the cracks at the mid span began to widen and propagate towards the compression face as the wall experienced a rapid increase in deflection. As the load was increased further, one or two cracks in the constant moment region continued to widen. At these crack locations, the concrete crushed then the PVC panels on the compression side of the wall buckled.

The final failure varied depending on the area of the steel reinforcement. For specimens reinforced with 10M rebars, one of the PVC panels on the tension side of the wall would rupture. For specimens with 15M rebars, the PVC panel in compression (top) would continue to buckle, and partially lift off the concrete surface.

a – Failure by steel yielding followed by concrete crushing then PVC bubbling then rupture of PVC panel. (PF-7-10)

b – Failure by steel yielding followed by concrete crushing then PVC bucking (PF-8-15)

Figure 4.6: Modes of failure for PVC encased walls with flat panels (PF)

4.3.3 Flexural Behaviour

4.3.3.1 Load-Deflection

All of the specimens had similar load deflection behaviour. Figure 4.7 shows typical load versus deflection curves for the 152 mm (6inch) thick PVC encased walls with flat panels. The vertical axis represents the load (kN) and the horizontal axis represents the mid span deflection (mm) as recorded by the external string pots. Initially, the load increased with

minimal deflection (<2 mm) until the specimen cracked at mid span. After cracking, the load continued to increase as the deflection increased until the steel yielded. After yielding, the slope of the curve was shallower than the post cracking slope. Past the yielding point, the load versus deflection curves for both specimens were similar but not identical. For the specimens reinforced with 10M rebars, the load increased with deflection until the curve plateaued with increasing deflection and a constant load. Finally, the load slowly started to drop off this plateau until failure was reached at a deflection of 300 mm. For the specimens reinforced with 15M rebars, the load increased with deflection until reaching a peak. Then, the load started to decrease gradually with increasing deflection until reaching a deflection of 100 mm. Past 100 mm deflection, the load dropped linearly as deflection increased until failure.

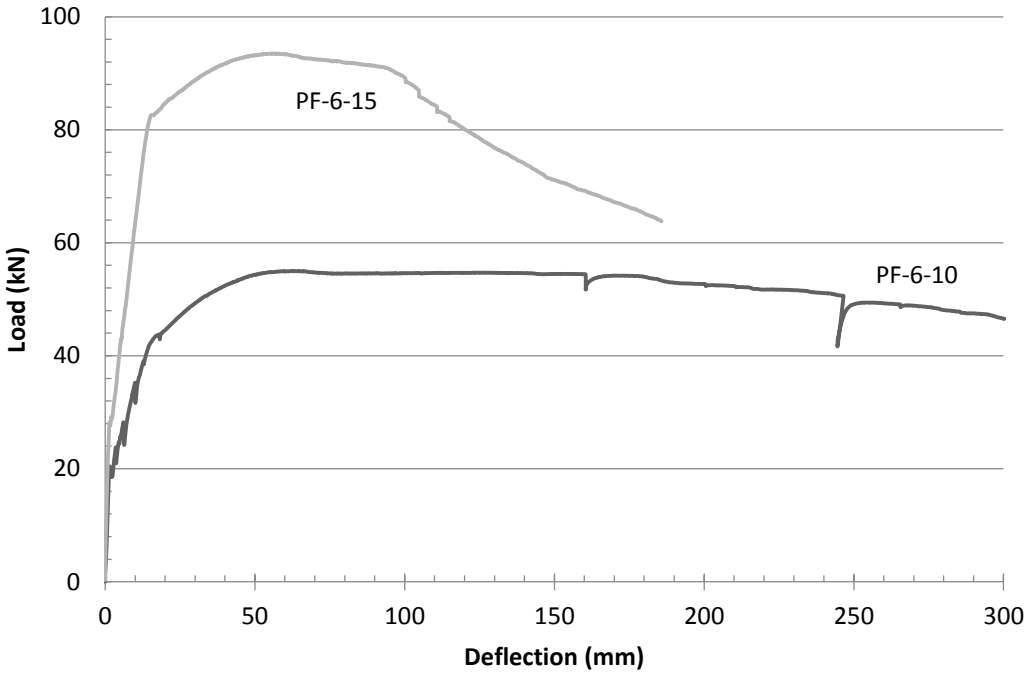

Figure 4.7: Load versus deflection curve for PF-6-10 and PF-6-15

Figure 4.8 compares the two flat panel specimens (PF-6-10 and PF-6-15) to their equivalent control walls. The flat panel specimens showed significant improvements in the applied load and ductility. Table 4.2 shows the crack, yield, peak, and ultimate loads, as well as their corresponding deflections. In addition, the table shows the percentage of increase in load and deflection over the control walls.

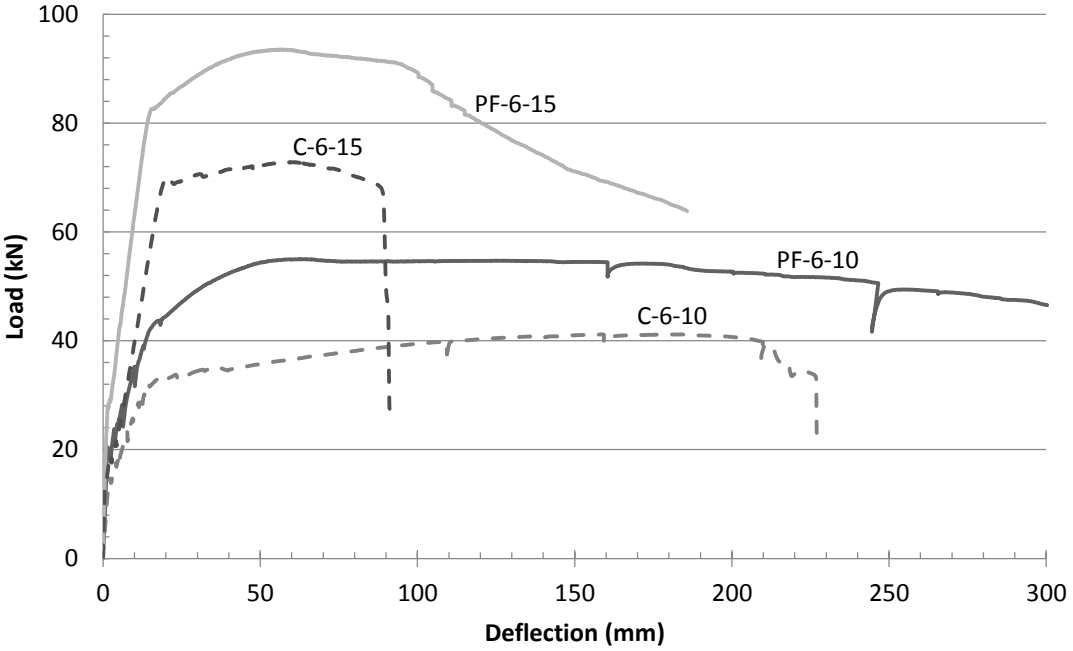

Figure 4.8: Load versus deflection curves for PVC encased walls with flat panels and their equivalent control walls (C-6-10 & C-6-15)

Table 4.2: Test results for PVC encased walls with flat panels

Reinforcement	P_{crack} (kN)	P_{yield} (kN)	P_{peak} (kN)	$\Delta_{cracking}$ (mm)	Δ_{yield} (mm)	Δ_{ult} (mm)	Ductility index	Toughness (kNmm)
Thickness: 152 mm (6")								
3-10M	20	43	55	1.4	15.4	300	19.5	15318
Improvement	**37%**	**34%**	**34%**			**33%**	**24%**	**80%**
3-15M	27.5	82.5	93	1.4	15.1	185	12.3	14862
Improvement	**62%**	**20%**	**20%**			**106%**	**167%**	**155%**
Thickness: 178 mm (7")								
3-10M	30	54	72	1.3	9.8	255	26.0	18429
Improvement	**71%**	**21%**	**30%**			**83%**	**113%**	**160%**
3-15M	31	96	111	1	14.1	178	12.6	16824
Improvement	**55%**	**14%**	**22%**			**78%**	**120%**	**109%**
Thickness: 203 mm (8")								
3-10M	33	64	89	0.9	8.2	262	32.0	22515
Improvement	**50%**	**21%**	**35%**			**93%**	**137%**	**170%**
3-15M	41	120	138	0.9	10.9	209	19.2	26190
Improvement	**95%**	**18%**	**21%**			**32%**	**60%**	**57%**

i – Cracking Load

The cracking load for the 152 mm (6 inch) thick PVC encased walls with flat panels was 20 kN and 27.5 kN for the 10M and 15M reinforced walls, an increase of 37% and 62% over the controls walls respectively. The cracking load of the 178 mm (7 inch) thick PVC encased specimens with flat panels was 30 kN and 31 kN, an improvement of 71% and 55% over the equivalent 10M and 15M reinforced control specimens. The increase in the cracking load for the 178 mm thick specimens was 63%. Finally, the cracking load for the 203 mm (8 inch) thick flat panel specimens was 33 kN and 41 kN for the 10M and 15M reinforced walls, an increase of 50% and 95% over the respective control walls.

The cracking loads for a given thickness increased as the reinforcing ratio increased. This makes sense as the transformed moment of inertia of the reinforced concrete walls increases

as the quantity of steel increases. There was no distinct correlation between the test variables and the observed improvement in the cracking load. As the concrete in the control specimens was subject to local areas of honeycombing, effectively reducing the effective wall cross-section, any further observations outside of the recorded improvement is difficult.

The deflection at cracking for the PVC encased specimens with flat panels varied between 1 mm and 1.5 mm. On average, they were close to the deflections of the equivalent control walls at cracking.

ii – Yield Load

PVC encased walls with flat panels showed a higher yield load than the equivalent control specimens. The enhancement was influenced by the quantity of reinforcing steel, with specimens reinforced with 3-10M rebars showing greater improvement than specimens with 3-15M rebars. The yield loads for the PVC encased walls reinforced with 10M rebars were 43 kN, 54 kN, and 64 kN for the 152 mm, 178 mm, and 203 mm thick walls, respectively. The equivalent control specimens showed yield loads of 32 kN, 44.5 kN, and 53 kN, respectively. Therefore, the increase in the yield load was 34%, 21%, and 21% for the 152 mm, 178 mm, and 203 mm thick walls, respectively.

The yield load for the flat panel encased walls reinforced with 3-15M rebars was 82.5 kN, 96 kN, and 120 kN for the 152 mm, 178 mm, and 203 mm thick walls, respectively. The equivalent control walls showed yield loads of 69 kN, 89 kN, and 102 kN for the 152 mm, 178 mm, and 203 mm thick walls, respectively. Therefore, the increase in the yield load for

the walls reinforced with 3-15M rebars was 20%, 14%, and 18% for the 152 mm, 178 mm, and 203 mm thick walls, respectively.

The observed improvement in the yield load can be attributed to the PVC panel on the tension side of the wall providing a supplementary tensile force within the cross-section. The improvement in yield load was most significant for the 10M reinforced walls as the tensile force in the PVC was the largest relative to the force in the yielding steel bars.

The yield deflection for the PVC encased walls with flat panels and the control walls was similar. Hence, the presence of the PVC panels did not have a significant influence on the yield deflection.

iii – Peak Load

The PVC encased walls with flat panels showed an increase in the peak load over the control specimens. Similar to the yield load results, specimens reinforced with 3-10M rebars showed a greater improvement than specimens reinforced with 3-15M rebars. The peak loads for the flat panel encased specimens with 3-10M bars were 55 kN, 72 kN, and 89 kN for 152 mm, 178 mm, and 203 mm thick walls, respectively. The peak loads for the equivalent control specimens were 41 kN, 55.5 kN and 66 kN for 152 mm, 178 mm, and 203 mm thick walls, respectively. Therefore, the increase in peak load for the walls reinforced with 3-10M rebars was 34%, 30%, and 35% for the 152 mm, 178 mm, and 203 mm thick walls, respectively.

The peak loads for flat panel encased walls reinforced with 3-15M rebars were 93 kN, 111 kN, and 138 kN for 152 mm, 178 mm, and 203 mm walls, respectively. The equivalent control specimens showed peak loads of 77.2 kN, 91 kN and 114 kN, respectively. Hence,

the PVC encasement increased the peak loads by 20%, 22%, and 21% for the 152 mm, 178 mm, and 203 mm thick walls, respectively.

As was discussed with the yield load, 10M reinforced walls showed the most significant improvement as the PVC was able to contribute a more significant portion of the tensile force within the cross-section. In addition, the high strain values observed in the PVC (>15000 με) indicate that the PVC was at or approaching the maximum stress value, further increasing the polymer's contribution to the cross-section.

The ultimate deflection for the walls with flat panels was significantly higher than the ultimate deflection for the control walls. The increase in ultimate deflection varied between 32% and 106% as shown in Table 4.2. In addition, the walls were more ductile than their equivalent control walls, with the ductility index of the specimens varying between 19.2 and 32. For a given wall thickness, the ductility index decreased, as the rebar diameter increased from 10M to 15M. However, for a given rebar diameter, the ductility index increased, as the concrete core thickness increased. The presence of the PVC panels increased the ductility index by a minimum of 24% and a maximum of 167%.

This increased ductility was also reflected in the toughness of the flat panel encased walls. Improvement in toughness varied from 57% to 170%. For walls reinforced with 3-10M steel bars, the amount of improvement increased as the wall thickness increased. Conversely, for walls with 3-15M steel bars, the amount of improvement decreased as the wall thickness increased. Overall, the presence of the PVC panels significantly improved the energy

absorption of the walls. This was due to the PVC containing the crushed concrete surfaces on the compression side of the walls, prolonging the ultimate failure.

4.3.3.2 Summary of key findings

The following points can be concluded from the load versus deflection behaviour of the PVC encased walls with flat panels;

1. Cracking load: the flat panels increased the cracking load by an average of 70% but the cracking deflection remained almost the same.
2. Yield load: the PVC encasement with flat panels increased the yield load of the concrete walls. The increase depended on the rebar diameter and the concrete core thickness.
    a) The average yield load increase for walls with 3-10M rebars was 25%. For walls with 3-15M rebars, the average yield load increased 17%. These results indicated that as the reinforcing ratio increased, the enhancement of the flat panels to the yield load decreased.
    b) the yield deflections were not influenced by the PVC encasement.
3. Peak load: The contribution of the flat panels to the peak load decreased as the reinforcing ratio increased.
    a) PVC encased specimens reinforced with 3-10M rebars showed an average increase in the peak load of 33% over the control walls. For walls with higher reinforcement ratios (3-15M bars), the load enhancement dropped to 21% on average.

b) From the literature, in previous similar tests, the increase in peak load was influenced by the wall thickness. As the wall thickness increased, the effect of the PVC system on the peak load decreased. This trend was not apparent in the results reported here. The average increase in peak load for the 152 mm, 178 mm, and 203 mm thick walls was 27%, 26%, and 28%, respectively.

c) The encasement increased the ultimate deflection and ductility. The increase in ultimate deflection varied between 32% and 106%. The ductility index for the walls with flat panels was also improved over the control specimens. The improvement of ductility index varied from 24% to 167%.

d) The toughness of the PVC encased walls increased significantly for all wall specimens. The improvement to toughness ranged from 57% to 170% over the equivalent control walls.

4.3.3.3 Load-Tensile Strain

Tensile forces within the wall specimens were resisted by the steel rebar, PVC panels, and portions of the PVC connector that were continuous through the wall. Figure 4.9 shows a typical load versus tensile strain behaviour of the steel and PVC panel. The vertical axis represents the load (kN) and the horizontal axis represents the strain gauge readings ($\mu\varepsilon$). From Figure 4.9, the strains in the PVC and steel were small until the cracking load was reached (30 kN). After the concrete cracked, the strains in the steel and PVC panels increased linearly with the load until the steel yielded at 56 kN. Past yielding, the steel strain gauge failed while the PVC gauge continued to read steadily increasing strain while the load

increased. Figure 4.10 shows the mid span deflection versus the strain in the steel and the PVC. However, the load plateaued at strain gauge reading of 25000 με, the strains in the PVC increased with deflection as shown in Figure 4.10, until failure occurred.

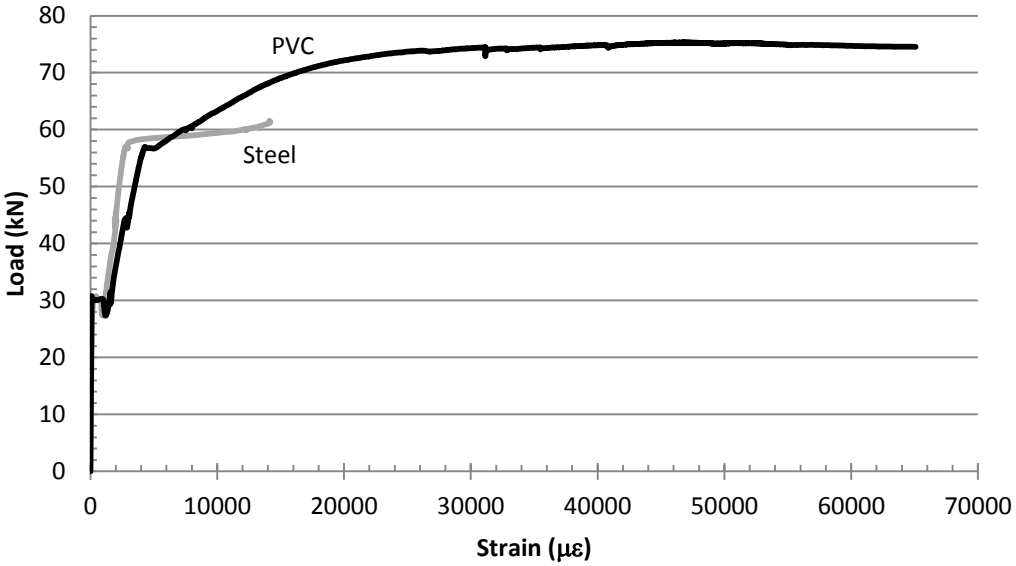

Figure 4.9: Load versus tensile strain for flat panel wall (PF-7-10)

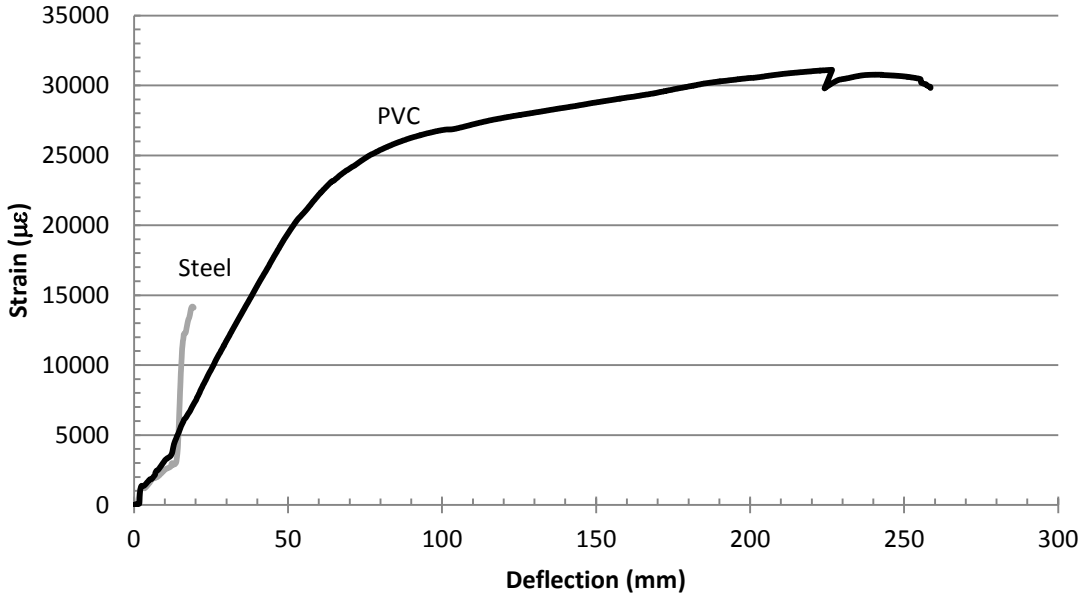

Figure 4.10: Strain versus mid span deflection (PF-7-10)

4.3.3.4 Load-Compressive Strain

The compressive forces in the wall were resisted by the concrete, the PVC panels on the compression side of the specimen, and the continuous portions of the PVC connectors that were above the neutral axis of the specimen. Figure 4.11 provides a typical load versus compressive strain behaviour for the concrete and the PVC panels. The vertical axis represents the load (kN) and the horizontal axis represents the compressive strain (με). Strains in both materials were low and increased linearly until the cracking load was reached (30 kN). The strains in the concrete and the PVC panels were similar until the steel yielded. Beyond the yield load (56 kN), the strain gauge readings of the concrete and PVC panels increased more rapidly. The concrete crushed at a strain gauge reading of -3000 με, while the PVC continued to experience compressive strains up to -8300 με.

Figure 4.12 provides the strain versus mid span deflection behaviour for the flat panel encased walls. The vertical axis represents the compressive strain (in με) and the horizontal axis represents the mid span deflection in mm. As the concrete strain reaches -3000με, crushing occurs, however the PVC strain continues to increase, indicating the concrete and PVC have ceased to act as a composite cross-section.

It is worth noting that the specimen presented (PF-7-10) failed primarily due to rupture of the PVC panels on the tension face. Prior to rupture of the panels, the PVC was buckled on the compression face but the specimen continued to resist the applied load until complete failure. The PVC strains at failure ranged from -3000 με to -15000 με, depending on the proximity of the gauge to the failure location. The average PVC compressive strain at failure was -10000 με.

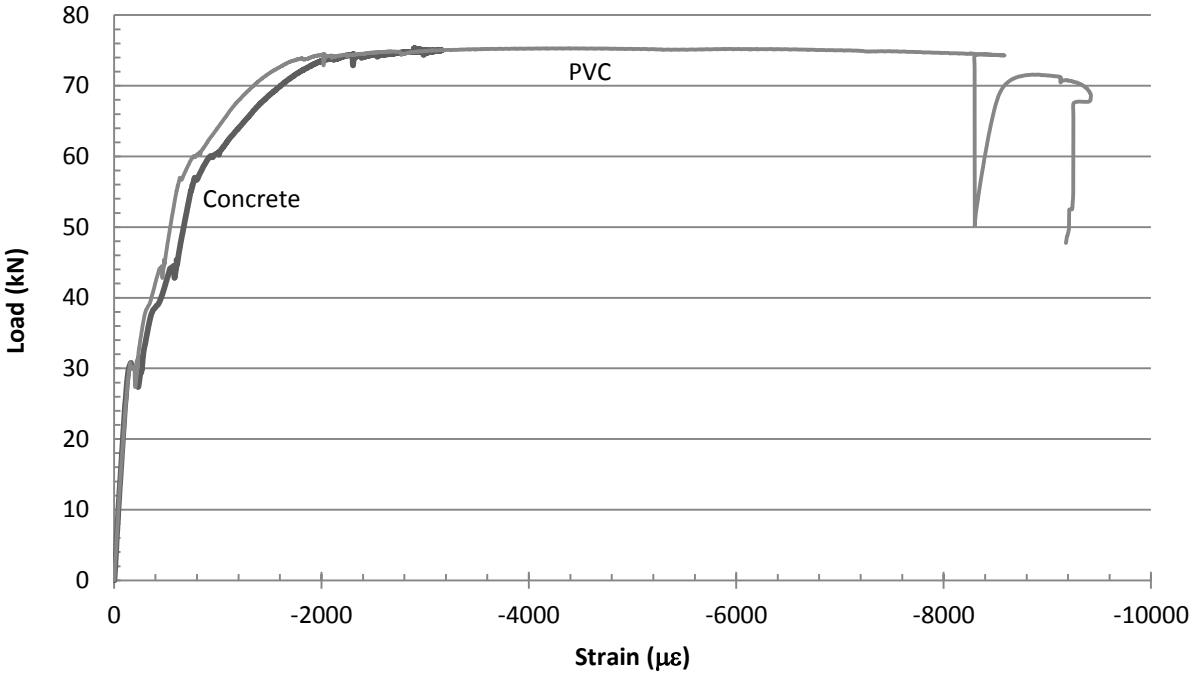

Figure 4.11: Load versus compressive strain (με) (PF-7-10)

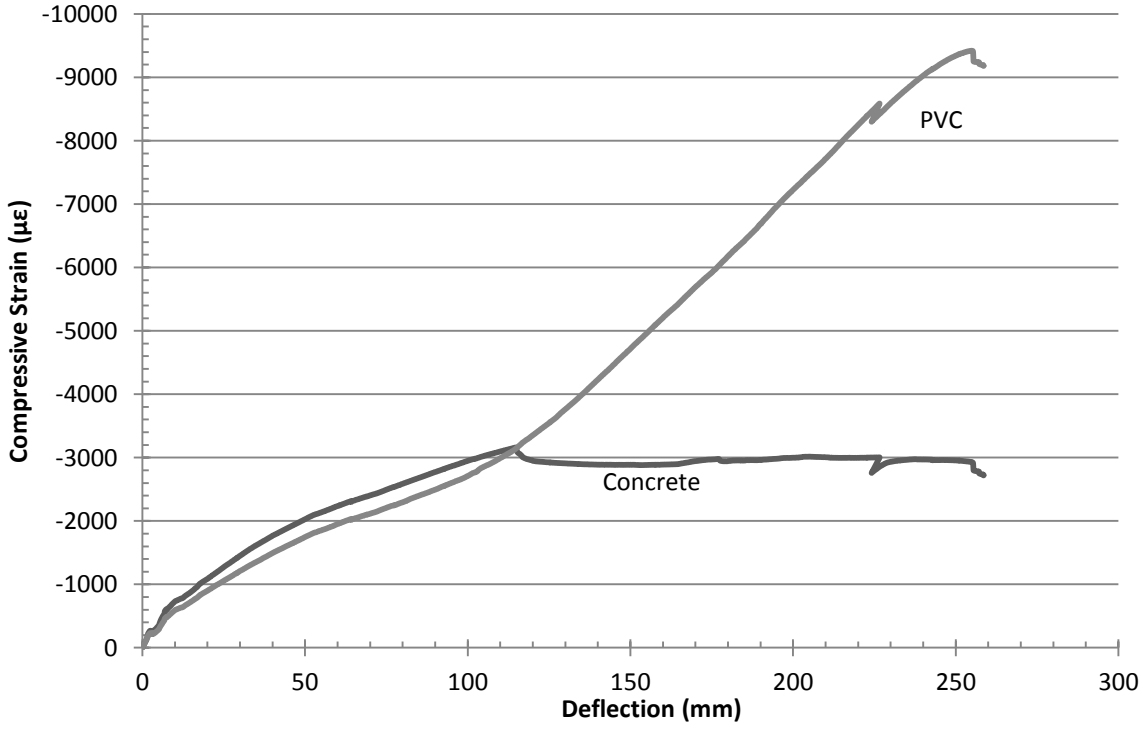

Figure 4.12: Load versus deflection behaviour (PF-7-10)

4.3.3.5 Strain Profile

Figure 4.13 presents the strain profile for the flat panel encased wall PF-7-10. Strain values were taken from the concrete in compression, reinforcing steel in tension, and the PVC panel in tension. The strain distribution was taken at several load levels as a percentage of the peak load. The three strain readings (concrete, steel, and PVC) were connected in a line to form the strain profile. If a gauge was damaged during the test, the data point at the corresponding load level was removed from the distribution. Up to 60% of the peak load the depth of the neutral axis remains constant. Beyond 60% of peak load the strain levels of the concrete and PVC increase greatly and the neutral axis depth decreases. Beyond 60% the steel reinforcement had reached yielding, which resulted in highly increased strain in the steel and PVC with a lesser increase in load resistance from the section.

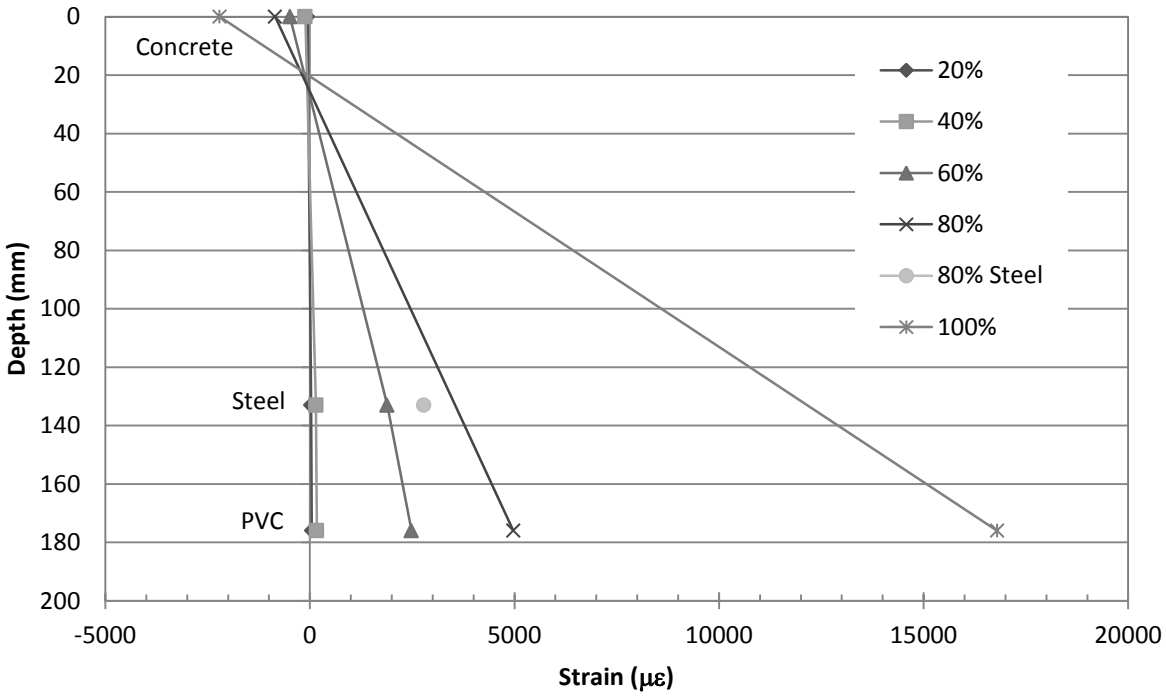

Figure 4.13: Strain profile for wall PF-7-10

4.4 Behaviour of PVC Encased Specimens with Hollow Panels

4.4.1 Modes of Failure

The PVC specimens with the hollow PVC panel encasement (PH) experienced failure in a similar fashion to the flat panel encased walls. Failure started with the steel reinforcement yielding, followed by concrete crushing with the compression PVC panel buckling or 'lifting off' the concrete surface (Figure 4.14). A new phenomenon was observed during the testing of these specimens, which was the slip of the panels resisting the tensile forces (tension panel slip). This behaviour will be discussed in more details in the subsequent sections. The tension panel slip occurred multiple times after the steel yielded and at a significantly higher load level.

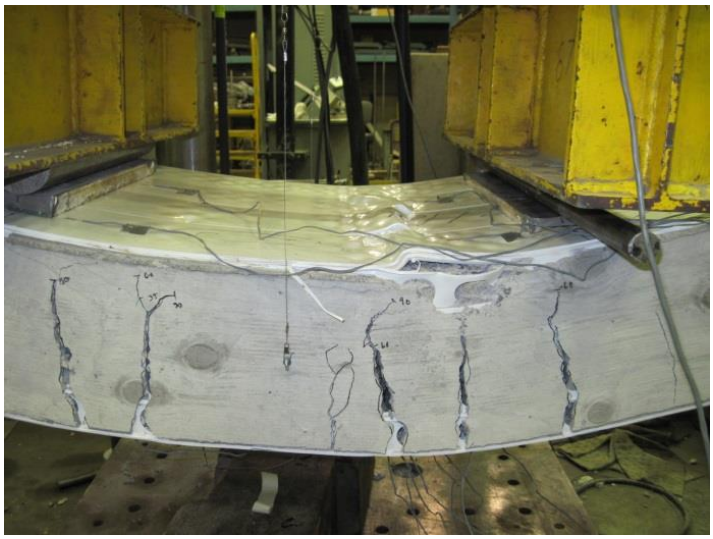

Figure 4.14: Failure mode for PVC encased specimens with hollow panels

4.4.2 General Behaviour

The specimens showed the same cracking behaviour when subjected to loading, similar to the PVC encased walls with flat panels. Cracks first appeared on the tension side of the wall

between the two loading points. As the load increased, several tension cracks appeared just outside of the constant moment region. After the steel yield point was reached, the cracks in the constant moment region widened as the specimen began to deflect excessively. For each of the specimens the location of the widening cracks was to the right of the centerline of the beam in the constant moment region. As the load continued to increase, crushing cracks were observed on the sides of the specimens, directly above the widening cracks. Then, the PVC panels in compression began to 'bubble' on the surface (Figure 4.15). The bubbled surface propagated from the right loading point to left, and became more pronounced as the load increased. Eventually, failure occurred when the crushed concrete tried to push up on the PVC panel, which in turn buckled excessively and folded over (Figure 4.15). This PVC buckling occurred at midspan or just underneath the right loading point.

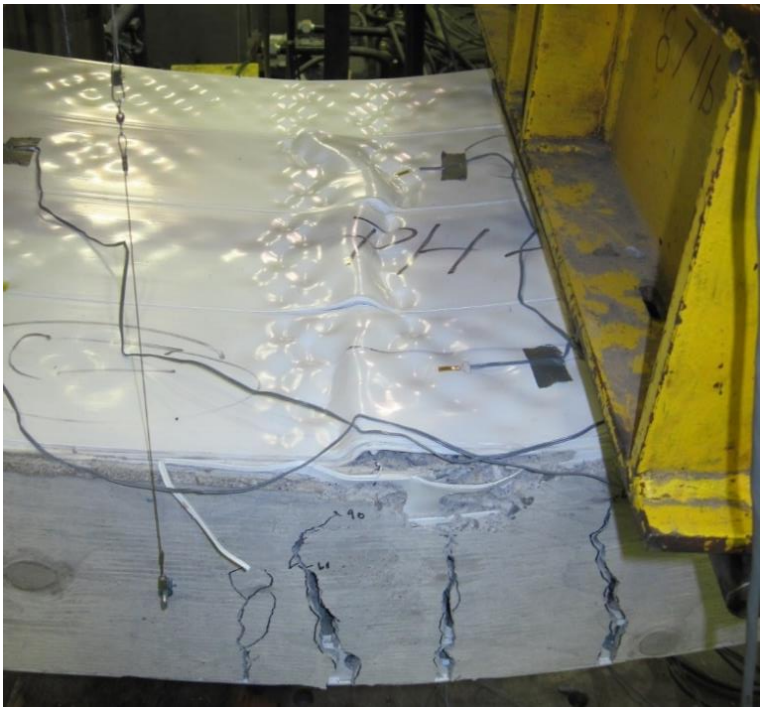

Figure 4.15: Bubbling on PVC surface and buckling of compression panel (PH-8-10)

As mentioned previously, each of the tested specimens experienced PVC tension panel slip. After the steel yielded and as the load increased, the contribution of the PVC panels to resisting the tensile forces increased. However, the total applied load did not provide enough clamping or frictional forces at the supports. Unlike the flat panels, the hollow panels did not have nubs to interlock with concrete specimen. Therefore, the tension panels experienced differential elongation under loading (Figure 4.16). This was most pronounced in the 152 mm (6") thick specimens. As the walls increased in thickness, and the applied load increased, the friction between PVC and concrete increased, reducing the extent of the slips.

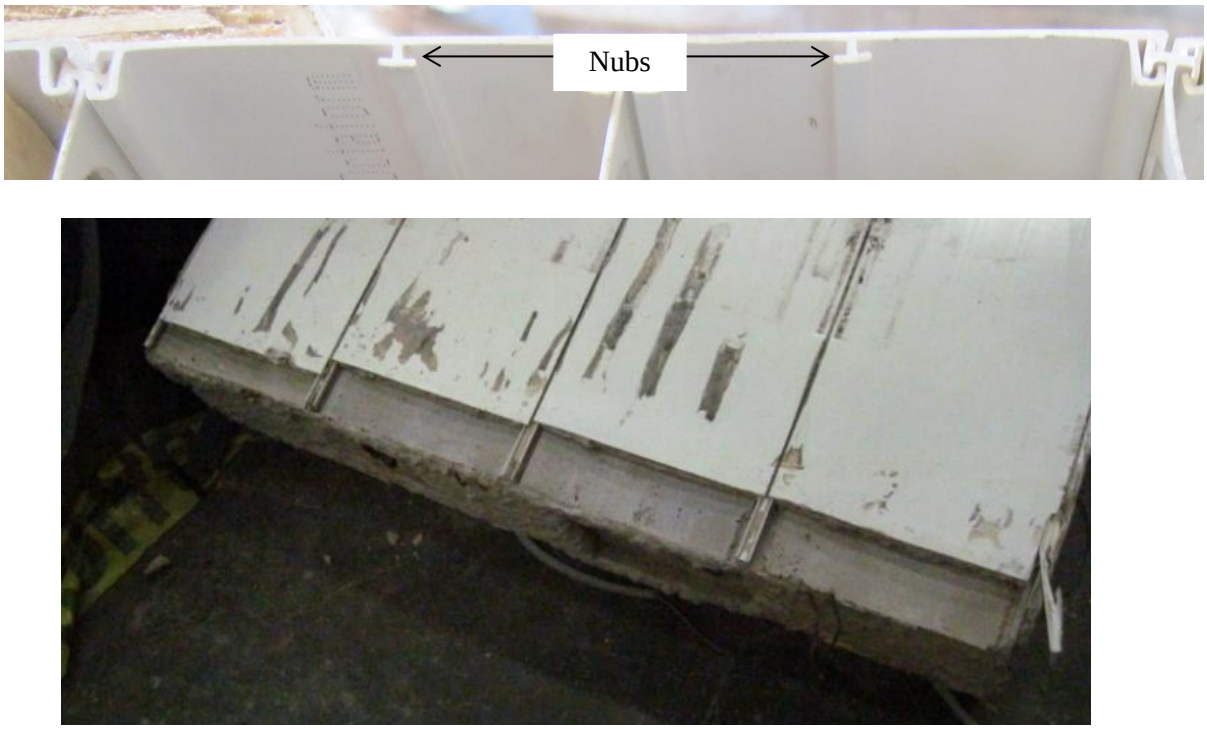

Figure 4.16: Tested specimen showing tension panel slip (PH-6-10)

4.4.3 Flexural Behaviour

4.4.3.1 Load Deflection

The load versus deflection behaviour for all of the hollow panel specimens was similar to the flat panel encased walls. Figure 4.17 shows a typical load versus deflection curve for two 152 mm thick PVC encased specimens with hollow panels. The vertical axis represents the applied load (kN) and the horizontal axis represents the mid span deflection (mm). Initially, the load increased with minimal deflection (<3mm) until concrete cracks formed on the tension side in the constant moment region. After cracking, the deflection and load increased until the steel yielded. Past the yielding point, load and deflection continued to rise, but at an increasingly shallower slope.

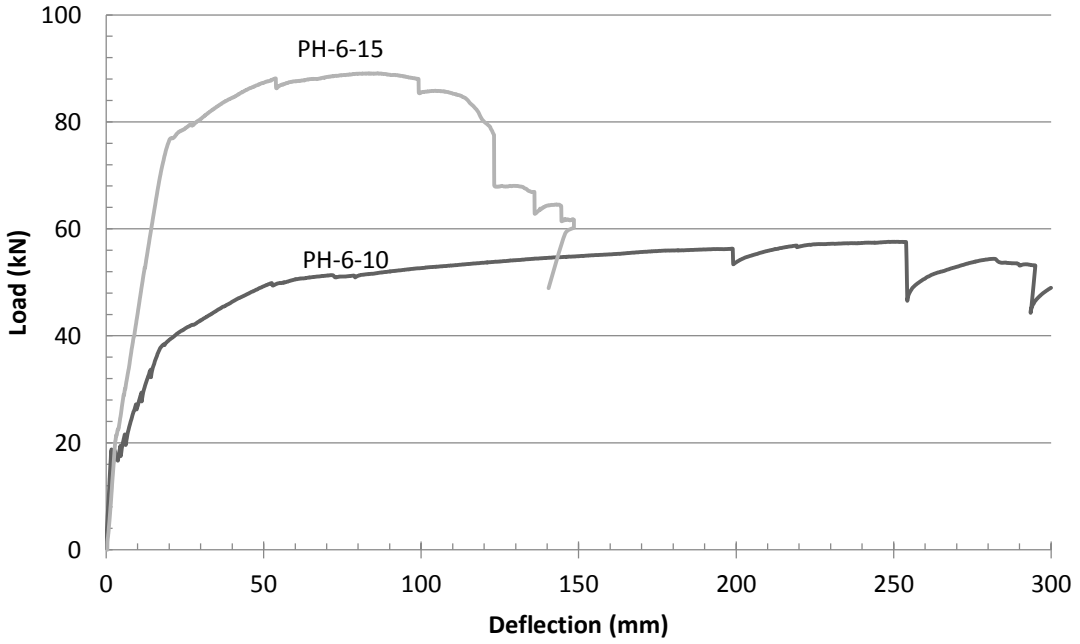

Figure 4.17: Load versus deflection for PVC encased walls with hollow panels (PH)

The behaviour past the yielding point differed depending on the amount of steel reinforcement in the specimen. For walls reinforced with 3-10M rebars, the peak load was achieved through a gradual plateau whereas specimens reinforced with 3-15M rebars reached their peak load more quickly and deflected much less. Sudden drops in the load were observed in both curves. These drops were attributed to the PVC panels slipping on the tension side of the wall. Regardless of this slip phenomenon, the load versus deflection behaviour for the PVC encased specimens with hollow panels showed enhancement in load and deflection over their equivalent control walls (Figure 4.18). Table 4.3 summarizes the cracking, yield, and peak loads and their corresponding deflections for the PVC specimens with hollow panels and compares them to their equivalent control walls.

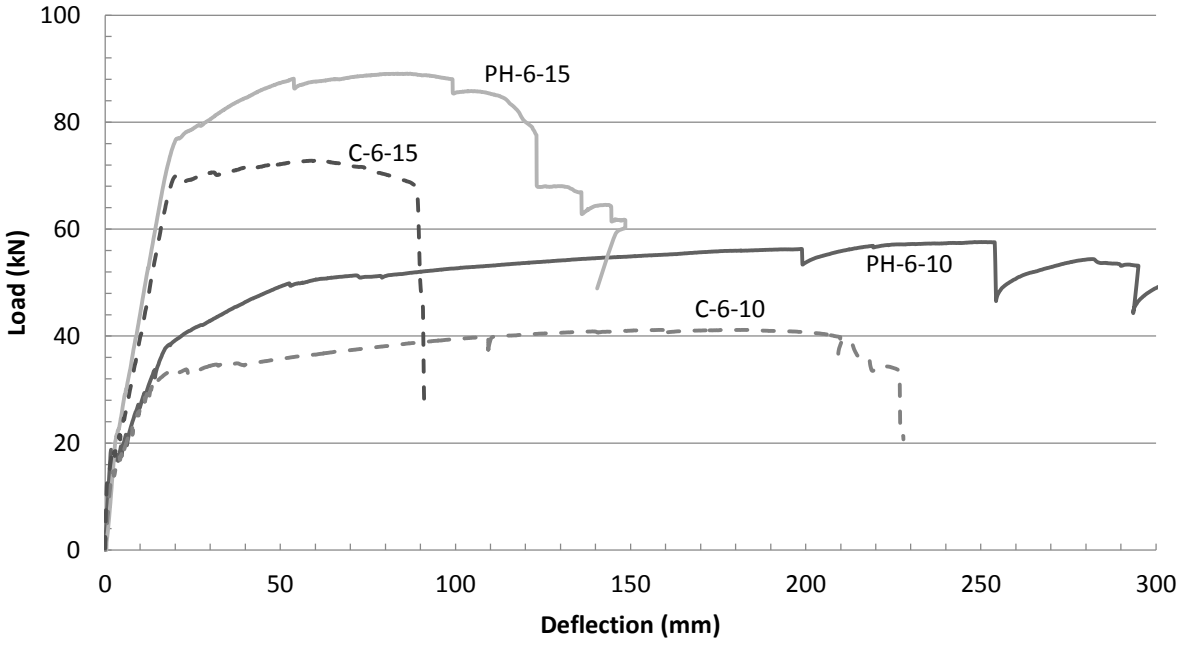

Figure 4.18: Load versus deflection for PVC encased walls with hollow panels and their equivalent control walls (C-6-10 & C-6-15)

Table 4.3: Test results for PVC encased walls with hollow panels

Reinforcement	$P_{Cracking}$ (kN)	P_{Yield} (kN)	P_{Peak} (kN)	$\Delta_{cracking}$ (mm)	Δ_{yield} (mm)	Δ_{ult} (mm)	Ductility index	Toughness (kNmm)
Thickness: 152 mm (6")								
3-10M	18	38	57	2.6	17.6	311	17.7	17719
Improvement	**23%**	**19%**	**39%**			**38%**	**13%**	**108%**
3-15M	22	76	89	3.1	20.4	135	6.6	11362
Improvement	**29%**	**10%**	**15%**			**50%**	**44%**	**95%**
Thickness: 178 mm (7")								
3-10M	25	46	75	2.2	14.6	143	9.8	9683
Improvement	**42%**	**3%**	**35%**			**3%**	**-20%**	**37%**
3-15M	24	85	104	1	17.1	124	7.3	12389
Improvement	**20%**	**1%**	**14%**			**24%**	**26%**	**54%**
Thickness: 203 mm (8")								
3-10M	31	60	95	1.1	9.6	216	22.5	18228
Improvement	**41%**	**13%**	**44%**			**59%**	**67%**	**119%**
3-15M	35	103	135	1.3	12.3	154	12.5	18297
Improvement	**67%**	**1%**	**18%**			**-3%**	**5%**	**10%**

i – Cracking Load

The cracking load for the 152 mm thick PVC encased specimens was 18kN and 22kN for the 10M and 15M reinforced walls respectively, an increase of 23% and 29% over the equivalent control walls. The cracking load for the 178 mm thick specimens with hollow panels was 25kN and 24kN, an increase of 42% and 20% over the 10M and 15M control walls. Finally, the 203 mm thick specimens encased in hollow panels had cracking loads of 31kN and 35kN, an increase of 41% and 67% over the equivalent control walls.

The cracking deflection for the hollow panel specimens ranged from 1 to 3 mm. The panels did not have a significant effect on the cracking deflection.

ii – Yield Load

As discussed earlier, the yield load is a function of the amount of steel reinforcement and the wall thickness. The yield load increased as the reinforcing bar diameter increased and/or the concrete core thickness increased. PVC encased walls with hollow panels showed a higher yield load than the equivalent control specimens. Similar to the walls with flat panels, the specimens reinforced with 3-10M rebars showed greater enhancement to the yield load than specimens with 3-15M rebars. For hollow panel encased specimens with 3-10M rebars, the yield loads were 38 kN, 46 kN, and 60 kN for wall thicknesses of 152 mm, 178 mm, and 203 mm, respectively. The yield loads for the equivalent control walls were 32 kN, 44.5 kN, and 53 kN, respectively. Therefore, the increase in the yield load for the PVC encased walls with hollow panels reinforced with 3-10M rebars was 19%, 3%, and 13% for wall thicknesses of 152 mm, 178 mm, and 203 mm, respectively.

The yield load for hollow panel encased walls reinforced with 3-15M rebars was 76 kN, 85 kN, and 103 kN for 152 mm, 178 mm, and 203 mm thick walls, respectively. The equivalent control walls had yield loads of 69 kN, 84 kN, and 103 kN, respectively. Therefore, the increase in yield load for the specimens reinforced with 3-15M bars was 10%, 1%, and 1% for 152 mm, 178 mm, and 203 mm thick walls, respectively.

The increase in yield load for all specimens was due to the PVC panel in tension providing an additional tensile force to the wall cross-section, improving the resistance. The improvements were minimal; due to the steel reinforcement being placed at a shallower depth as a result of hollow panel's thickness, thus negating some of the benefit from the

additional material in the hollow panels. This observation is further discussed in Section 4.5.1 – Wall Cross-section Comparison. In addition, the strain levels observed in the PVC at yielding resulted in a material stress significantly lower than the potential peak stress. The PVC was not fully engaged and therefore only provided a mild enhancement to the cross-section.

The yield deflection for the encased walls with hollow panels and the control walls were similar. The presence of the hollow panels did not have an influence on the yield deflection.

iii – Peak load

The PVC encased walls with hollow panels showed an increase in the peak load over the control specimens. Similar to the yield load results, specimens reinforced with 3-10M rebars experienced a greater improvement than the walls reinforced with 3-15M rebars. The peak loads for hollow panel encased specimens reinforced with 3-10M bars were 57 kN, 75 kN, and 95 kN for 152 mm, 178 mm, and 203 mm thick walls, respectively. The peak loads for the equivalent controls walls were 41 kN, 55.5 kN and 66 kN, respectively. Therefore, the increase in peak load for the hollow panel encased specimens was 39%, 35%, and 39% for 152 mm, 178 mm, and 203 mm thick walls, respectively.

The peak loads for PVC encased walls reinforced with 3-15M rebars were 89 kN, 104 kN, and 135 kN for 152 mm, 178 mm, and 203 mm thick walls, respectively. The equivalent control specimens had peak loads of 77.2 kN, 91 kN and 114 kN, respectively. The specimens with hollow panels reinforced with 3-15M showed an increase in the peak load of 15%, 14%, and 18%, respectively.

As was seen in the flat panel encased walls, the improvement to load resistance was higher at the peak load level than at yield load level. The high strains associated with the peak load indicated that the PVC was approaching or was at peak tensile stress, offering substantially more improvement than at the yield load level. In addition, the observed improvements for the 10M walls were higher than the respective flat panel walls. The enhancement was achieved despite the shallower steel depth, indicating the benefit of effectively doubling the PVC cross-sectional area within the cross-section.

The ultimate deflection for the PVC encased walls with hollow panels was higher than the ultimate deflection for the control walls for most of the specimens. The increase in ultimate deflection varied between 3% and 59% as shown in Table 4.3. The ductility index of the hollow panel encased specimens varied between 6.6 and 22.5. For a given wall thickness, the ductility index decreased, as the rebar diameter increased from 10M to 15M. The presence of the PVC panels increased the ductility index by a minimum of 5% and a maximum of 67%.

The toughness of each hollow panel encased wall was higher than the equivalent control wall. The improvement in toughness ranged from 10% to 119%. For the walls reinforced with 3-15M steel bars, the effect of the panels decreased as the thickness of the wall increased. No trend was apparent for wall reinforced with 3-10M steel bars.

4.4.3.2 Summary of key findings

1. Cracking load: the walls encased with hollow panels increased the cracking load by an average of 45%. The deflection at cracking remained the same as the deflection for the control walls.

2. Yield load: the walls with hollow panels provided a minimal increase in the yield load of the control walls

    a) The average yield load increase for walls with 3-10M rebars was 12%. For walls with higher reinforcement ratios (3-15M rebars), the average yield load increase was 4%. Similar to the previous findings by Wahab et al (2013), these results indicate that as the reinforcing ratio increases, the effect of the PVC encasement with hollow panels on the yield load decreases.

    b) The yield deflection was not influenced by the PVC system.

3. Peak load: Similar to the yield load, the effect of the PVC encasing system on the peak load decreases as the reinforcing ratio increases.

    a) PVC encased specimens with hollow panels and reinforced with 3-10M rebars showed an average increase in the peak load of 39% over the control specimens. For walls with higher reinforcement ratios (3-15M bars), the increase in peak load dropped to 16% on average.

    b) In previous tests of PVC encasing, the increase in the peak load was influenced by the wall thickness. As the thickness of the specimens increased, the effect of the PVC encasement decreased. This trend was not apparent in the results as the average increase in the peak load for 152 mm, 178 mm, and 203 mm thick walls was 27%, 25%, and 31%, respectively.

4. Deflection: The encasement with hollow panels provided an increase in ultimate deflection and ductility. The increase in ultimate deflection varied between 3% and

59%. The improvement of ductility index varied from 5% to 67%. Toughness also improved with the presence of hollow panels, with a range of improvement from 10% to 119%.

4.4.3.3 Load-Tensile Strain

Figure 4.19 shows a typical load versus tensile strain in the steel and the PVC panels. The vertical axis represents the load (kN) and the horizontal axis represents the strain (με). Figure 4.20 shows the mid span deflection versus the strain in the steel and the PVC panels. From Figure 4.19, the strains in the PVC and steel were small until cracking occurred at 30 kN. After the concrete cracked, the load increased linearly with the strain gauge readings for both the steel and the PVC panels until steel yielded at 56 kN. One of the PVC strain gauges was attached to a panel that slipped, which can be observed in a sudden drop in strain value. Figure 4.20 displays the inconsistency of the slips between the two panels recorded. The dashed line shows a continual increase in strain as the specimen experiences deflection, while the solid line shows the panel slip and eventual failure.

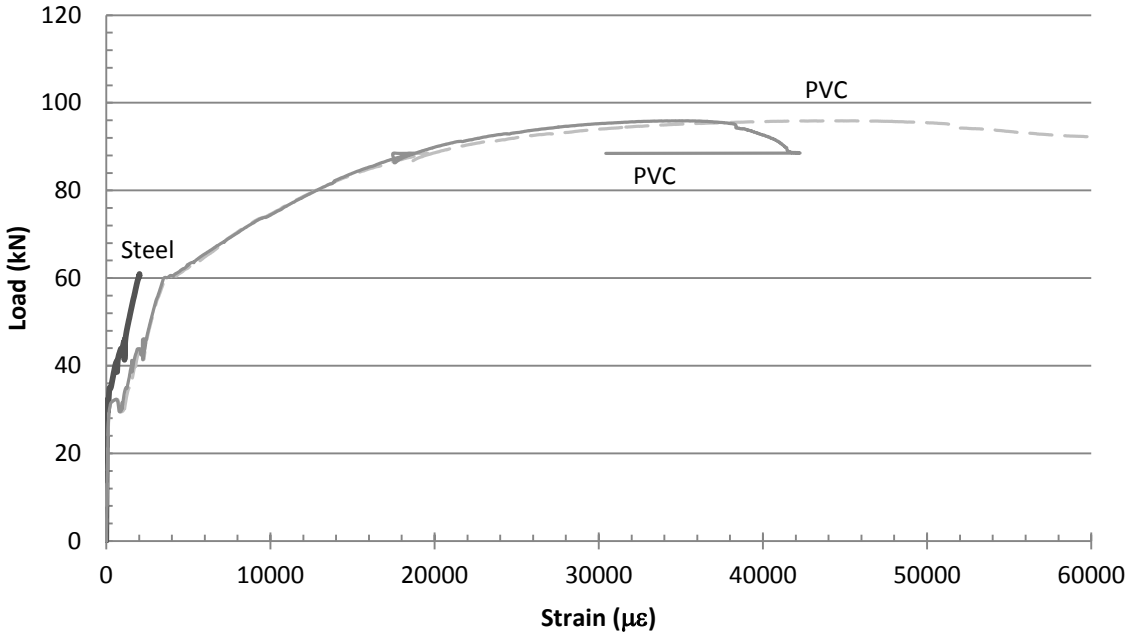

Figure 4.19: Load versus tensile strain for hollow panel wall (PH-8-10)

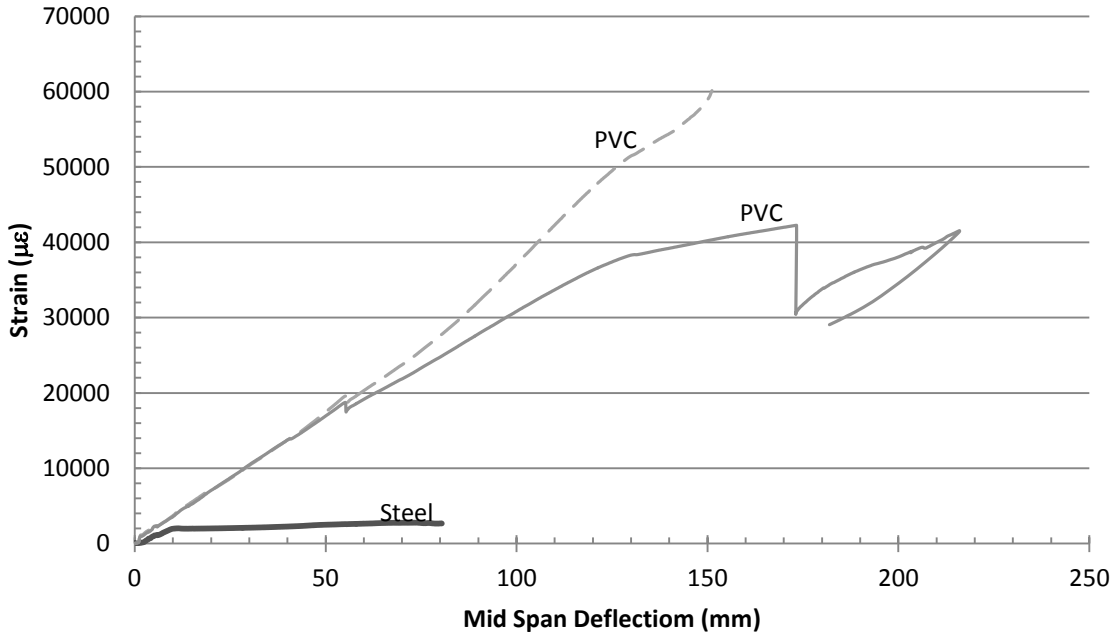

Figure 4.20: Strain versus mid span deflection (PH-8-10)

4.4.3.4 Load-Compressive Strain

Figure 4.21 provides a typical load versus compressive strain behaviour for the concrete and PVC panels. The vertical axis represents the load (kN) and the horizontal axis represents the compressive strain (με). The readings of three strain gauges are presented on the figure, a gauge attached to the concrete surface (grey), a gauge attached to the inner face of the PVC panel (dashed), and a gauge attached to the outside face of the PVC panel (solid). Strains in both materials were low and increased linearly until the concrete cracked at 20 kN. At the cracking load, the strains in the concrete and inner panel of PVC remained similar but the strain in the PVC on the outside panel increased more rapidly, due to the increase in deflection of the wall. This difference in strains remained through the specimen yielding (76kN) and eventual failure. Concrete crushed at -3000με, while the PVC continued to experience compressive strains beyond -8000με.

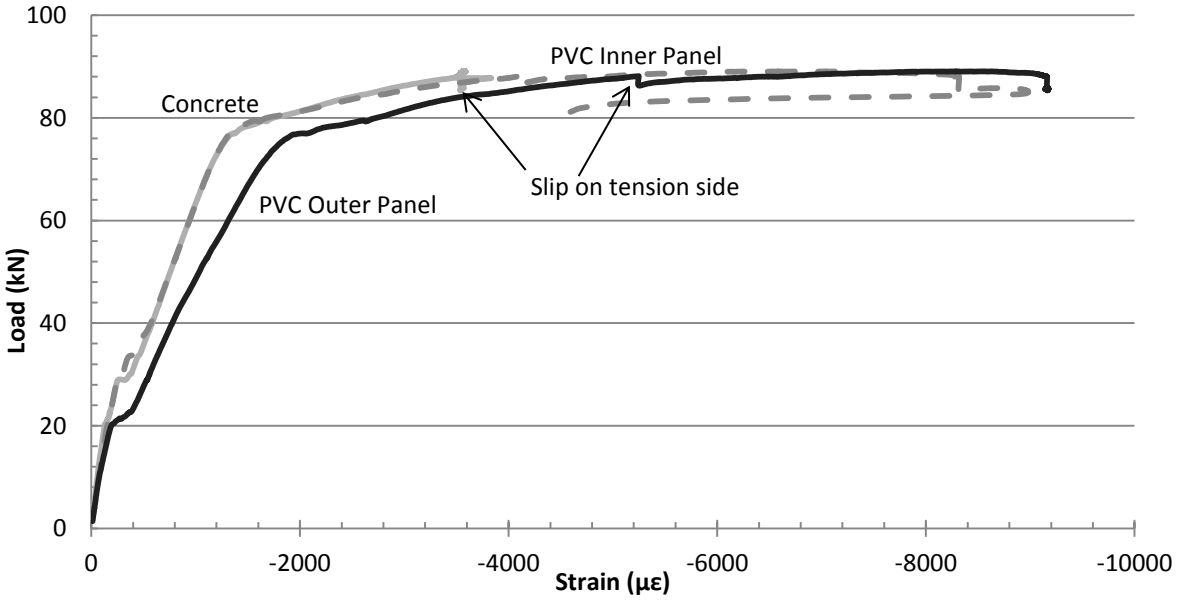

Figure 4.21: Load versus compressive strain for hollow panel encased wall (PH-6-15)

It is worth noting that the specimen presented experienced panel slip on the tension face but the compressive strains were maintained despite these slips. The recorded strains in the PVC panels at failure ranged from -6000 με to -14000 με, depending on the failure location. The average strain at failure for both the outside and inside PVC panels was -10000 με, which was the same average compressive strain for specimens with flat panels.

4.4.3.5 Strain Profile

Figure 4.22 presents an example strain profile for a hollow panel encased wall. Strain values were taken at 6 locations; from the upper and lower PVC panels on the compression and tension sides, the concrete surface and the steel reinforcing. The strain distribution was taken at several load levels as a percentage of the peak load. The six strain gauge readings were connected in a line to form the strain profile. If a gauge was damaged during the test, the data point at the corresponding load level was removed from the distribution. At low load levels, all of the data points fell on a straight line. As the load increased, there was no strain gradient between the outer and inner panels on the tension side. At peak load level a distinct difference in compression strain level between the outside and inside panels was recorded. This strain gradient was not reflected in the tension side of the wall.

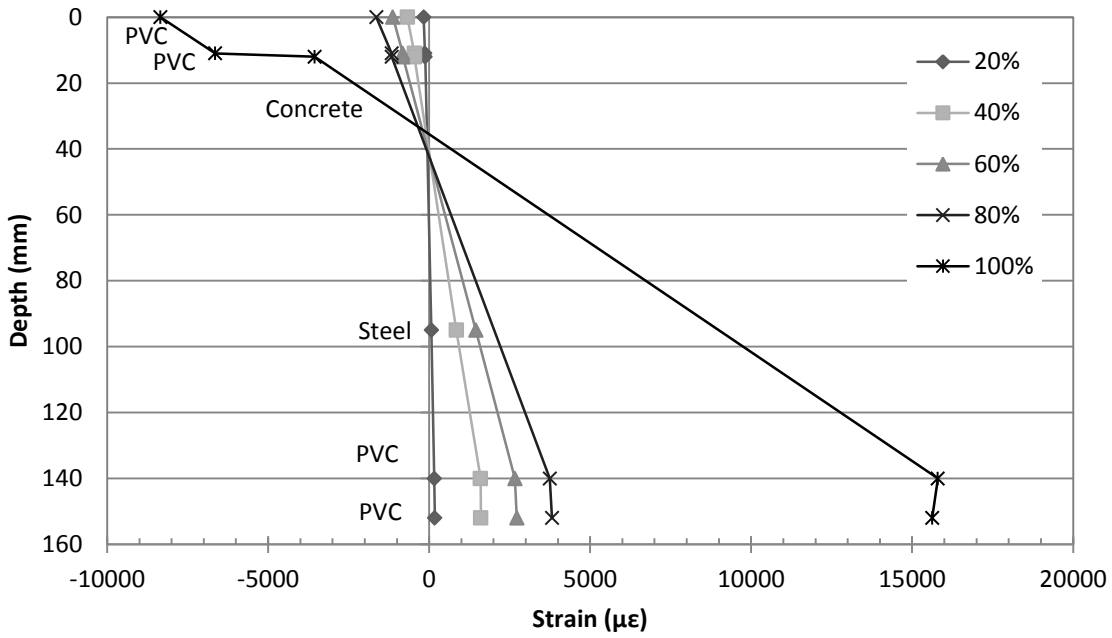

Figure 4.22: Strain profile for hollow panel encased wall PH-6-15

4.5 Effect of Panel Type (Hollow versus Flat)

Two types of PVC panels were tested in this study, flat panels and hollow panels. The following section will highlight and discuss recurring trends that were observed during the testing of these two panel types.

4.5.1 Wall Cross-Section Comparison

Figure 4.23 provides a single-cell cross-section for each of the three wall types tested; a control wall with bare concrete, a PVC encased wall with flat panels, and a PVC encased wall with hollow panels. The depth of the steel reinforcement is also shown. As discussed earlier, all of the walls were cast with a clear concrete cover of 38 mm on the tension side of the wall.

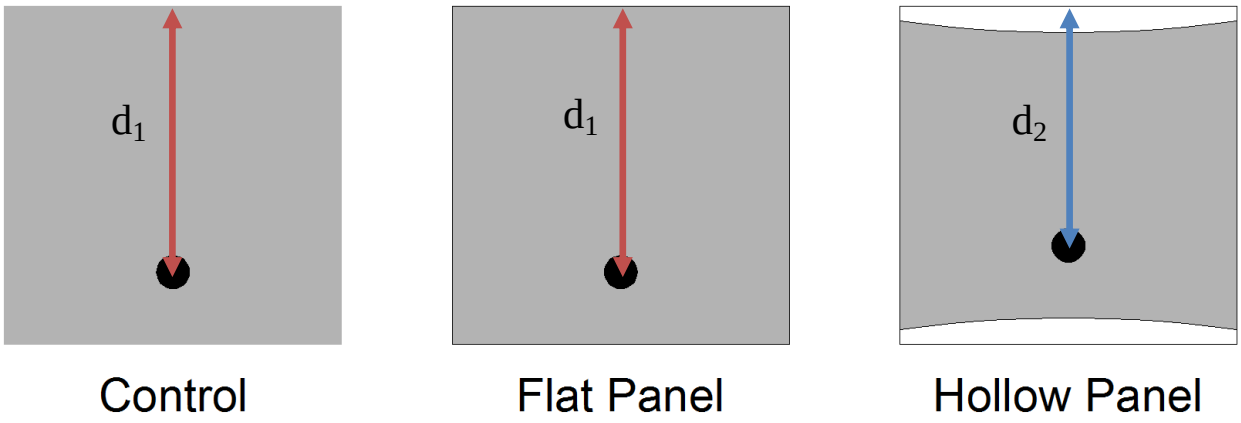

Figure 4.23: Tested cross-sections: control, flat panel, and hollow panel

Three significant observations can be made from studying these cross-sections. First, the hollow panels double the quantity of PVC material versus the original flat panel. Theoretically, this additional material could provide more resistance to flexure-induced forces on the wall than the flat panel specimens, particularly when achieving peak load.

A second observation was made regarding the position of the reinforcing steel in the cross-sections. Each of the tested walls had a specified concrete clear cover of 38 mm (1½"). Clear cover is defined as the distance from the exterior concrete surface to the surface of the reinforcing steel. For the PVC encased walls with hollow panels, the reinforcing steel was at a shallower depth d_2 (102 mm for a 152 mm thick wall) than the depth d_1 of the control and flat panel cross sections (114 mm for a 152 mm thick wall). This difference in depths would have an effect on the yield load and ultimate load of the walls with hollow panels and will be discussed further in the following section.

Finally, due to the thickness of the hollow panels, the effective thickness of the encased concrete was less than the equivalent control and flat panel walls. This reduction in concrete section would reduce the effect of the PVC encasement on increasing the cracking load.

4.5.2 Flexural Behaviour

Figure 4.24 compares a typical load versus deflection behaviour for PVC encased walls with hollow and flat panels. The walls were 152 mm thick and reinforced with 3-10M rebars (PF-6-10 & PH-6-10). Table 4.4 compares the cracking, yield and peak loads and deflections for the three types of tested specimens.

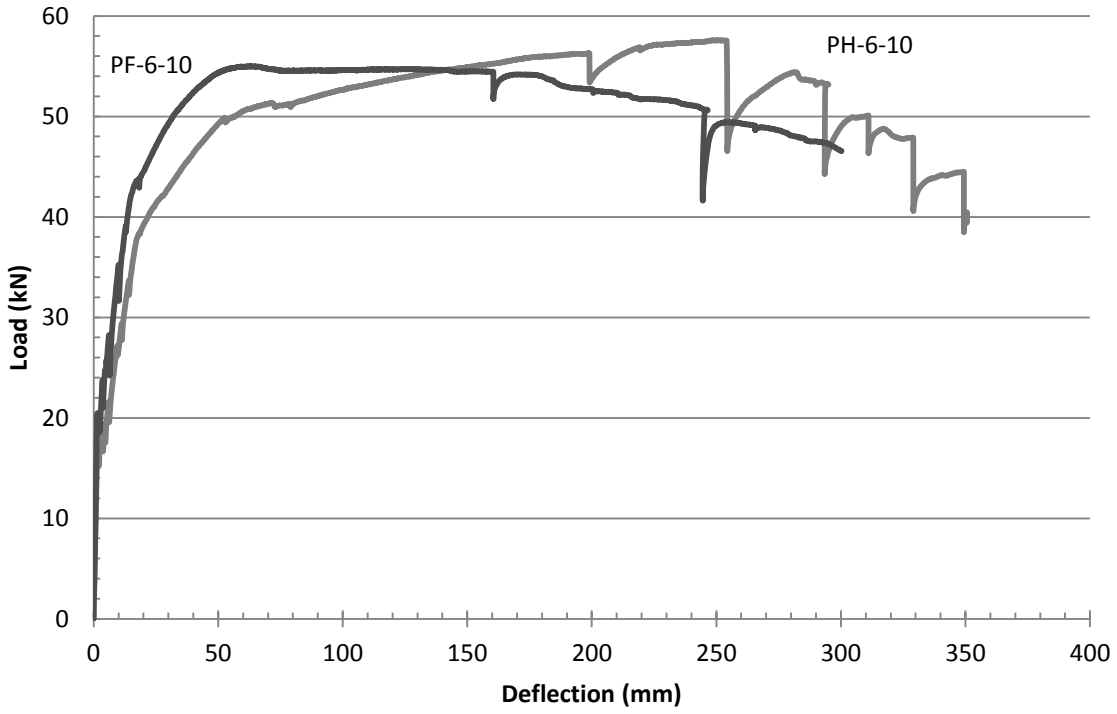

Figure 4.24: Load vs deflection behaviour for equivalent walls with flat and hollow panels.

Table 4.4: Test results for all specimens

Specimen	P_{crack} (kN)	P_{yield} (kN)	P_{peak} (kN)	$\Delta_{cracking}$* (mm)	Δ_{yield} (mm)	Δ_{ult} (mm)	Ductility index	Toughness
Thickness = 152 mm (6 inches)								
C-6-10	14.6	32	41	1.9	14.4	226	15.7	8505
PF-6-10	20	43	55	1.4	15.4	300	19.5	15318
PH-6-10	18	38	57	2.6	17.6	311	17.7	17719
C-6-15	17	69	77.2	1.3	19.6	90	4.6	5820
PF-6-15	27.5	82.5	93	1.4	15.1	182	12.3	14862
PH-6-15	22	76	89	3.1	20.4	135	6.6	11362
Thickness = 178 mm (7 inches)								
C-7-10	17.5	44.5	55.5	1.6	11.4	139	12.2	7090
PF-7-10	30	54	72	1.3	9.8	255	26.0	18429
PH-7-10	25	46	75	2.2	14.6	143	9.8	9683
C-7-15	20	84	91	2.1	17.4	99.9	5.7	8058
PF-7-15	31	96	111	1	14.1	178	12.6	16824
PH-7-15	24	85	104	1	17.1	124	7.3	12389
Thickness = 203 mm (8 inches)								
C-8-10	22	53	66	1.2	10.1	136	13.5	8315
PF-8-10	33	64	89	0.9	8.2	262	32.0	22515
PH-8-10	31	60	95	1.1	9.6	216	22.5	18228
C-8-15	21	102	114	1	13.2	158	12.0	16775
PF-8-15	41	120	138	0.85	10.9	209	19.2	26190
PH-8-15	35	103	135	1.3	12.3	154	12.5	18297

The cracking loads for the specimens with flat and hollow panels were 20 kN and 18 kN, respectively. The lower cracking load for the hollow panel specimen was attributed to the smaller effective thickness of concrete present in the walls with hollow panels. This trend of lower cracking loads was consistent for all specimens tested (Table 4.4). Regardless, the PVC encased walls with hollow panels still recorded an increased cracking load when compared with the control walls.

Similar to the cracking load results, the wall with hollow panels yielded at 38 kN, whereas the wall with flat panels yielded at 43 kN. This difference can be primarily attributed to the shallower steel reinforcement depth in the hollow panel specimen. The specimens with hollow panels had less improvement in yield load over the control walls than their corresponding walls with flat panels. For the example presented, the wall with hollow panels (PH-6-10) showed a 19% improvement over the control wall, as opposed to a 34% improvement for the wall with flat panels (PF-6-10).

When comparing the peak loads of the walls with hollow panels with the flat panels, the findings were consistent for a given reinforcement. For walls reinforced with 3-10M rebars, the specimens with hollow panels showed equivalent or slightly higher peak load values (increase of 3% to 10%) than the specimens with flat panels. However, for specimens reinforced with 3-15M rebars, the specimen with flat panels achieved slightly higher load capacity (increase of 2% to 6%) than the equivalent specimen with hollow panels. Therefore, it could be safely assumed that the specimens with hollow panels showed almost the same peak load as the specimens with flat panels, in spite of the reduced depth of the reinforcing steel and the reduced cross-sectional area of concrete. This behaviour can be attributed to the relative influence of the panel type. As the hollow panels have twice the area of PVC, there is an increased contribution of the panel in ultimate flexural resistance.

The walls with hollow panels showed a reduced ductility compared with the equivalent walls with flat panels due to the tension panel slip. As the slipped occurred, resulting in differential elongation between the panels and the tension side of the concrete face, the PVC and concrete ceased to act as a pure composite. The reinforced concrete core predictably

failed as expected (steel yielding followed by concrete crushing), but without an effective bond to the encasing panels, the concrete failure promoted the wall failure sooner than an equivalent flat panel encased specimen, where the bond between PVC and concrete was maintained for a longer duration.

4.5.3 Reduction of Wall Thickness

Figure 4.25 compares load deflection behaviour of a 152 mm wall encased with flat panels to a control wall with a core thickness of 178 mm. Both walls were reinforced with 3-15M rebars. Since the PVC encased walls with flat panels showed a superior behaviour compared with the hollow panel encased walls, hollow panel walls were eliminated from this comparison. The solid line represents the PVC encased specimen and the dashed line represents the control specimen.

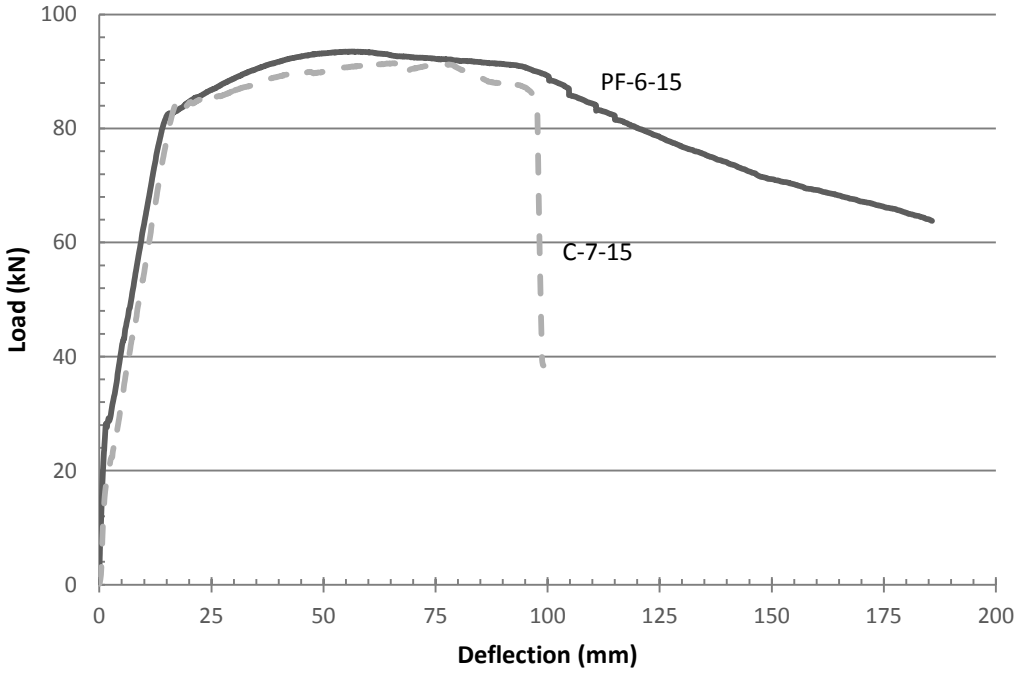

Figure 4.25: Load vs. deflection for C-7-15 and PF-6-15

The 152 mm thick PVC encased wall behaved very similarly to the 178 mm thick concrete wall, with the PVC specimen having yield and ultimate loads nearly identical to the thicker control wall. Three other sets of results were summarized, comparing flat panel encased walls with a control wall with the same quantity of steel reinforcement whose core thickness was increased by 25 mm. These results are presented in Table 4.5. It is clear that PVC encased specimens with a reduced 25 mm core thickness provided comparable yield and ultimate loads to the corresponding control walls. In addition, the ultimate deflection was significantly improved.

Table 4.5: Comparison of for PVC encased walls with 25 mm thicker control walls

Specimen	Yield load (kN)	**Percentage of control**	Peak load (kN)	**Percentage of control**	Δ_{ult} (mm)	**Percentage of control**
C-7-10	44.5		55.5		139	
PF-6-10	43	**97%**	55	**99%**	300	**216%**
C-7-15	84		91		99.9	
PF-6-15	82.5	**98%**	93	**102%**	185	**185%**
C-8-10	53		66		136	
PF-7-10	54	**102%**	75	**114%**	255	**188%**
C-8-15	102		114		158	
PF-7-15	96	**94%**	111	**97%**	178	**113%**

4.5.4 Hollow Panel Slip

As discussed earlier, the walls with hollow panels experienced tension panel slip, where the elongated PVC panel would slide against the concrete surface as seen in Figure 4.26. The panels that slipped were still recording positive strain, but the effective elongation of the panel was less than the potential elongation as seen on the tension face of the concrete wall. These slips were most apparent in the 152 mm and 178 mm specimens. As seen in Figure

4.27, the majority of the slips occurred where the walls were approaching the peak load and at high deflections, with the panels experiencing high strain values.

Figure 4.26: Panel slips observed on wall PH-6-10

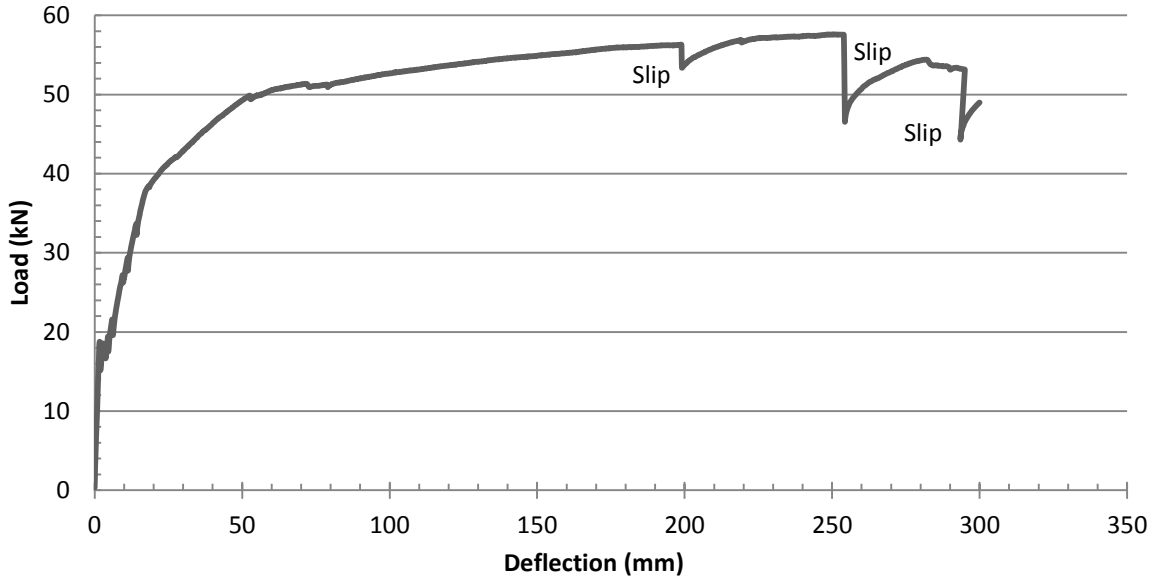

Figure 4.27: Load versus deflection illustrating panel slips

For specimens with core thicknesses of 203 mm, sudden slip of the panels were not observed but there was a gradual difference in the elongation, revealing the concrete underneath as the test progressed. In addition, upon removing the applied load at the end of

the test, the panels slipped. This change in behaviour can be attributed to the increased loads applied to the thicker walls. These loads provided higher frictional forces at the supports and acted as a clamping force; effectively preventing sudden slips. At the completion of the tests, the applied load was rapidly removed. At this sudden change, the 'clamping force' that had been restraining the tension PVC panels from moving was gone, resulting in a general slip of the panels as the stress was relieved. The slips observed indicated that the PVC hollow panels and concrete were not acting in pure composite behaviour, reducing the effective contribution of the PVC to the cross-section.

4.5.5 Damage Investigation of PVC Encased Walls

After the completion of a flexure test, portions of the panels from each PVC encased wall were removed to expose the concrete surface. The exposed surfaces were examined to gain insight into how the previously discussed failure modes occurred, and to further understand the interaction between the PVC and concrete.

At failure, the top compressive fibres of the control walls experienced concrete crushing. The concrete effectively crumbled in these areas and began to lift away from the core of the wall (Figure 4.28). As there was no steel reinforcement in the compression zone of the wall providing confinement, the compression block could be easily observed and even removed entirely from the wall in large chunks after testing (Figure 4.29).

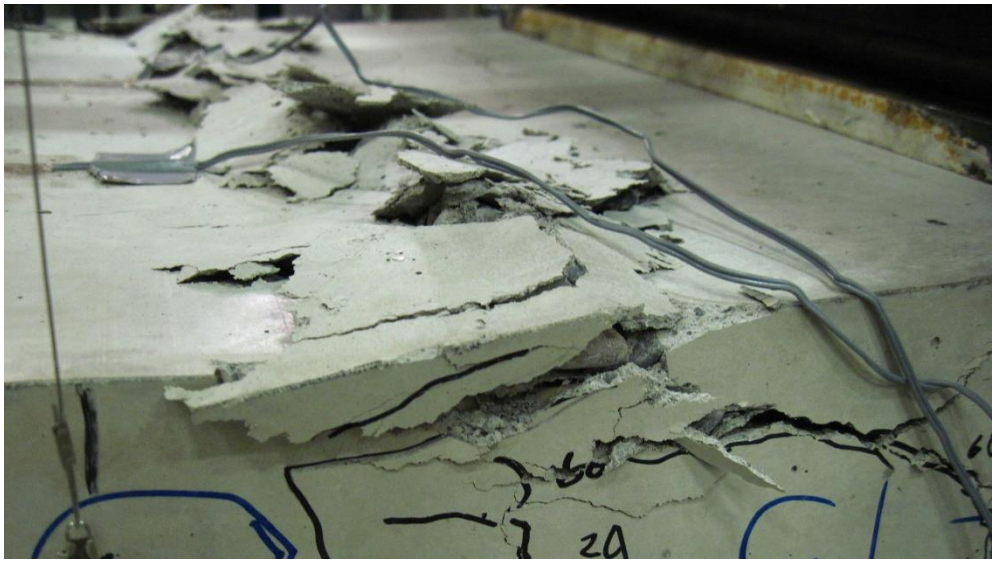

Figure 4.28: Control wall at failure with crushed concrete lifting at surface.

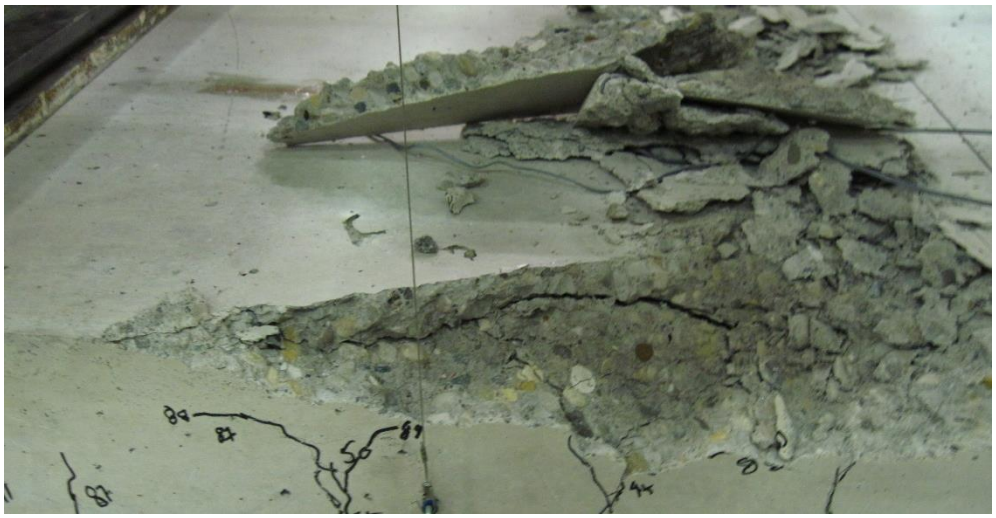

Figure 4.29: Concrete compression block removed from control wall.

During tests of the PVC encased walls, this separation of concrete from the wall was not observed. Figure 4.30 presents the compression face of a wall encased in flat panels during testing. Bumps or bubbles in the PVC panel can be seen across the width of the wall. At location where the panels are linked to PVC connectors, these bumps are either less

pronounced or not present. When the PVC panels were removed at the 'bump' locations, crushed concrete was observed underneath the wall. As the concrete was contained by the panels and connectors throughout testing, the exposed concrete was effectively pulverized (Figure 4.31).

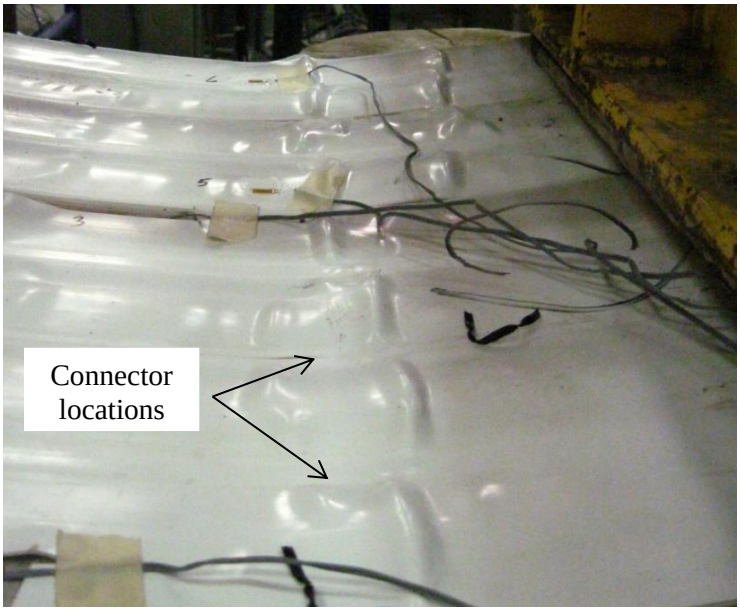

Figure 4.30: Bubbled surface of flat panel encased wall.

Figure 4.31: Pulverized concrete under bubbled location.

As previously discussed, flat panel encased walls did not experience panel slip during testing. As the panels were removed, portions of the PVC were more difficult to take off than the hollow panels. The underside of each flat panel had two nubs (Figure 4.32). These nubs had concrete paste attached to them as the panels were removed, implying that some mechanical bond was present in connecting the concrete to the panel. In contrast, the hollow panels had a completely smooth surface, giving further indication that there was only frictional bond present in the hollow panel encased specimens.

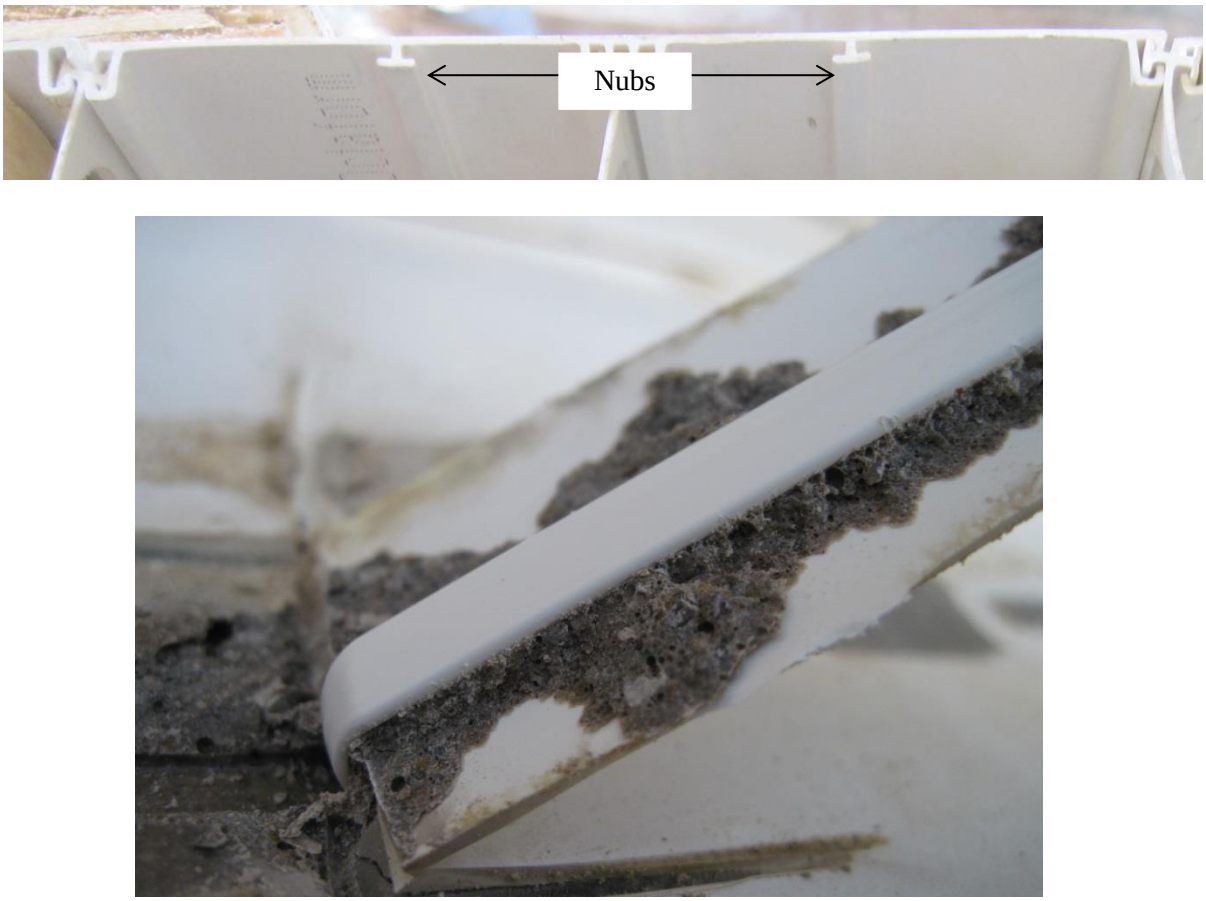

Figure 4.32: Concrete paste attached to PVC ‘nubs’.

Despite the lack of mechanical connection to the concrete surface, removing the hollow panels after testing yielded additional observations. As was seen in the flat panel walls, the hollow panels contained the failure surface of the concrete. In areas outside of the failure locations, removal of the panels revealed a smooth, clean concrete surface (Figure 4.33).

Figure 4.33: Failure location and smooth surface of hollow panel formed concrete.

4.6 Effect of PVC Encasement on Concrete Strength

It was suggested that the SIP system may provide an increase in concrete compressive strength over the conventionally formed walls. With a permanent formwork layer against the concrete, mix water would be restricted from exiting the walls, prolonging the curing process. After the flexural tests were completed, three wall specimens were selected for core sampling. Table 4.6 shows the walls selected and the number of cores taken from each wall. The cores were tested to determine the actual compressive strength of the control and PVC

encased walls. The core strengths were compared with the remaining cylinders from the concrete cast.

Table 4.6: Cores drilled from tested specimens

Type		Number of specimens	Average compressive strength (MPa)
Control cores	C-8-10	4	27.5±1.3
PVC Encased cores	PH-8-10	2	28.2 ± 1.3
	PH-8-15	2	
Cylinders	Cylinders	8	26.7±0.7

The compressive test results and confidence intervals are presented in Table 4.6. The concrete cores taken from the PVC encased walls showed a minimal improvement over the control specimen and cylinders. However, due to the small sample size and confidence interval presented in Table 4.6, it can be concluded that the PVC encasing does not appear to provide any significant benefit to concrete strengths.

4.7 Summary from Experimental Test Program

Based on the test results, it was found that the use of the PVC system enhanced the flexural behaviour of the reinforced concrete walls in terms of mode of failure, load capacity, and deflection. The main findings of the experimental work reported here can be summarized as follow.

4.7.1 Modes of Failure

All of the control specimens failed by steel yielding followed by concrete crushing at mid span. The location of the crushing point varied from the centre of the constant moment region to underneath the loading points.

Failure for flat panel encased PVC walls depended on the reinforcing ratio. For specimens reinforced with 3-10M rebars, the walls failed by steel yielding at mid span, followed by concrete crushing at mid span, then bubbling or buckling of the PVC panels on the compression face, and finally PVC rupture on the tension side of the wall. Specimens reinforced with 3-15M rebars did not experience PVC panel rupture on the tension side, as the tensile strains at failure were significantly lower for the more heavily reinforced sections.

All of the hollow panel encased PVC walls showed a similar mode of failure. Failure started with steel yielding at mid span, followed by concrete crushing at mid span, and PVC panels buckling on the compression face. Slipping of the hollow panels on the tension side of the wall was also observed.

4.7.2 Loads and Deflections

Cracking Stage: The flat panel and hollow panel walls improved the cracking load by an average of 71% and 45%, respectively. The walls with hollow panels showed less improvement as the geometry of the panel reduced the thickness of the concrete specimen.

Yielding Stage: The effect of the PVC on the yield load decreases as the reinforcement ratio increases.

- PVC encased walls with flat panels increased the yield load by at least 21% for specimens reinforced with 3-10M rebars and at least 14% for specimens reinforced with 3-15M rebars.
- PVC encased walls with hollow panels and reinforced with 3-10M rebars showed an increase in the yield load by 12% on average, and 4% on average for walls

reinforced with 3-15M rebars. It is worth mentioning that the depth of the steel reinforcement for the walls with hollow panels was less than the walls with flat panels, which reduced the potential increase in the yield load.

- The yield deflection was not affected by the presence of the PVC panels.

Peak Stage: The contribution of the PVC system to the peak load decreases as the reinforcement ratio increases.

- PVC encased walls with flat panels showed an increased peak load by at least 30% for specimens reinforced with 3-10M rebars and at least 20% for specimens with 3-15M rebars, when compared with the equivalent control walls.
- PVC encased walls with hollow panels and reinforced with 3-10M rebars showed an increased peak load by 38% on average, and 16% on average for walls reinforced with 3-15M rebars. The greatest improvement was observed in the 203 mm thick specimens due to the high clamping force that prevented sudden slips in the PVC tension panels.

Ultimate deflection: The increase in ultimate deflection for the flat and hollow paneled PVC encased walls varied from 3% to 106%.

4.7.3 Strains in the PVC Panel

- Compressive strains: Strain values for concrete and PVC remained consistent until concrete crushing. The PVC strain gauge readings continued to increase until buckling of the PVC. The average strain in the PVC at failure was -10000με and -4000 με for concrete.

- Tensile strains: The strain gauges readings of both the PVC and steel were consistent. Very high strain values were recorded on the PVC tension panels in multiple tests at failure (>50000με).

4.7.4 Effect of PVC Encasing on Concrete Strength

Concrete cores were taken from control and hollow panel specimens. When compared with the cast cylinders, there was no significant difference found in the compressive strength. Therefore, the PVC encasement does not have a significant impact on the compressive strength of concrete over bare reinforced concrete.

Chapter 5: Analytical Investigation

5.1 Introduction

The following section will outline the model developed for calculating the flexural resistance of PVC SIP formed concrete walls at yield and ultimate load levels. Results from the model will be compared with the experimental data.

5.2 Assumptions of the Model

Strain compatibility analysis has been used to determine the flexural resistance of various reinforced concrete elements. In this method a force balance of concrete acting in compression and reinforcing steel in tension is determined from a linear strain distribution through the element. The following assumptions are made to validate the analysis:

- plane sections remain plane after bending,
- a perfect bond exists between the reinforcing steel and concrete,
- the concrete provides zero tension resistance, and;
- concrete crushes when reaching the crushing strain $\varepsilon_{cu} = 0.0035$

The mode of failure of the element depends on the strains in the concrete and the steel. If steel yields before concrete crushes, the flexural element fails in a ductile manner and is classified as under-reinforced (CSA A23.3-04). In this situation, additional load applied beyond the yield point results in significant deflection and eventual crushing of the concrete in compression. If the concrete crushes before the steel yields, the flexural element fails in a more brittle manner and is classified as over-reinforced.

The model presented here calculates the capacity of PVC encased walls. Therefore, a third material, PVC, is included in the strain compatibility analysis and equilibrium. In addition to the previous assumptions, the following assumptions are made.

- perfect bond exists between the PVC and concrete,
- both the PVC panels on the tension and compression face contribute to the resistance of the wall,
- continuous portions of the PVC connectors contribute to resisting tensile forces and,
- continuous portions of the PVC connectors in the compression zone are neglected due to small strain values.

Further details of the material properties are discussed in the next section.

5.3 Material Properties

5.3.1 Concrete

For compressive strengths less than 41 MPa, concrete is assumed to follow a parabolic stress strain relationship as seen in Figure 5.1. The stress in the concrete versus the corresponding strain can be expressed using Equation 5-1 (Collins and Mitchell 1987). CSA A23.3-04 recommends a strain value ε_o of 0.0025 corresponding to the 25MPa concrete compressive strength and a crushing strain ε_{cu}, of 0.0035 and.

$$f_c = f_c' \left(\frac{2\varepsilon}{\varepsilon_o} - \left(\frac{\varepsilon}{\varepsilon_o} \right)^2 \right) \qquad [5\text{-}1]$$

$$\varepsilon_o = \frac{2f_c'}{E_c}$$

$$E_c = 4500\sqrt{f_c'}$$

Where,

f_c: the concrete stress corresponding to a given concrete strain (ε) (MPa),

f_c': the concrete compressive strength (MPa),

ε: the concrete strain corresponding to a given concrete stress (f_c),

ε_o: the concrete strain corresponding to the concrete compressive strength (f_c'), and

E_c: the Young's modulus of concrete (MPa).

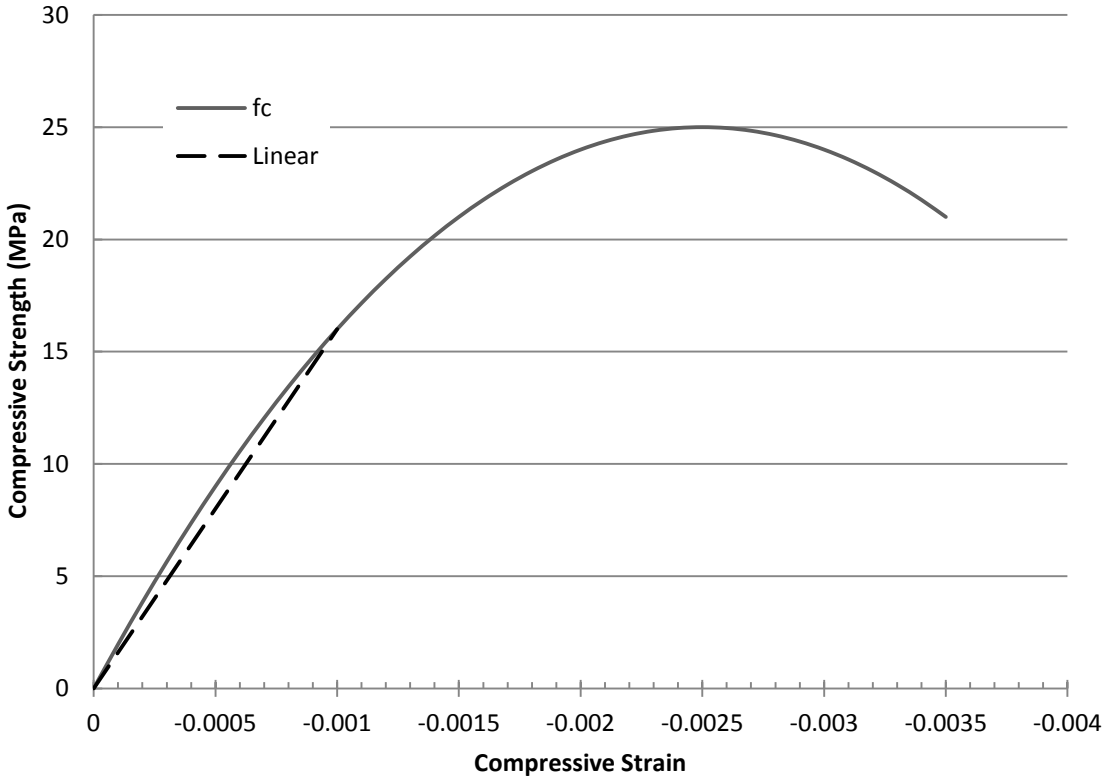

Figure 5.1: Idealized concrete stress-strain relationship.

The use of an equivalent rectangular concrete stress block has been adopted for design in multiple codes (CSA A23.3-04, ACI 318) and in previous models developed for PVC

encased walls (Kuder et al. (2009), Rtiel et al.(2008), and Wahab et al.(2013)). The parabolic stress-strain curve in Figure 5.1 is transformed to a rectangular block using modification factors, α_1 and β_1. The stress and depth modification parameters, (α_1 and β_1) are calculated at any given strain values using equations 5-2 and 5-3 (Collins and Mitchell 1987).

$$\alpha_1\beta_1 = \frac{\varepsilon}{\varepsilon_o} - \frac{1}{3}\left(\frac{\varepsilon}{\varepsilon_o}\right)^2 \quad [5\text{-}2]$$

$$\beta_1 = \frac{4 - \frac{\varepsilon}{\varepsilon_o}}{6 - \frac{2\varepsilon}{\varepsilon_o}} \quad [5\text{-}3]$$

Where,

α_1: the ratio of the average stress in the compression stress block to the concrete strength, and

β_1: the ratio of the depth of the compression stress block to the depth of the neutral axis

5.3.2 Steel

The tension reinforcement is assumed to be elastic until yielding then plastic with a 1% strain hardening slope (bi-linear behaviour). The idealized stress-strain relationship is shown in Figure 5.2, with the yield stress taken as 486 MPa for the 10M reinforcing bar or 478 MPa for the 15M reinforcing bar as reported by the reinforcing steel manufacturer. Equations 5-4 and 5-5 give the expressions for steel stress versus strain.

$$f_s = \varepsilon_s E_s \qquad \varepsilon_s < \varepsilon_y \quad [5\text{-}4]$$

$$f_s = f_y + 0.01E_s(\varepsilon_s - \varepsilon_y) \qquad \varepsilon_s \geq \varepsilon_y \quad [5\text{-}5]$$

Where,

f_s: the steel stress corresponding to a given steel strain (ε_s) (MPa),

f_y: the steel stress corresponding to the steel yield strain (ε_y) (MPa),

E_s: Young's modulus for reinforcing steel before yielding, taken equal to 200 GPa,

ε_s: steel strain corresponding to a given stress, and;

ε_y: steel strain according to the yield stress.

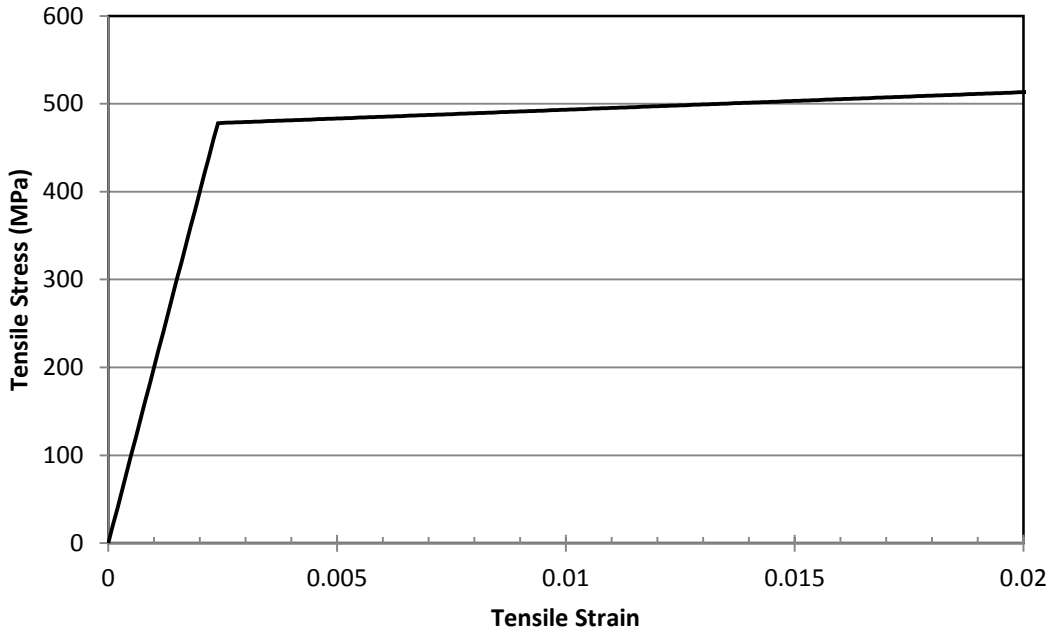

Figure 5.2: Stress versus strain relationship for reinforcing steel.

5.3.3 PVC

Figure 5.3 shows the stress-strain relationship of the PVC. The relationship can be expressed according to the following equation.

$$f_{PVC} = -71518\varepsilon_{PVC}^2 + 3412.1\varepsilon_{PVC} \quad [5\text{-}6]$$

Based on the experimental test results, once the strain in the PVC reaches 25000με, a constant value of 40.6MPa is assumed (solid line) as the PVC encased wall

specimens maintained a consistent load resistance plateau through a large deflection. This behaviour is particularly evident in the flat panel specimens reinforced with 10M bars that experienced high strains until failure.

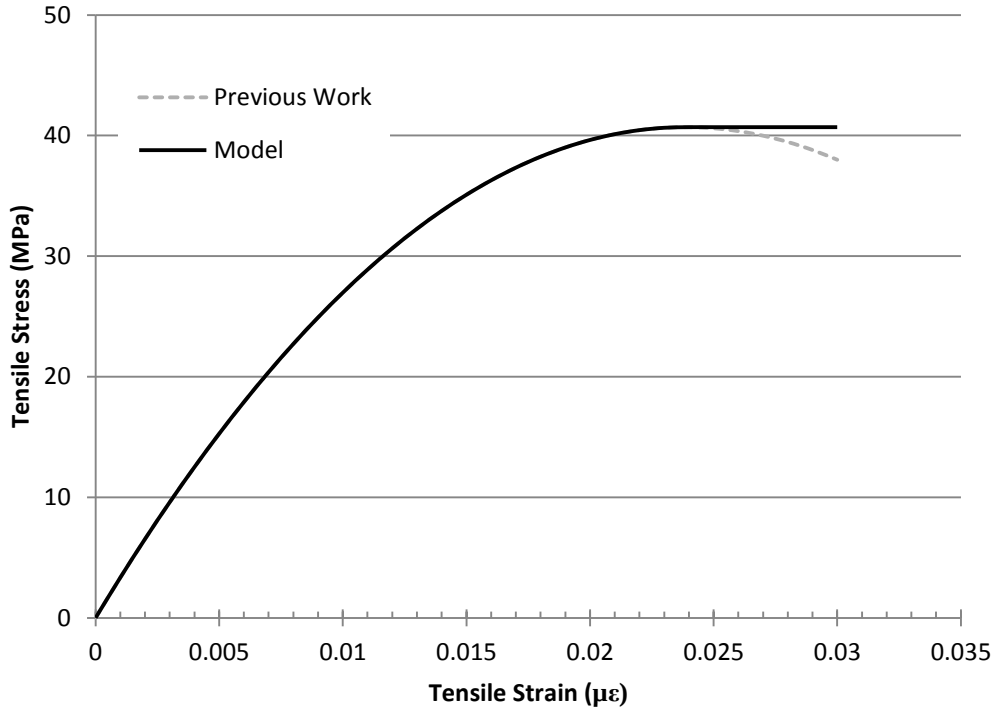

Figure 5.3: Stress-strain curve for PVC panels and connectors.

Figure 5.4 presents a typical PVC connector used to construct the PVC encased walls. Critical portions of the connector (continuous in the longitudinal direction) that are utilized in the model are identified.

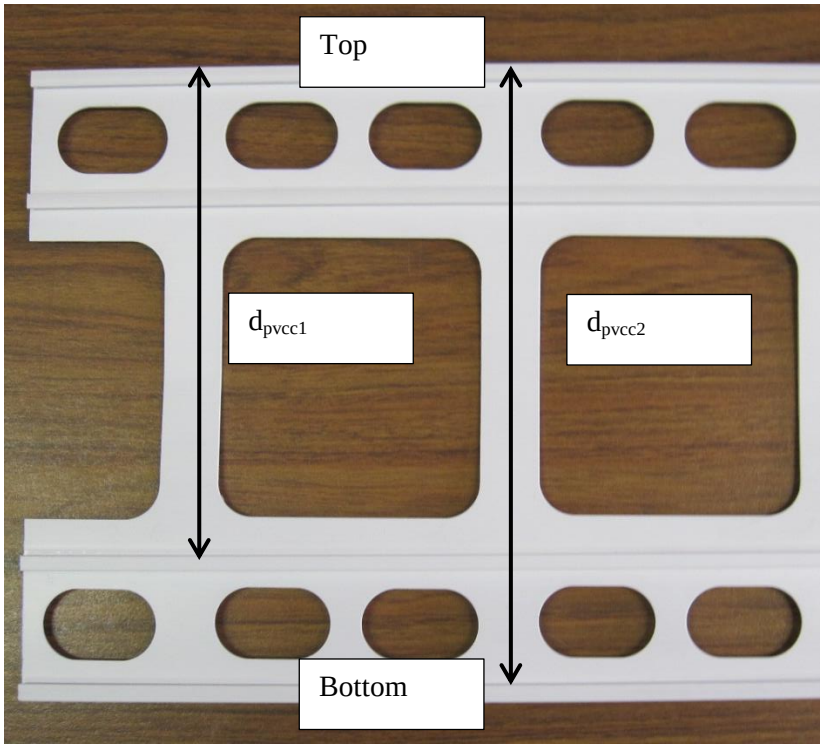

Figure 5.4: PVC connector

5.4 Yield Load Analysis

5.4.1 Control Specimens

The strain and corresponding stress distribution of a singly reinforced concrete wall at yielding, as described by Pillai et al. (2007), is provided in Figure 5.5. At yielding, the stresses in the concrete can be reasonably approximated as linear from the neutral axis to the top compression fibre. During testing the concrete strains at yield were recorded between 700 and 1000με, resulting in a concrete stress of less than 0.5 f'_c (Figure 5.1). Figure 5.5a shows the effective cross-section consists of the reinforcing steel at a depth (d), and the concrete compression block with a width (b) and a depth (kd). The depth of the neutral axis can be determined using elastic theory, where the cracked cross-section is transformed into

an effective section of concrete (Figure 5.5b). The steel is equated to concrete area through the use of a modular ratio ($n_s=E_s/E_c$). The centroid of this transformed area is equal to the depth of the neutral axis (kd). Equating moments of area about the neutral axis allows the neutral axis depth to be determined (Equation [5-7]).

$$\frac{b(kd)^2}{2} = nA_s(d - kd) \qquad [5\text{-}7]$$

Where:

b: the width of the wall (mm),

d: the depth to the centroid of reinforcing steel (mm),

A_s: the cross-sectional area of the reinforcing steel (mm^2),

n_s: the ratio of Young's Modulus of steel to concrete, and

k: the fraction of the depth from the compression face to the N.A location.

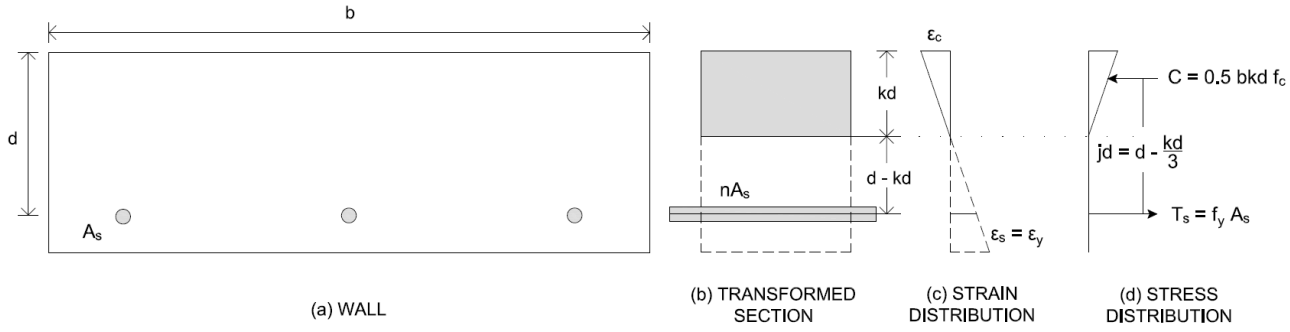

Figure 5.5: Sectional analysis at yield load.

Once the depth of the compression block (kd) is determined from Equation [5-7], the yield moment can be calculated from the resultant stress distribution as shown in Figure 5.4d and given by Equation [5-8].

$$M_y = T_s jd \qquad [5\text{-}8]$$

$$M_y = A_s f_y (d - \frac{kd}{3})$$

From this moment value the applied load on the specimen can be determined using Equation [5-9].

$$P_{yield} = \frac{2M_y}{shear\ span} \quad [5\text{-}9]$$

Where; the shear span is equal to 770 mm.

5.4.2 PVC SIP Formed RC Specimens

Elastic theory was extended to walls encased in PVC. In addition to the concrete compression block and steel reinforcement, four portions of the PVC forming system were included in the analysis; the compression and tension panels (C_{pvcpc}, T_{pvcpt}), and the continuous portions of the connectors acting close to the extreme tension side of the wall (T_{pvcc1},T_{pvcc2}). The additional components of the analysis are summarized for simplicity in a single cell wall with hollow panels in Figure 5.5.

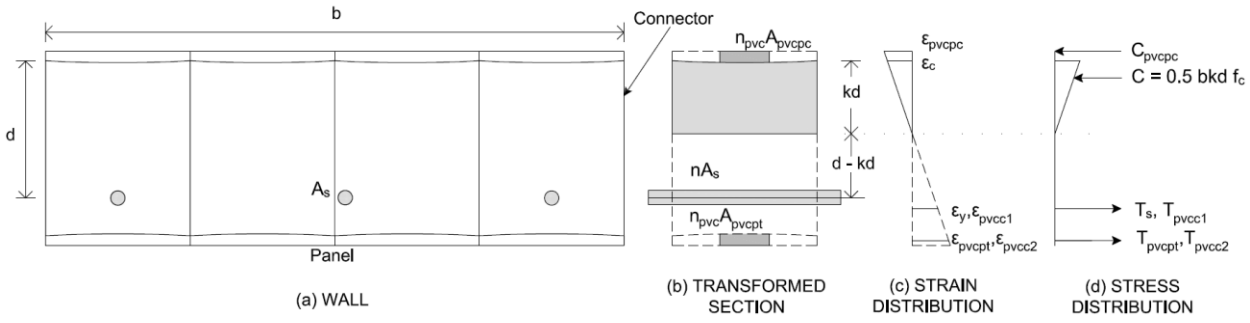

Figure 5.6: Section analysis of PVC encased concrete walls at yield load.

In order to determine the depth of the neutral axis (kd), moments of area of the cracked transformed section are equated resulting in Equation [5-10].

$$kdb\frac{(kd)}{2}+\left(kd+\frac{t_p}{2}\right)n_{PVC}A_{PVCPC}=n_sA_s(d-kd)+n_{PVC}\begin{bmatrix}A_{PVCC1}\left(d_{PVCC1}-t_p-kd\right)\\+A_{PVCC2}\left(d_{PVCC2}-t_p-kd\right)\\+A_{PVCPT}(h-1.5t_p-kd)\end{bmatrix} \quad [5\text{-}10]$$

Where:

n_{PVC}: modular ratio between PVC and concrete,

d_{PVCC1}: depth of the first continuous portion of the connectors acting in tension measured from the compression PVC panel (mm),

d_{PVCC2}: depth of the second continuous portion of the connectors acting in tension measured from the compression PVC panel (mm),

h: total thickness of the wall (mm),

t_p: thickness of the PVC panels (mm) (11.5mm for hollow panels, flat panels assumed 0 thickness),

A_{PVCC1}: cross-sectional area of the first continuous portion of the connectors acting in tension (mm^2),

A_{PVCC2}: cross-sectional area of the second continuous portion of the connectors acting in tension (mm^2),

A_{PVCPC}: cross-sectional area of the PVC panels acting in compression (mm^2), and

A_{PVCPT}: cross-sectional area of the PVC panels acting in tension (mm^2)

Using the linear strain distribution shown in Figure 5.6, and knowing that the strain in the steel is equal to the yield strain, the strains in the PVC panels and connectors will be determined as given by Equation [5-11].

$$\frac{\varepsilon_c}{d-kd} = \frac{\varepsilon_{pvcpc}}{kd+t_p} = \frac{\varepsilon_{pvcc1}}{d_{pvcc1}-t_p-kd} = \frac{\varepsilon_{pvcc2}}{d_{pvcc2}-t_p-kd} = \frac{\varepsilon_{pvcpt}}{d_{pvcpt}-1.5t_p-kd} \quad [5\text{-}11]$$

The stresses in the PVC panels and connectors are computed using Equation [5-12]

$$f_{PVC} = -71518\varepsilon_{PVC}^2 + 3412.1\varepsilon_{PVC} \quad [5\text{-}12]$$

With the material stresses calculated, the resulting yield moment can be calculated using Equation [5-13].

$$\begin{aligned} M_y = T_s j_1 + T_{PVCC1} j_2 + T_{PVCC2} j_3 + T_{PVCPT} j_4 + C_{PVCPC} j_5 \\ = A_s f_y \left[d - t_p - \frac{kd}{3}\right] + f_{PVCC1} A_{PVCC1} \left[d_{PVC1} - t_p - \frac{kd}{3}\right] \\ + f_{PVCC2} A_{PVCC2} \left[d_{PVC2} - t_p - \frac{kd}{3}\right] + f_{PVCPT} A_{PVCPT} \left[h - 1.5t_p - \frac{kd}{3}\right] \\ + f_{PVCPC} A_{PVCPC} \left[\frac{kd}{3} + \frac{t_p}{2}\right] \end{aligned} \quad [5\text{-}13]$$

Where,

T_s: tension force in the reinforcing steel (N)

T_{PVCC1}: tension force in the first portion of the connector (N)

T_{PVCC2}: tension force in the second portion of the connector (N)

T_{PVCPT}: tension force in the PVC panel (N)

C_{PVCPC}: compression force in the PVC panel (N)

f_y: yield stress in reinforcing steel (MPa)

f_{PVCC1}: stress in the PVC connector due to the estimated strain, ε_{pvcc1} (MPa)

f_{PVCC2}: stress in the PVC connector due to the estimated strain, ε_{pvcc2} (MPa)

f_{PVCPT}: stress in the PVC panel due to the estimated strain, ε_{pvcpt} (MPa)

f_{PVCPC}: stress in the PVC connector due to the estimated strain, ε_{pvcpc} (MPa)

5.4.3 Comparison between Calculated and Experimental Yield Loads

Table 5.1 and Figure 5.7 present the experimental yield load results with the values calculated using section analysis. The calculated values for the control specimens were consistently overestimated with the model exceeding the test results by an average of 8% (19% maximum for only one specimen). However, the results for the PVC encased specimens were consistently conservative by an average error of 5% (16% maximum for one specimen.)

Table 5.1: Summary of Experimental vs Calculated Yield load for test program

		Yield Load		
	Specimen	Experimental (kN)	Calculated (kN)	Error (%)
Control	C-6-10	32	38.1	-19%
	C-6-15	69	70.9	-3%
	C-7-10	44.5	47.3	-6%
	C-7-15	84	88.7	-6%
	C-8-10	53	56.6	-7%
	C-8-15	102	106.7	-5%
Flat Panel	PF-6-10	43	42.1	2%
	PF-6-15	82.5	75	9%
	PF-7-10	54	51.8	4%
	PF-7-15	96	93.3	3%
	PF-8-10	64	61.5	4%
	PF-8-15	120	111.6	7%
Hollow Panel	PH-6-10	38	37.6	1%
	PH-6-15	76	64.1	16%
	PH-7-10	46	47.3	-3%
	PH-7-15	85	82.3	3%
	PH-8-10	60	57.2	5%
	PH-8-15	103	100.7	2%

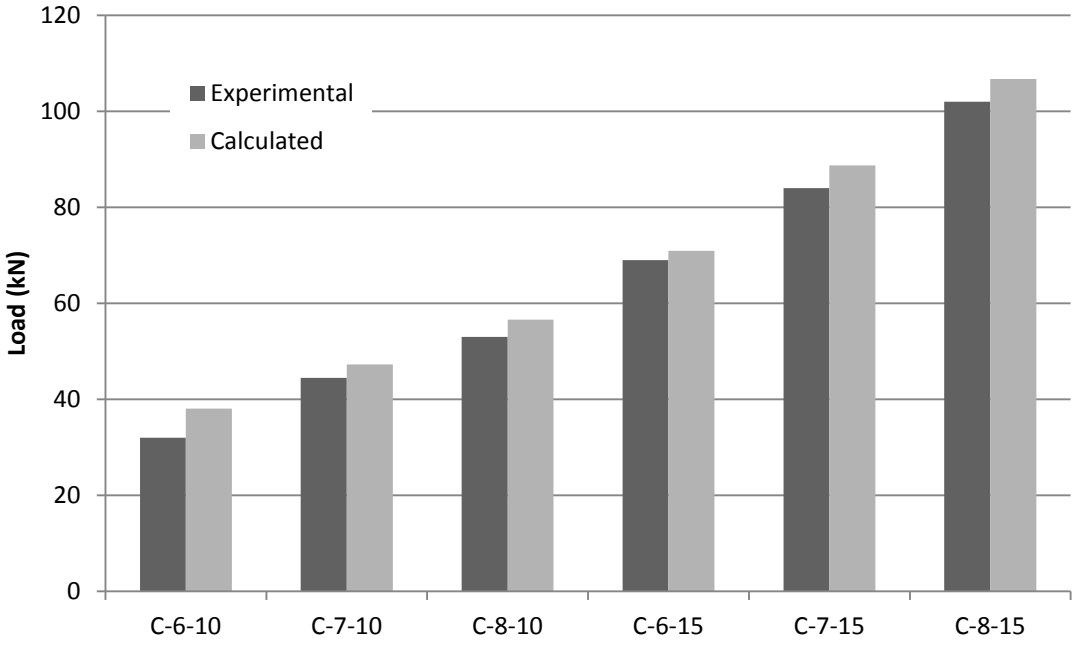

a) control walls

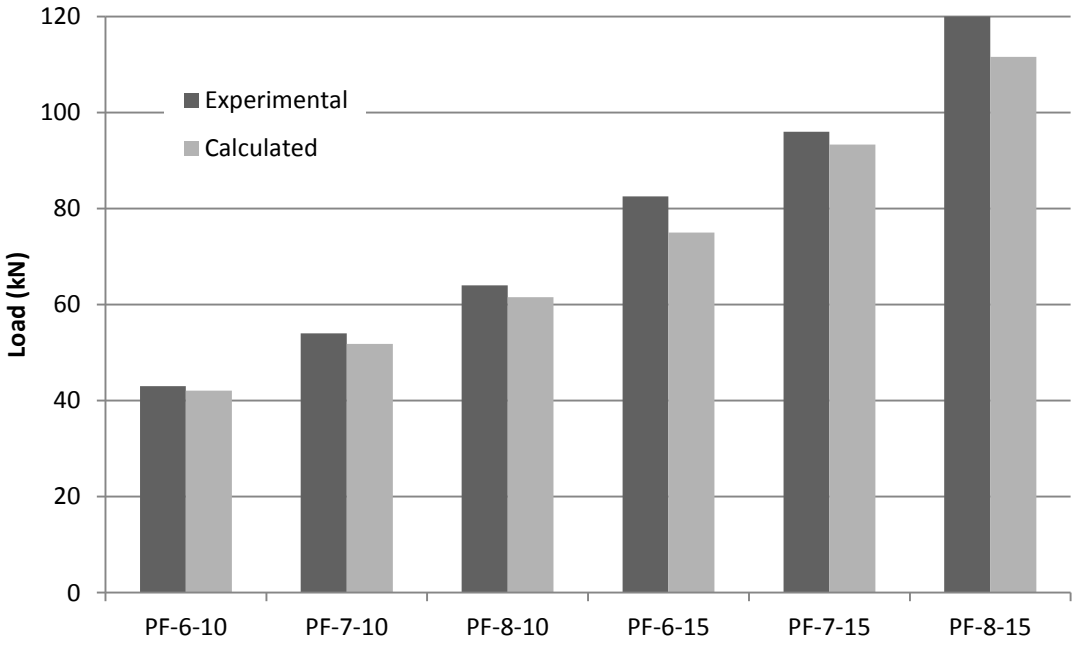

b) PVC encased walls with flat panels

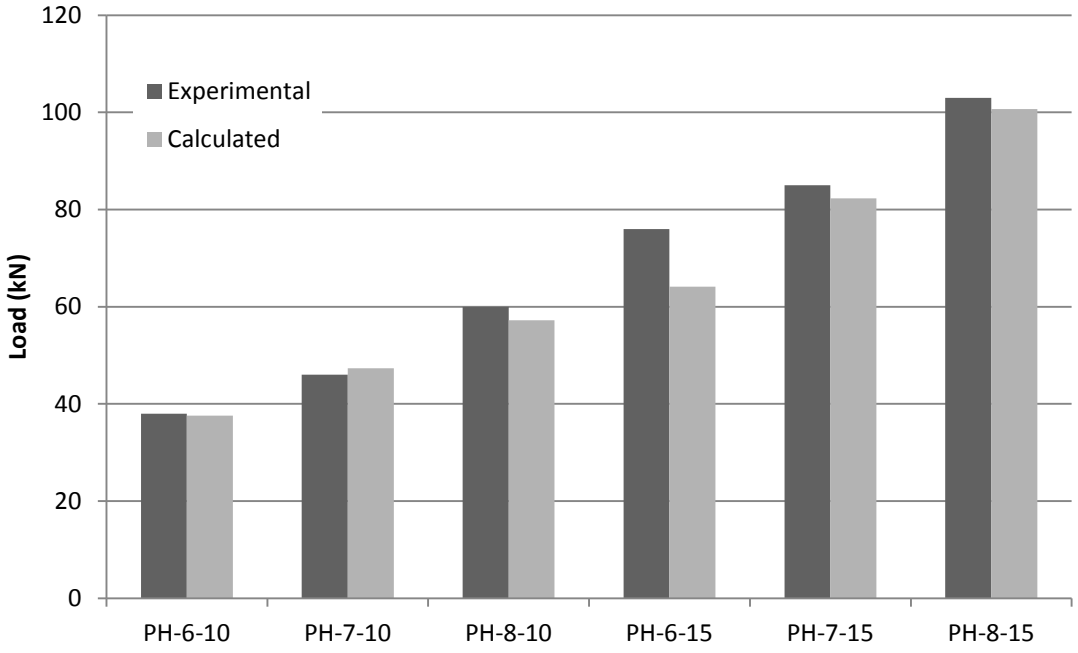

c) PVC encased walls with hollow panels

Figure 5.7: Experimental versus calculated yield loads for tested walls

5.5 Ultimate Load Analysis

5.5.1 Control Specimens

Figure 5.8 presents the strain and stress distributions of a singly reinforced concrete wall at ultimate load. At ultimate load conditions, the strain in the steel reinforcement is well above the yield strain ($\varepsilon_s >> \varepsilon_y$) and the concrete in the top compressive fibres has reached crushing strain (ε_{cu}). An iterative method is used to determine the location of the neutral axis (c). The strain in the top compressive fibre is set equal to the concrete crushing strain ($\varepsilon_c = 0.0035$). The stress in the concrete now reflects a non-linear relationship with strain and can be equated into a concrete compression stress block using stress and depth parameters α_1 and β_1 respectively. From the resulting strain profile a value of 'c' is determined and compression and tension forces are equated to satisfy internal equilibrium.

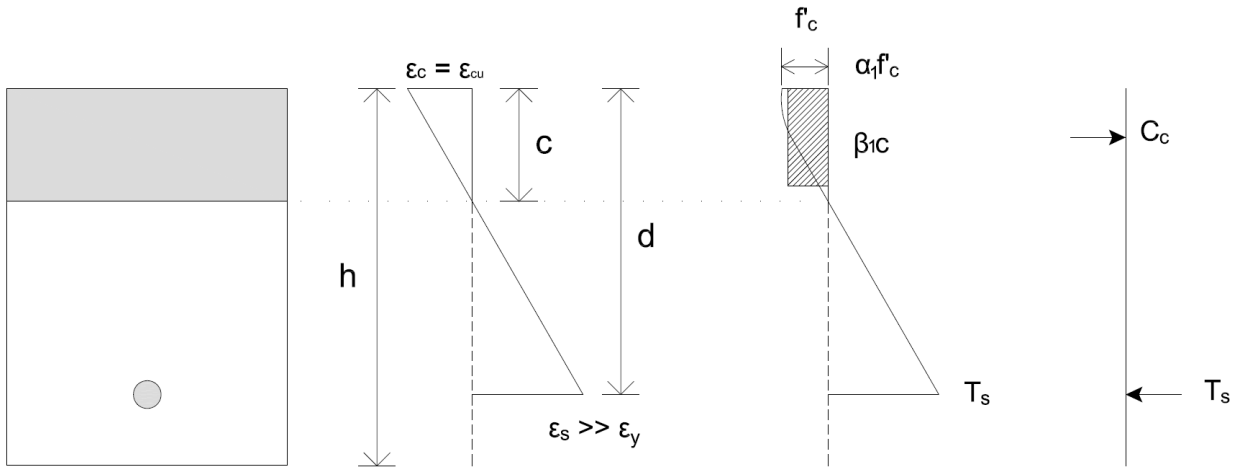

Figure 5.8: Stress and strain distributions for reinforced concrete walls at ultimate limit state

$$C_c = T_s \quad [5\text{-}14]$$

$$C_c = \alpha_1 \beta_1 c b f_c'$$

$$T_s = [f_y + 0.01(\varepsilon_s - \varepsilon_y)E]A_s$$

Where;

C_c: the force in the concrete compression block (N), and;

T_s: the force in the steel reinforcing (N)

If internal equilibrium is not satisfied, the steel strain is incrementally increased, subsequently reducing the neutral axis depth until C=T. The moment resistance of the wall can be calculated by a summation of moments about the concrete compression stress block as given by Equation [5-18].

$$M_{ult} = T_s j d \quad [5\text{-}15]$$

$$M_{ult} = T_s (d - \frac{\beta_1 c}{2})$$

The applied load at ultimate, (P_{ult}) for a given wall in the test program can be calculated from the Equation [5-16].

$$P_{ult} = \frac{2M_{ult}}{shear\ span} \quad [5\text{-}16]$$

Where; the shear span is equal to 770 mm.

5.5.2 PVC SIP Formed RC Specimens

A similar approach is taken to determine the ultimate load capacity of PVC encased concrete walls. Figure 5.9 shows the strain compatibility and resulting stress profiles for the six forces considered. The strain in each material (concrete, steel, and PVC) can be determined from linear strain analysis as given by Equation [5-17].

$$\frac{\varepsilon_c}{c} = \frac{\varepsilon_{PVCPC}}{c + t_p} = \frac{\varepsilon_s}{d - c - t_p} = \frac{\varepsilon_{PVCC1}}{d_{pvcc1} - c - t_p} = \frac{\varepsilon_{PVCC1}}{d_{pvcc2} - c - t_p} = \frac{\varepsilon_{PVCPT}}{h - c - t_p} \quad [5\text{-}17]$$

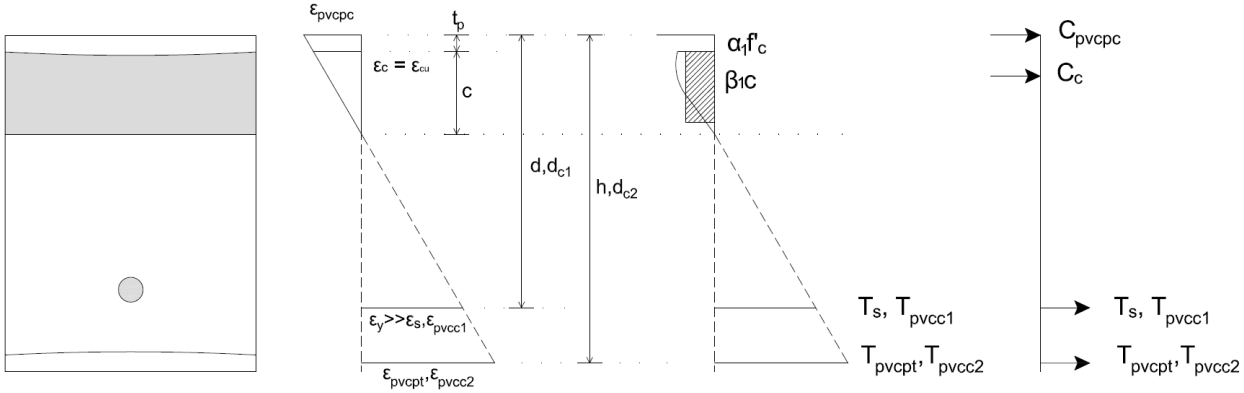

Figure 5.9: Stress-strain diagrams for single cell PVC encased wall with hollow panels at ultimate limit state

An iterative method is used to determine a neutral axis location that satisfied internal equilibrium. The strain at the top compressive concrete fibre ε_c was set to the concrete crushing strain ($\varepsilon_c = 0.0035$) while an arbitrary value of strain in the tension PVC panel, ε_{pvcpt}, is selected. From these conditions, the depth of the neutral axis could be determined (Equation [5-18]).

$$c = \frac{h}{\varepsilon_{PVCPT}} \cdot \frac{1}{\left(\frac{1}{\varepsilon_{cu}} + \frac{1}{\varepsilon_{PVCPT}}\right)} \quad [5\text{-}18]$$

Once the depth of the neutral axis 'c' is calculated, the remaining strain values of the steel and PVC are be determined. From these strain values, forces in the PVC, concrete and steel are be calculated and used to check for internal equilibrium conditions (Equations [5-19] and [5-20]).

$$C = T \quad [5\text{-}19]$$

$$C_c + C_{pvcpc} = T_s + T_{pvcc1} + T_{pvcc2} + T_{pvcpt} \quad [5\text{-}20]$$

$$C_c = \alpha_1 \beta_1 c b f_c'$$

$$C_{pvcpc} = \sigma_{PVCPC} A_{pvcpc}$$

$$T_s = [F_y + 0.01(\varepsilon_s - \varepsilon_y)E]A_s$$

$$T_{pvcc1} = \sigma_{PVCC1} A_{pvcc1}$$

$$T_{pvcc2} = \sigma_{PVCC2} A_{pvcc2}$$

$$T_{pvcpt} = \sigma_{PVCPT} A_{pvcpt}$$

If the compressive forces (C) exceed the tensile forces (T), the assumed strain in the PVC panel strain is increased, and the process is repeated until internal equilibrium is satisfied (Equation [5-20]). Once internal equilibrium was satisfied, moments were summed about the concrete compression block to calculate the moment of resistance of the wall (Equation [5-21]).

$$M = T_s\left(d - t_p - \frac{c\beta_1}{2}\right) + T_{pvcc1}\left(d_{pvcc1} - t_p - \frac{c\beta_1}{2}\right) + T_{pvcc2}\left(d_{pvcc2} - t_p - \frac{c\beta_1}{2}\right) + T_{pvcpt}\left(h - t_p - \frac{c\beta_1}{2}\right) + C_{pvcpc}\left(t_p + \frac{c\beta_1}{2}\right) \quad [5\text{-}21]$$

5.5.3 Comparison between Calculated and Experimental Ultimate Loads

Table 5.2 and Figure 5.10 compare the experimental ultimate load results to the values calculated using strain compatibility. The control specimens are in close agreement to the test results with each calculated load falling within ±4% of the experimental load values. The calculated ultimate load for the walls encased in flat panels are conservative (or underestimated) by an average of 4% (8% max for only one wall). Finally, walls encased with hollow PVC panels are underestimated by an average of 6% (15% max for only one wall). In conclusion, the calculated and experimental ultimate loads are in good agreement except for one specimen (PH-6-15).

Table 5.2: Summary of experimental versus calculated ultimate load

		Ultimate Load		
	Specimen	Experimental (kN)	Calculated (kN)	Error (%)
Control	C-6-10	41	42.8	-4%
	C-6-15	77.2	74.1	4%
	C-7-10	55.5	54.4	2%
	C-7-15	91	95	-4%
	C-8-10	66	66.7	-1%
	C-8-15	114	116.8	-2%
Flat Panel	PF-6-10	55	56.9	-3%
	PF-6-15	93	85.7	8%
	PF-7-10	75.3	71.4	5%
	PF-7-15	111	110.5	0%
	PF-8-10	89	86.2	3%
	PF-8-15	138	135.4	2%
Hollow Panel	PH-6-10	57	55.3	3%
	PH-6-15	89	75.5	15%
	PH-7-10	72	70.7	2%
	PH-7-15	104	101.2	3%
	PH-8-10	95	86.5	9%
	PH-8-15	135	127.5	6%

The model is significantly conservative for one specimen in particular, PH-6-15. The ultimate load of this wall is calculated to be 15% less than the experimental result. When reviewing the test data at yield load, the calculated load is 16% underestimated. Figure 5.11 shows the specimen after testing. The failure location for the wall was directly underneath the right loading point. Further investigation of the wall post testing revealed significant depression of the hollow panels at this load point, while the left load point had much less depression. Hence, there was a discrepancy in load between the two points, inadvertently shifting the load distribution and producing a higher resistance in the wall than first anticipated.

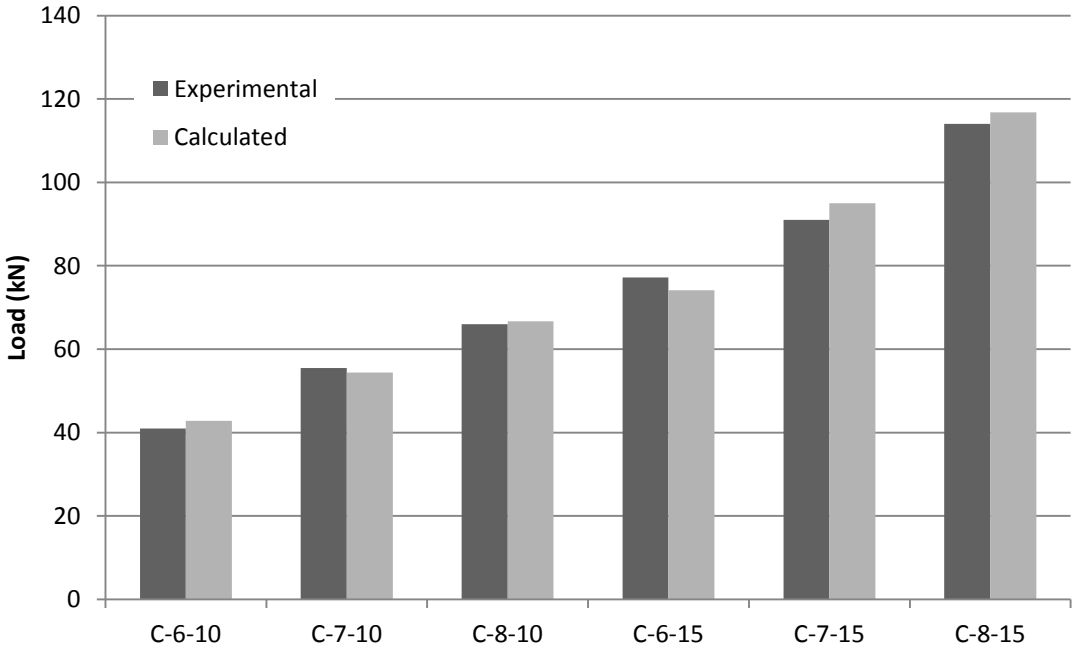

a) control walls

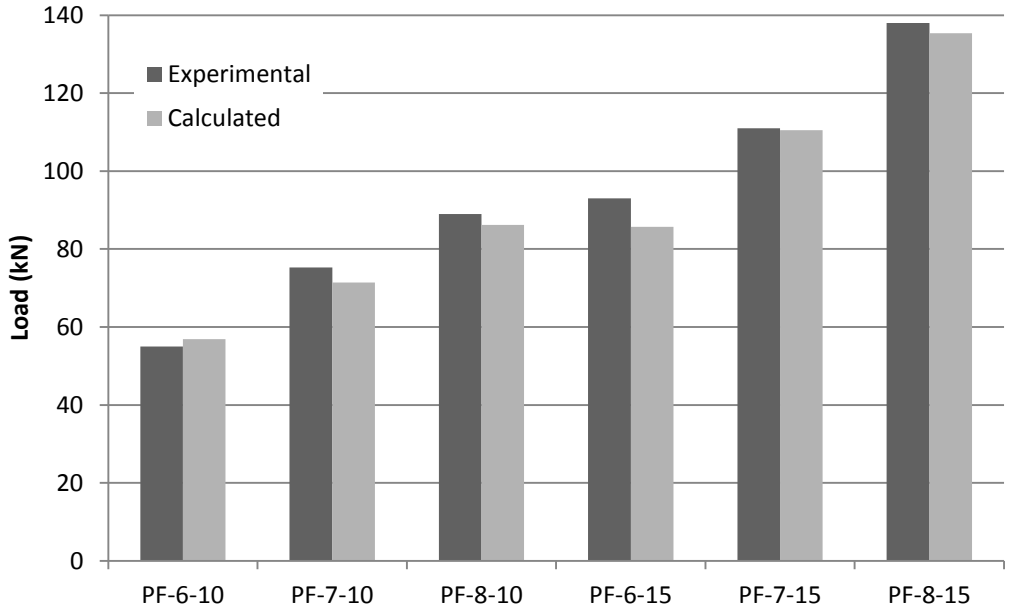

b) PVC encased walls with flat panels

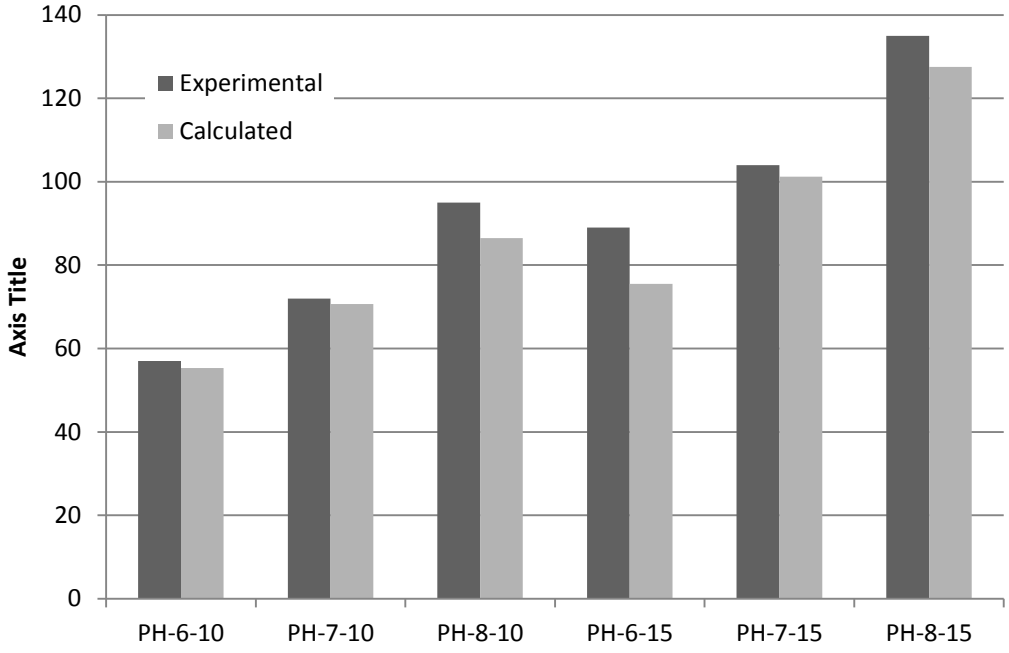

c) PVC encased walls with hollow panels

Figure 5.10: Experimental versus calculated ultimate load

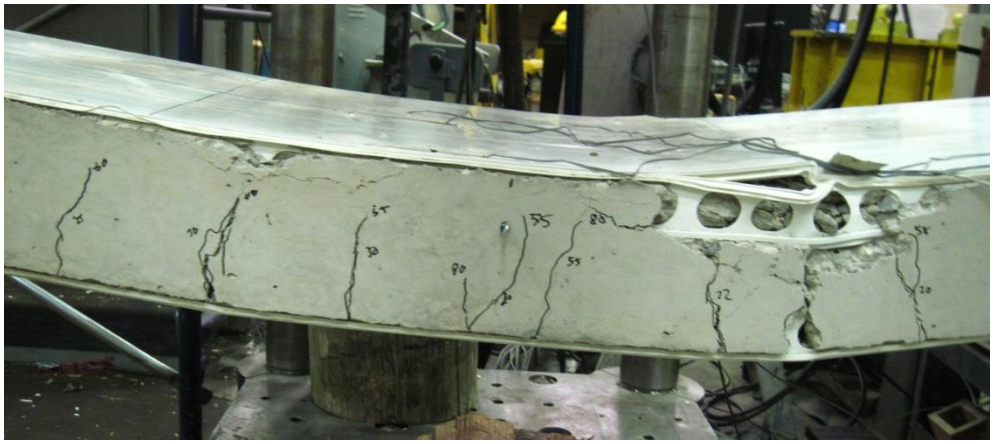

Figure 5.11: Failure at right loading point for wall PH-6-15.

The strain in the tension PVC panel (ε_{pvcpt}) as estimated by the model is compared with the experimental strain values recorded during testing. The results are presented in Tables 5.3 and 5.4. The experimental strain values are an average of the gauges readings at the ultimate load level. The recorded strain level is highly dependent on where the gauge is in relation to the failure location (crack locations) of the specimen. Overall, the calculated strains at ultimate load are in good agreement with the experimental results.

The largest overestimation of ultimate strain is for wall PF-6-10, a 6-inch thick wall encased with flat panels and reinforced with 10M rebars. The strain gauges on the PVC panel were not at the failure location of the specimen, reducing the recorded strain reading at ultimate load. For specimens encased with hollow panels, the greatest underestimation of ultimate strain is for wall PH-8-15. The recorded strain was nearly double the calculated strain (35000με vs 19700με). Despite this discrepancy, at the calculated strain value the wall achieved 97% of the recorded ultimate load.

Table 5.3: Comparison of ultimate tensile strain values for flat panels

	Tension Strain (με)			
Wall	Experimental	Calculated	Difference	Error (%)
PF-6-10	17000	27400	-10400	38%
PF-6-15	18500	15100	3400	23%
PF-7-10	35500	33000	2500	8%
PF-7-15	19000	18100	900	5%
PF-8-10	N/A	39000	N/A	N/A
PF-8-15	25400	21400	4000	19%

The flat panel strain values are closer on average than the corresponding hollow panel walls, with an average error of 18% (as compared with 24% for hollow panel walls). This lower variance could be attributed to the panel slips observed in the hollow panel specimens, as the model assumed perfect bond between the concrete and PVC.

Table 5.4: Comparison of ultimate tensile strain values for hollow panels

	Tension Strain (με)			
Wall	Experimental	Calculated	Difference	Error (%)
PH-6-10	21000	24900	-3900	16%
PH-6-15	15600	13500	2100	16%
PH-7-10	22600	30000	-7400	25%
PH-7-15	19000	16800	2200	13%
PH-8-10	36000	36000	0	0%
PH-8-15	35000	19700	15300	78%

A closer examination of the hollow panel strain values show that walls with 10M reinforcing bars overestimated the strain values and walls with 15M reinforcing bars are underestimated. As the loads experienced by the 10M reinforced walls are lower than corresponding 15M specimens, there is less ‘clamping force’ or applied friction at the supports to prevent the panels from slipping. The slips in the 10M specimens also

contributed to the experimental strains at ultimate being lower than the corresponding calculated ultimate strains, where a perfect composite bond was assumed.

In addition, the estimated and calculated strain values tend to be higher in walls with less steel reinforcing, exceeding 20000με in each case. This value of strain corresponds to the maximum stress in the PVC, increasing the likelihood for slips to occur. This stress within the panel would have the highest possibility of exceeding the frictional resistance between the concrete and PVC, as well as the clamping force at the supports. Conversely, walls with hollow panels reinforced with 15M bars showed experimental strain values higher than the calculated values. These conservative estimates (with the exception of wall PH-8-15) are within 16% of the experimental strains. The calculated strain values were also less than 20000με, showing the material had not reached a stress level promoting slip. Finally, due to higher loads experienced by these walls, the clamping force at the supports increased, reducing the severity and extent of panel slip.

The model was also used to calculate the wall curvature at the ultimate load level. This curvature was determined using the following equation [5-22]

$$\phi_{ult} = \frac{\epsilon_{cu}}{c} \qquad [5\text{-}22]$$

Where ϕ_{ult} is the ultimate curvature in mm^{-1}, ε_{cu} is the crushing strain of concrete, and c is the depth of the neutral axis. The experimental curvatures were calculated using the strain data at ultimate load. Table 5.5 presents a comparison between the experimental and

ultimate curvatures. Three wall specimens did not have concrete strain gauges to determine the experimental curvature.

Table 5.5: Comparison of Experimental and Ultimate Curvatures

	Ultimate Curvature (ϕ_{ult})		
Wall	Experimental	Calculated	Error
Flat Panel Encased			
PF-6-10	0.000138	0.000206	33%
PF-6-15	0.000149	0.00012	-24%
PF-7-10	0.000218	0.0002	-9%
PF-7-15	0.000123	0.000118	-4%
PF-8-10	N/A	N/A	
PF-8-15	0.000141	0.000116	-22%
Hollow Panel Encased			
PH-6-10	0.000174	0.000127	-37%
PH-6-15	0.000136	0.00012	-13%
PH-7-10	N/A	N/A	
PH-7-15	0.000123	0.000117	-5%
PH-8-10	N/A	N/A	
PH-8-15	0.000197	0.000115	-72%

The average error for the walls was -24%, with the model consistently underestimating the experimental curvature. The model used a concrete crushing strain of 3500με, however many of the walls exceeded this strain and crushed at approximately 4000με. If a strain value of 4000με is used the average error is reduced to 17%. This change resulted in most curvature estimates exceeding the experimental results, creating conservative estimates of the ultimate curvature. The adjustment in crushing strain changed the ultimate load resistance calculations by ±1%, and was therefore not a significant adjustment to the load estimation of the model.

5.6 Model Results with Modifications to Wall Cross-sections

Since the proposed model provided results in good agreement with the experimental results, two modifications to the PVC encased walls that were not tested in the experimental program are presented. The first modification adjusts the depth of reinforcing steel to be consistent for both flat and hollow panel walls. Second, an 'optimized' panel layout is explored, using a combination of hollow and flat panels to maximize yield and ultimate load levels. These new walls are shown in Figure 5.12.

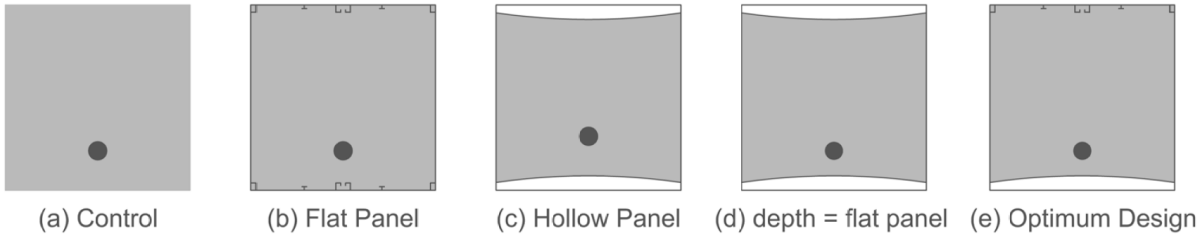

Figure 5.12: Summary of tested (a-c) and modified (d, e) wall cross-sections.

5.6.1 Effect of the steel reinforcing depth on yield and ultimate loads for hollow panel walls

For the walls with hollow panels and flat panels, the location of the reinforcing steel was inconsistent due to the panel thickness. The depth of the steel for walls encased with hollow panels was set in the model to match the reinforcement depth in the control and PVC encased walls with flat panels. Figure 5.13 presents the calculated yield load predictions for the tested walls, grouped with constant thickness and reinforcement (i.e., the data group labeled '6"-10' shows 6 inch thick walls reinforced with 10M reinforcing steel). The fourth column in each group shows results if the hollow panel encased walls had steel reinforcement depth equal to the walls with flat panels.

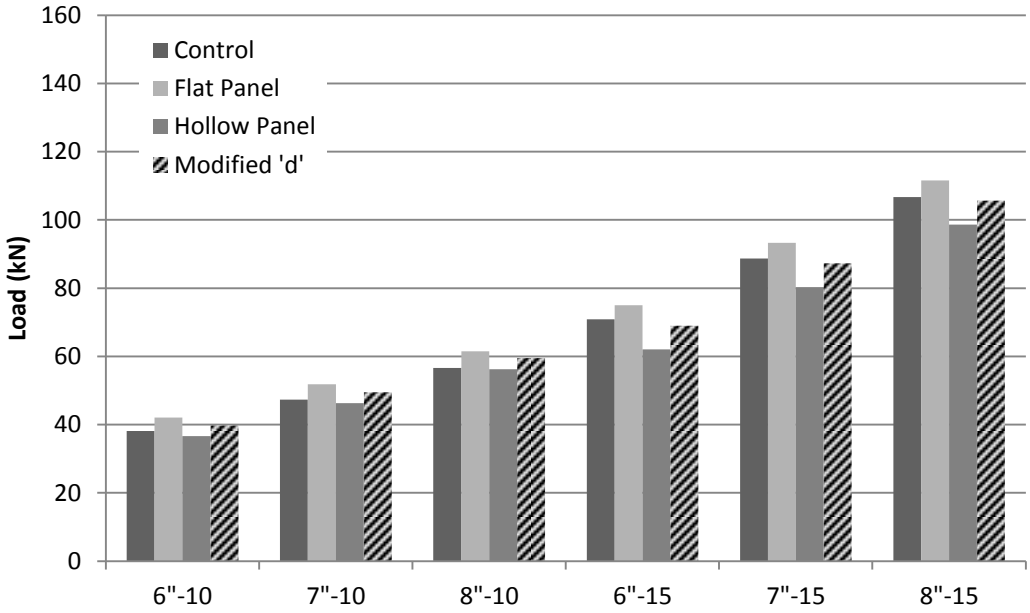

Figure 5.13: Effect of the steel reinforcement depth on the yield load

Increasing the depth of the steel reinforcement improves the yield load in each data set over the tested hollow panel encased specimens. The improvement is more pronounced in walls with more steel reinforcement. The calculated load for wall with 10M bars show an increased yield load by an average of 7%, while wall with 15M bars show an improved yield load by an average of 9%. This trend is expected as the PVC encased walls with greater amounts of reinforcement would be more sensitive to the location of the reinforcing steel. Higher reinforcement areas increase the tension force at the yielding point, assuming a greater portion of the tensile force felt within the cross-section (compared to PVC) to satisfy equilibrium. The anticipated improvement also depends on the thickness of the wall. Thinner walls (152 mm) show the highest improvement. For example, 152 mm thick walls reinforced with 15M bars improve yield load by 11% while 203 mm thick walls experience a 7.5% increase. Recall that the modification to the wall sections was an 11 mm increase in

the depth of reinforcement for all wall thicknesses, representing 7% and 5% of the thickness of 152 mm thick and 203 mm thick walls respectively. Hence, the sensitivity to this change is most apparent in thinner sections, resulting in the highest increase in the load resistance.

For all six data sets, the yield load achieved by the modified hollow panel encased specimens is less than the equivalent flat panel encased walls. In addition, walls reinforced with 15M bars achieve less yield load than the corresponding control specimens. This is due to the panel thickness reducing concrete core and thus the moment arm between the concrete compression block and steel tensile forces. Despite the concrete wall core reduction, walls with hollow panel reinforced with 10M rebars show a slight load increase over the respective control specimens. This is due to the PVC panel in tension having a greater influence in the moment resistance of the wall, offsetting the effective concrete section reduction.

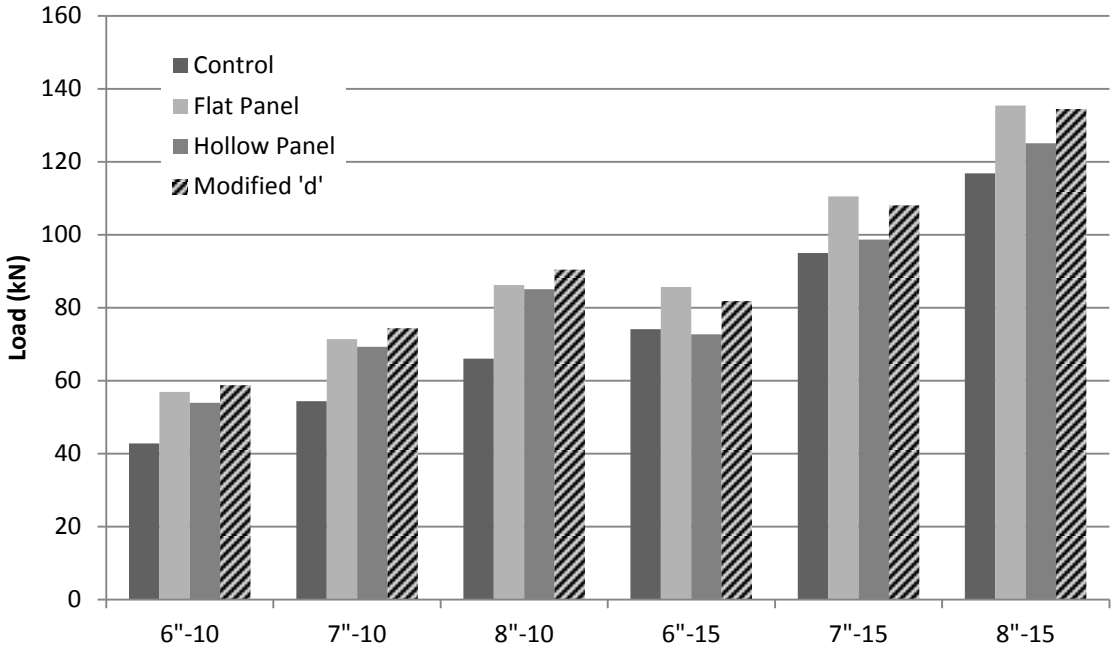

Figure 5.14: Ultimate load for wall sections with equivalent depth of steel reinforcement

Figure 5.14 presents the results of the modified hollow panel reinforcement depth for ultimate load conditions. Similar to the yield load results, the amount of improvement in the ultimate load results over the tested hollow panel encased walls depends on wall thickness and reinforcing quantity. The anticipated load from the model exceeds the equivalent anticipated load for the flat panel walls reinforced with 10M reinforced walls. However, for walls reinforced with 15M, the ultimate load prediction for the modified walls remains less than the walls with the flat panels. This difference is attributed to the reduction in the moment arm of the force couple between the concrete compression core and steel reinforcing. Regardless for all cases, the hollow panel encased walls with equivalent steel reinforcing depth shows a significant increase in ultimate load capacity over the corresponding control walls.

5.6.2 Yield and Ultimate Load prediction with Optimized Panel Layout

A second modification to the wall cross-section is analyzed. A flat panel is used on the compression side of the wall while a hollow panel is placed on the tension side. The depth of steel reinforcement is kept equal to the depth in the experimental test program flat panel and control walls. This proposed layout is deemed to be an optimal configuration of panels as it benefits from increased PVC cross-sectional area to resist tensile forces (hollow panel) without reducing the effective concrete area thickness. The configuration favours loading cases where bending is dominant in one direction, such as retaining walls and water/chemical holding tanks. Figure 5.15 presents the yield load results for this optimal section in comparison to the tested wall sections.

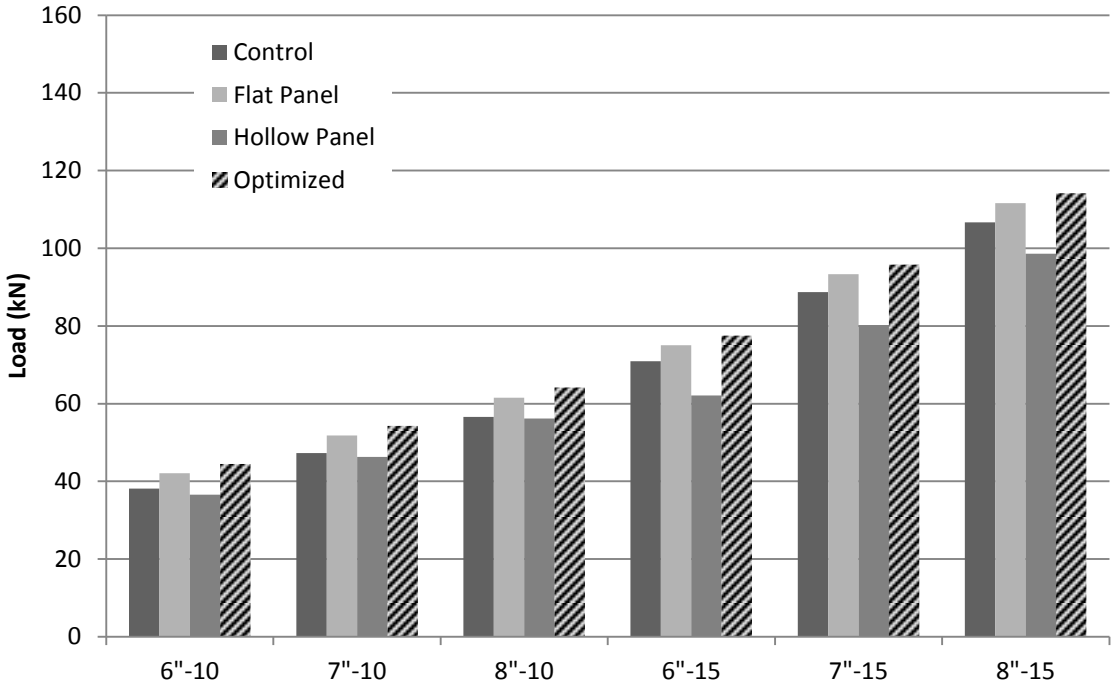

Figure 5.15: Yield load calculated for optimized PVC encasement

The optimized section results in the greatest increase in yield load over the control walls. The improvement observed depended on the quantity of steel reinforcement and the wall thickness. Walls reinforced with 10M bars show an average increase in yield load of 15%, while walls reinforced with 15M bars improve by an average of 8%. As the wall thickness increased, the expected improvement for yield load decreased. For example, walls with the optimized layout and reinforced with 10M bars show an increase in yield load of 17%, 15%, and 13% for 152 mm, 178 mm, and 203 mm thick walls, respectively.

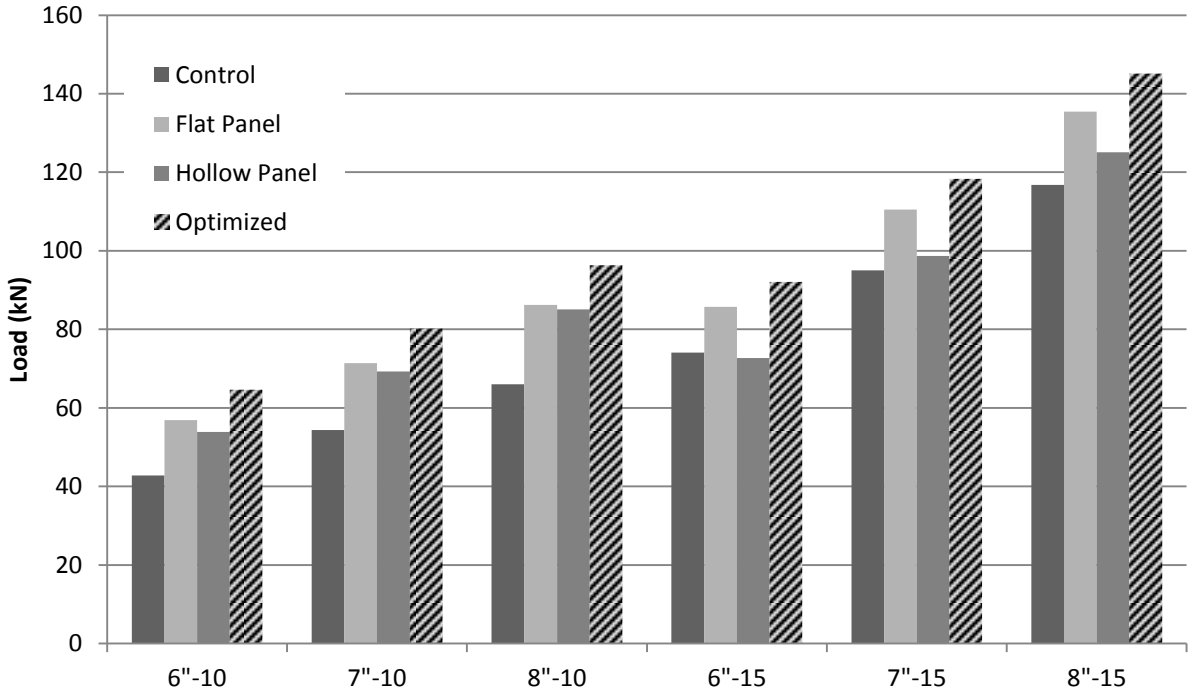

Figure 5.16: Ultimate load prediction for optimized PVC encased wall.

Figure 5.16 presents the ultimate load prediction for the optimized PVC encased section. At ultimate load level, the optimized PVC encased walls improve the load capacity by an average of 48% and 24% over their equivalent control walls reinforced with 10M and 15M rebars, respectively. This difference is expected as the effective contribution of the PVC at ultimate load decreases as the amount of reinforcement increases. For example, in 203 mm thick walls reinforced with 10M bars, the PVC panels contribute 34% of the tensile force at ultimate load. Conversely, 203 mm thick walls with 15M rebars experience PVC panel contribution of 21%, a reduction in effective contribution to the load resistance.

Finally, the predicted improvement is pronounced enough for the PVC encased walls to provide the same or greater ultimate load than a thicker conventionally reinforced concrete wall. For example, a 178 mm thick 15M rebar reinforced PVC encased wall utilizing the

proposed panel layout resulted in an ultimate load of 118 kN, while a 203 mm thick concrete wall without encasement resists a load of 116 kN.

5.7 Summary of Analytical Model Development

An analytical model was developed to estimate the yield and ultimate load level for PVC encased reinforced concrete walls. The following findings are concluded from the model results.

Yield Load

Elastic analysis is used to estimate the yield load resistance. The results from the model are found to be in good agreement with the test results, with an average error of 8% for the control walls and 5% for the encased walls.

Ultimate Load

Linear strain compatibility is used to estimate the ultimate load resistance. The results from the model are in good agreement with the experimental data. The average error for the control specimens is 3%. The flat panel encased walls have an average error of 3%, while the hollow panel encased walls have an average error of 6%.

Modified Cross-sections

With the model producing estimates in close agreement with the experimental results, the model is used to estimate the results for two more cross-section types; hollow panel encased walls with steel reinforcement depth equal to the test program depth, and a wall cross-section that utilized flat panels on the compression side and hollow panels on the tension side. The hollow panel cross-section with equivalent steel depth

improve the yield and ultimate loads by an average of 8% over the tested hollow panel wall. The later combination of panels results in the largest predicted increase in both yield and ultimate load levels. The average yield load improvement is 15% and 8% for 10M and 15M walls, while ultimate load improvement is 48% and 24% respectively.

In comparing the relative improvements in load of the PVC encased walls over the control walls, the effect is most apparent at the ultimate load level. The contribution of the PVC when steel is yielding is minimal as the strain levels observed and calculated reflect PVC stresses that are approximately 25% of the ultimate tensile stress. Conversely, at the ultimate condition, the PVC stress level is close to or at maximum, providing a much more significant portion of the cross sections resistance.

Chapter 6: Conclusions and Recommendations

6.1 Experimental Work

Experimental and analytical studies were conducted on the behaviour of reinforced concrete walls that were encased in PVC stay-in-place formwork. Eighteen reinforced concrete walls were cast and tested in four-point bending. Three test variables were examined; the type of PVC panel (flat or hollow), amount of steel reinforcing (3-10M or 3-15M bars), and wall thickness (152 mm, 178 mm, or 203mm). The following conclusions can be made from the experimental results.

- The mode of failure observed was different for each type of specimen. Control walls failed due to steel yielding followed by concrete crushing. For wall specimens encased in flat panel PVC and reinforced with 10M bars, the failure mode was through steel yielding, followed by concrete crushing, PVC buckling and finally PVC rupture. Flat panel encased walls reinforced with 15M bars experienced failure through steel yielding, followed by concrete crushing and PVC buckling. For walls encased in hollow panels, all specimens failed by steel yielding, followed by concrete crushing and PVC buckling.
- Unlike the modes of failure reported in the literature, PVC panel slip was observed during the testing of hollow panel encased walls. The majority of these slips occurred when the recorded strain values in the panels were approaching the strain at maximum stress, approximately 25000με.

- PVC encasement improved the load capacity of the reinforced concrete walls. For flat panel encased walls, the average improvement at yield and ultimate loads were 21% and 27% respectively. Hollow panel encased walls recorded average yield and ultimate load improvements of 8% and 27% respectively. Therefore, the flat panel encased walls showed better over improvement to load resistance. This is due to the shallow location of the steel reinforcement in the hollow panel encased walls, reducing the effective improvement given from the panels. The observed improvement was more significant at ultimate load conditions due to the higher stresses in the tension PVC panels contributing to the load resistance.
- The amount of load carrying improvement was found to be a function of the reinforcing ratio and wall thickness. The effect of the PVC encasement lessened as the reinforcing ratio or wall thickness increased. Lightly reinforced, thin walls had the highest improvement. As the reinforcing ratio increased, the strains in the tension side of the walls at failure were significantly lowered. As the PVC does not achieve maximum stress until high strains are reached, the contribution of the panels to resisting the applied loads is lessened. In addition, increasing the amount of steel reinforcement reduces the relative contribution of the PVC to the cross-section.
- A comparison was made between walls with the SIP PVC system and walls that were conventionally constructed and 25mm (1") thicker. The yield and peak loads were very similar in this comparison, suggesting the potential for using the SIP

system as a means to reduce the wall thickness and achieve the same structural performance.

- PVC encasement improved the ductility at ultimate load level and the toughness of the reinforced concrete walls. Flat panel encased walls improved ductility by an average of 71% and toughness by 122%. Hollow panel encased walls improved ductility by an average of 29% and toughness by 70%. Flat panel encased walls were determined to be better at improving ductility and toughness, as composite behaviour was achieved, while the hollow panels did not behave as a pure composite.
- There was no statistic difference observed in the concrete strength of PVC encased walls and traditionally formed concrete.

6.2 Analytical Work

In addition to the experimental testing, an analytical program was developed to estimate the yield and ultimate loads of PVC encased reinforced concrete walls. The model followed linear strain compatibility to estimate the internal forces of the wall elements. The following conclusions were made from the results of the model.

- Calculated yield loads were in good agreement with the experimental data, with an average error of 8% for the control walls and 5% for the PVC encased walls.
- Calculated ultimate (peak) loads showed good correlation with the experimental data. The average error for the control, flat panel and hollow panel encased walls were 3%, 3% and 6% respectively.

- Calculated and experimental PVC tensile strain values were in good correlation at ultimate load conditions. The average error for PVC tensile strain prediction was 21%.

- With the proposed model providing results in good agreement with the test data, other PVC encased wall cross-sections were explored. An optimized panel layout was proposed that utilized flat panels on the compression side of the wall and hollow panels on the tension side. This configuration of panels resulted in the greatest estimated improvement over the control walls at both yield and ultimate load levels.

6.3 Recommendations and Proposed Future Work

The following topics are proposed for further investigation in light of the work completed in this study.

- A new cross-section layout was examined using the model developed in this research. It is recommended that walls be cast and tested using this configuration of PVC encasement in order to confirm the predicted load resistance behaviour. This configuration is of particular interest in situations where one-way bending would dominate, such as retaining walls and holding tanks.

- The analytical model developed by this research assumed perfect bond between the concrete and PVC hollow panel. Slips were observed during testing of the hollow panel encased walls, suggesting that only partial bond exists. Frictional and bond tests between the PVC panels and concrete should be investigated.

- In order to assure bond and full composite action is achieved between the hollow panel PVC and concrete, the use of a gritting material should be considered. For instance, 152 mm (6”) thick walls encased in sand coated hollow panels should be tested to determine if the slip will occur or not.
- The nubs present on the interior face of the flat panels appeared to be sufficient in providing this composite behaviour. These nubs could be potentially be incorporated into the hollow panels as well.

References

ACI 440.R1-06. (2006). Guide for the Design and Construction of Structural Concrete Reinforced with FRP Bars. *ACI 440.1R-06*.

Bank, L. C., & Oliva, M. G. (2007). Pultruded FRP Plank as Formwork and Reinforcement for Concrete Members. *Advances in Structural Engineering*, 525-535.

Cement Association of Canada. (2006). *Concrete Design Handbook.* Ottawa.

Chahrour, A. H., Soudki, K. A., & Straube, J. (2005). RBS polymer encased concrete wall part I: experimental and theoretical provisions for flexure and shear. *Construction and Building Materials*, 550-563.

Collins, M. P., & Mitchell, D. (1997). *Prestressed Concrete Structures.* Toronto: Response Publications.

Dieter, D. A., & Dietsche, J. S. (2006). Concrete Bridge Decks Constructed with Fiber-Reinforced Polymer Stay-in-Place Forms and Grid Reinforcing. *Transportation Research Record*, 219-226.

Fam, A. Z., & Rizkalla, S. H. (2002). Flexural Behavior of Concrete-Filled Fibe-Reinforced Polymer Circular Tubes. *Journal of Composites for Construction*, 123-132.

Fam, A., & Nelson, M. (2014). Full bridge testing at scale constructed with novel FRP stay-in-place structural forms for concrete deck. *Construction and Building Materials*, 368-376.

Gia, X., & Darby, A. (2013). Experimental investigation into a ductile FRP stay-in-place formwork system for concrete slabs. *Construction and Building Materials*, 1013-1023.

Kuder, K. G., Gupta, R., Harris-Jones, C., Hawksworth, R., Hendersonq, S., & Whitney, J. (2009). Effect of PVC Stay-In-Place Formwork on Mechanical Performance of Concrete. *Journal of Materials in Civil Engineering*, 307-315.

McClelland, R. (2007). Permanent formwork for composite bridge decks. *Concrete*, 10-11.

Mohamed, H. M., & Masmoudi, R. (2012). Effect of Test Parameters on Flexural strength of Circular fiber-reinforced polymer-confined concrete beams. *Journal of Reinforced Plastics and Composites*, 897-914.

Ritchie, P. A., Thomas, D. A., Lu, L.-W., & Connelly, G. M. (1991). External Reinforcement of Concrete Beams Using Fiber Reinforced Plastics. *ACI Structral Journal*, 490-500.

Rteil, A. A., Soudki, K. A., & Richardson, D. J. (2008). Flexural behavior of octaform forming system. *ACI Special Publication*, 130-144.

Soudki, K., El-Salakawy, E., & Craig, B. (2007). Behavior of CFRP Strengthened Reinforced Concrete Beams in Corrosive Environment. *Journal of Composites for Construction*, 291-298.

Appendix A
Test Results

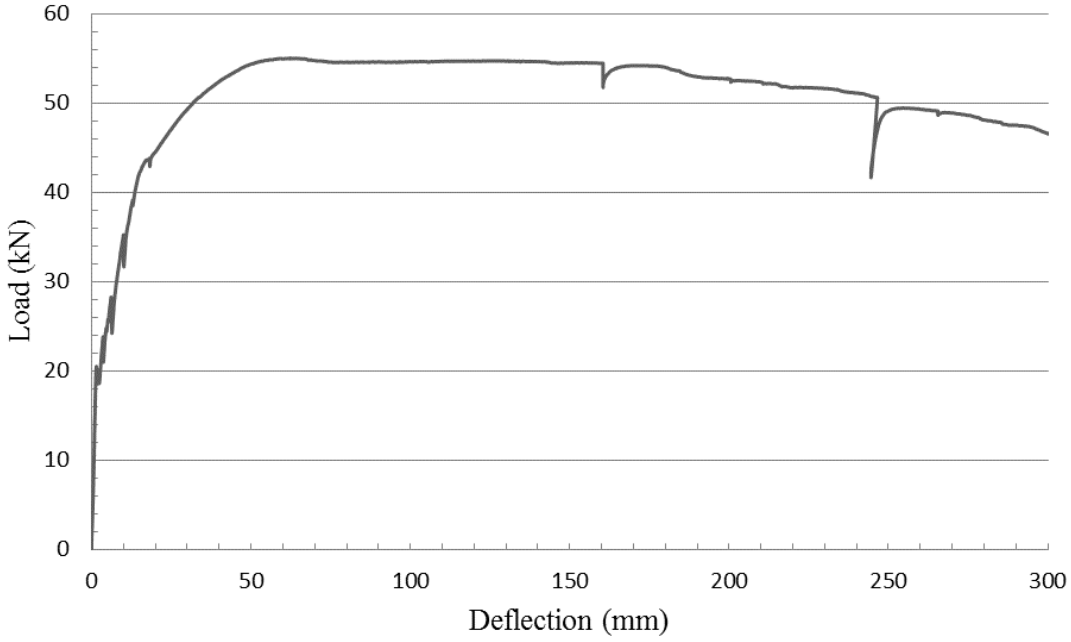

a – load versus mid span deflection

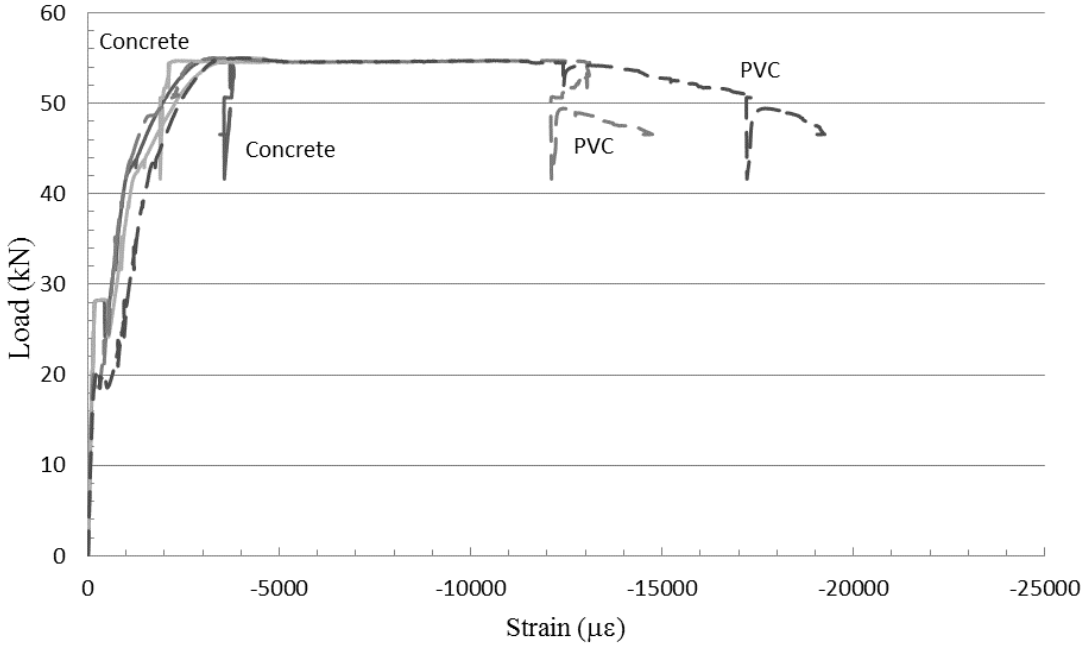

b – load versus compressive strain (Concrete and PVC Panel)

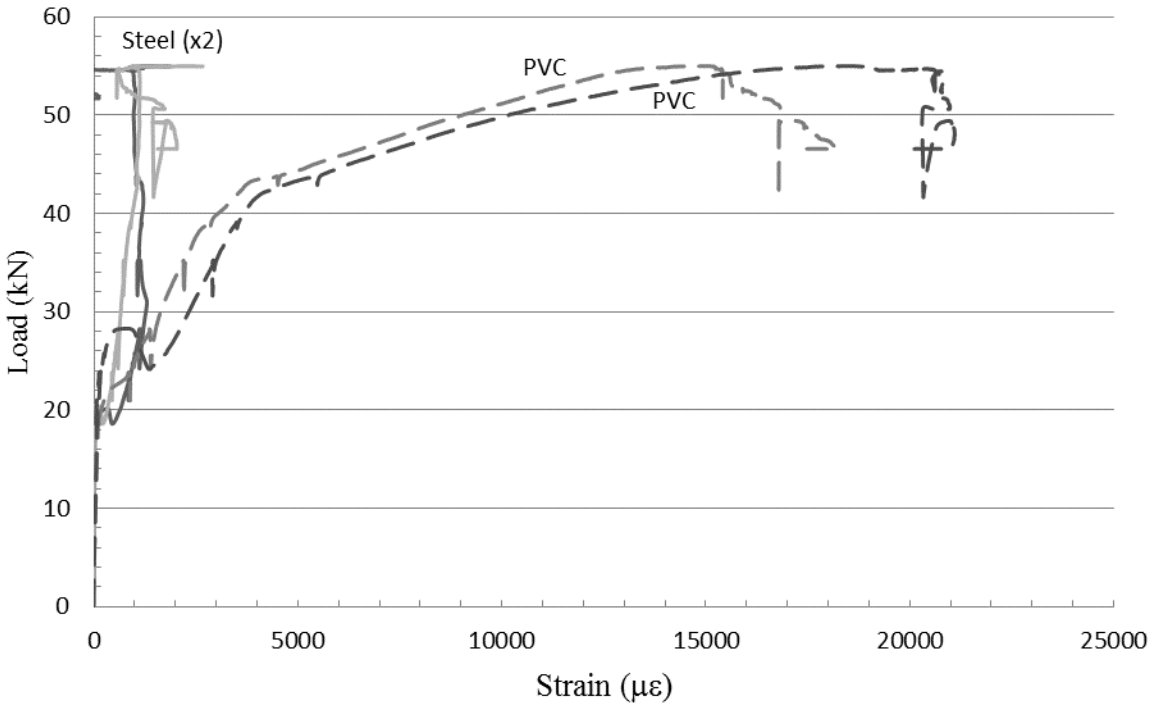

c – load versus tensile strain (steel and PVC panel)

Figure (A-1): Test Results for 6" thick walls reinforced with 3-10M bars

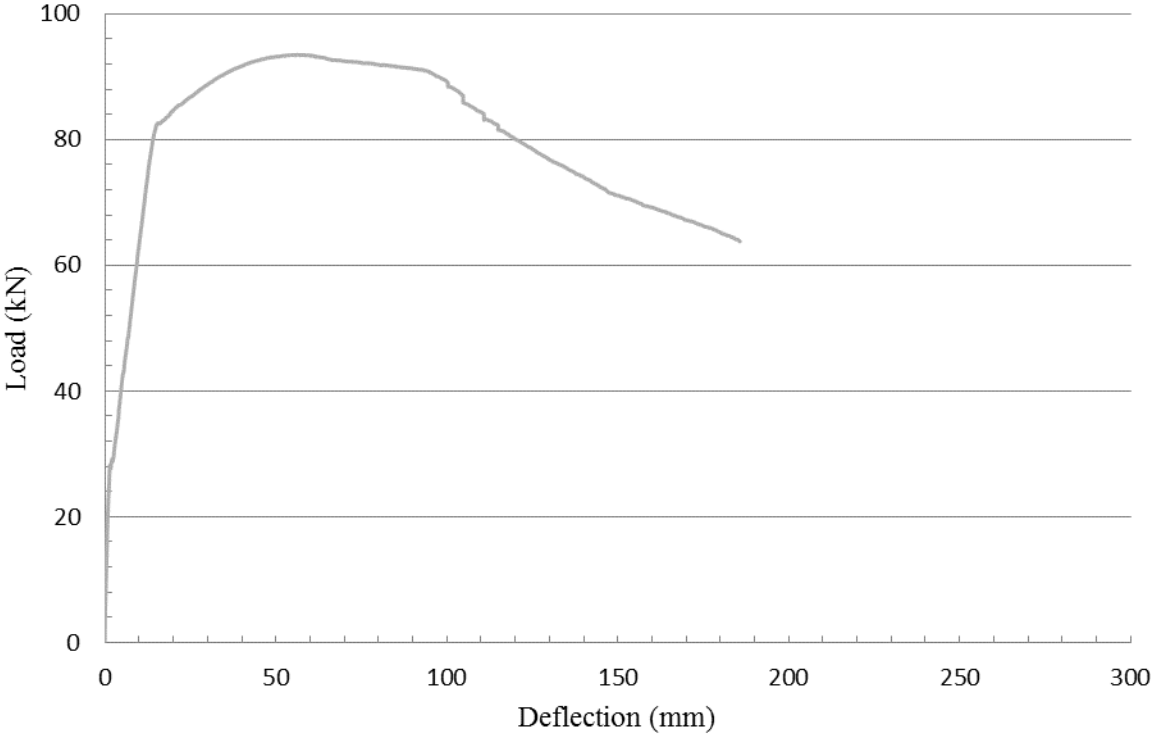

a – load versus mid span deflection

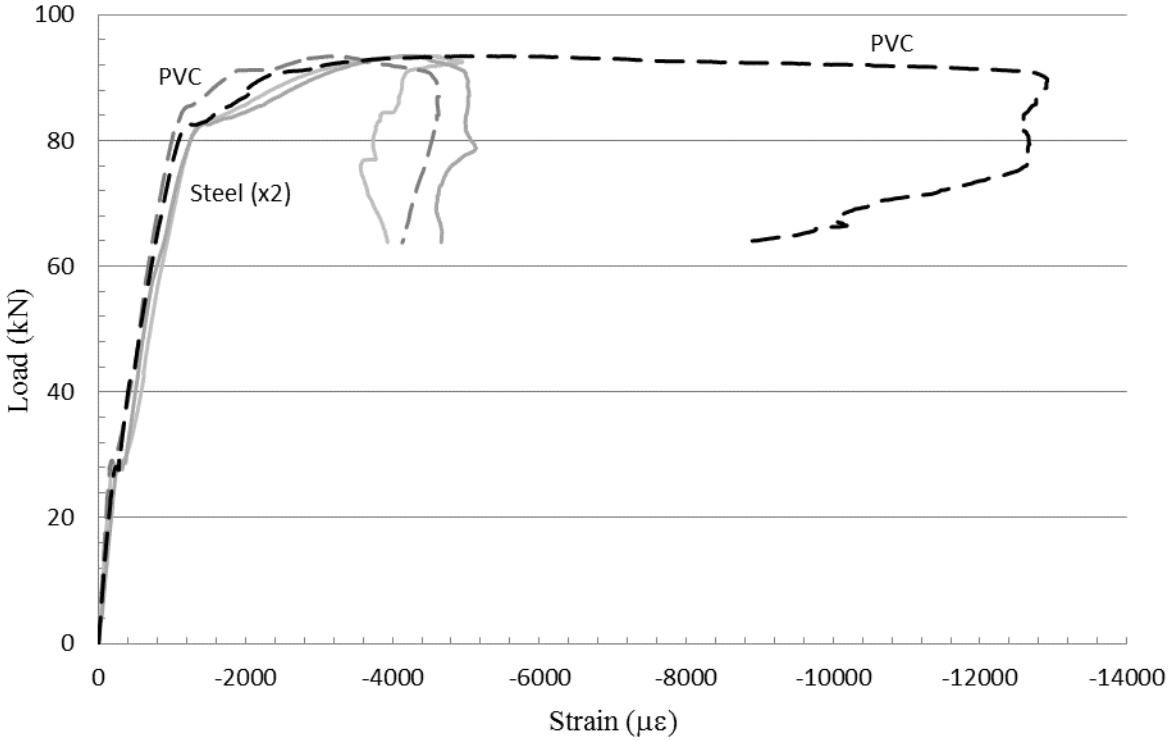

b – load versus compressive strain (Concrete and PVC panel)

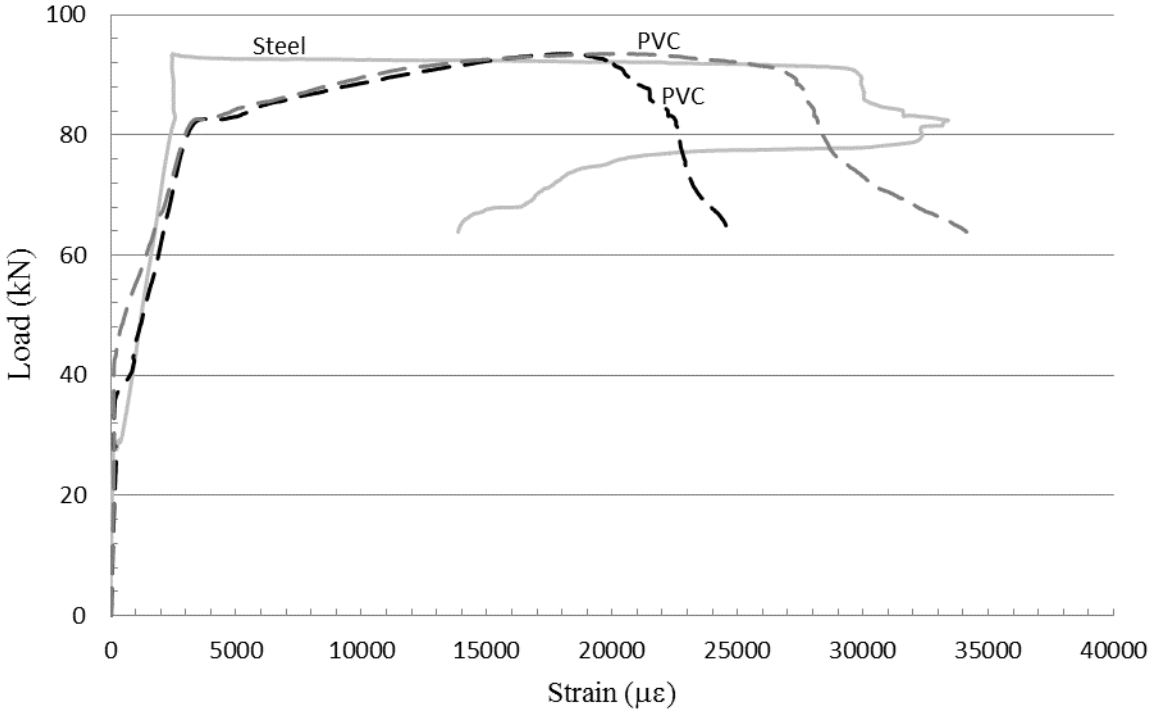

c – load versus tensile strain (steel and PVC panel)

Figure (A-2): Test Results for 6" thick walls reinforced with 3-15M bars

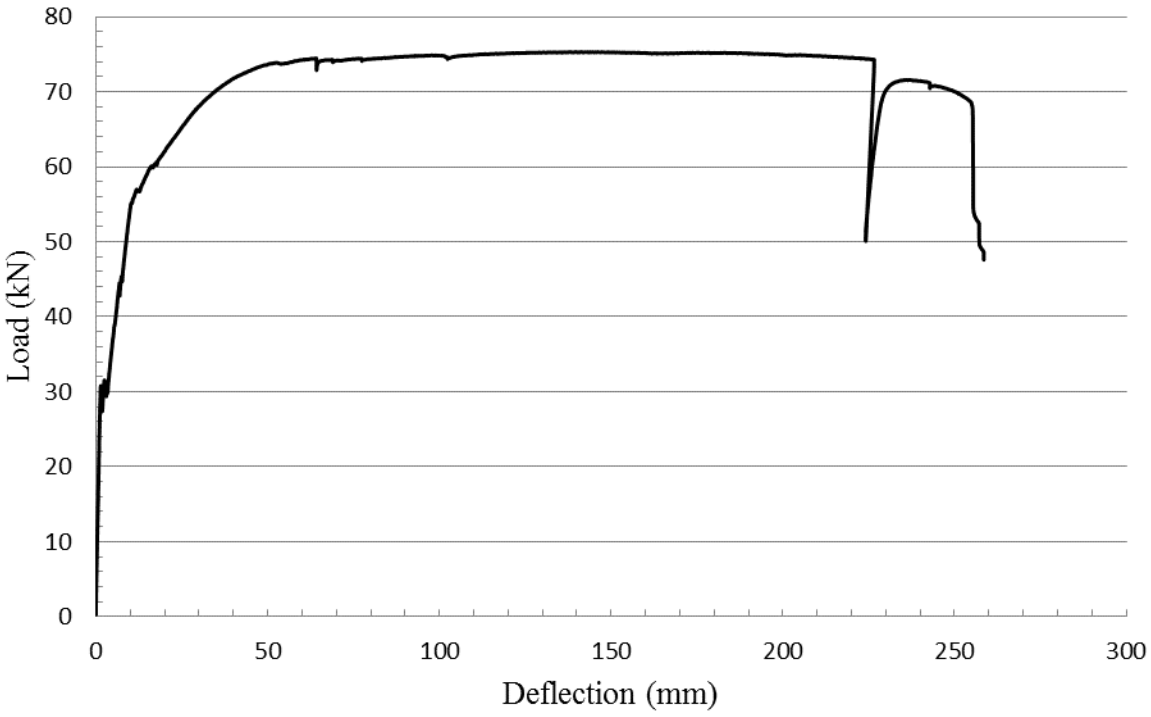

a – load versus mid span deflection

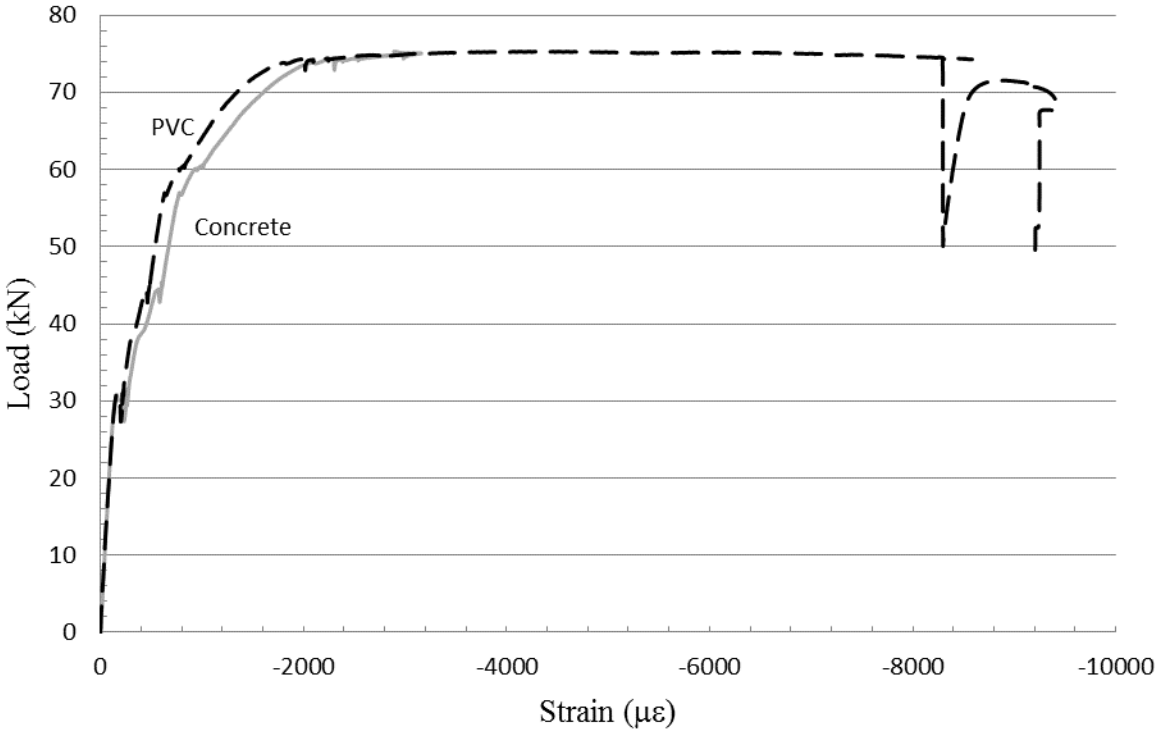

b – load versus compressive strain (concrete and PVC panel)

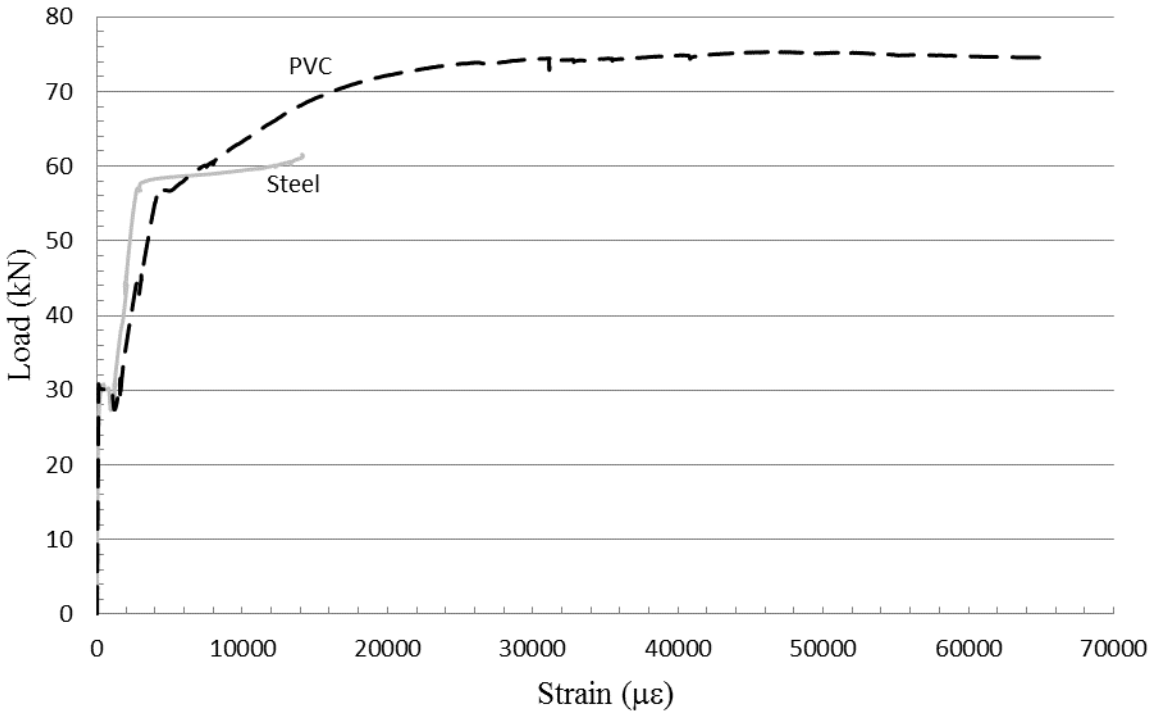

c – load versus tensile strain (steel and PVC panel)

Figure (A-3): Test Results for 7" thick wall reinforced with 3-10M bars

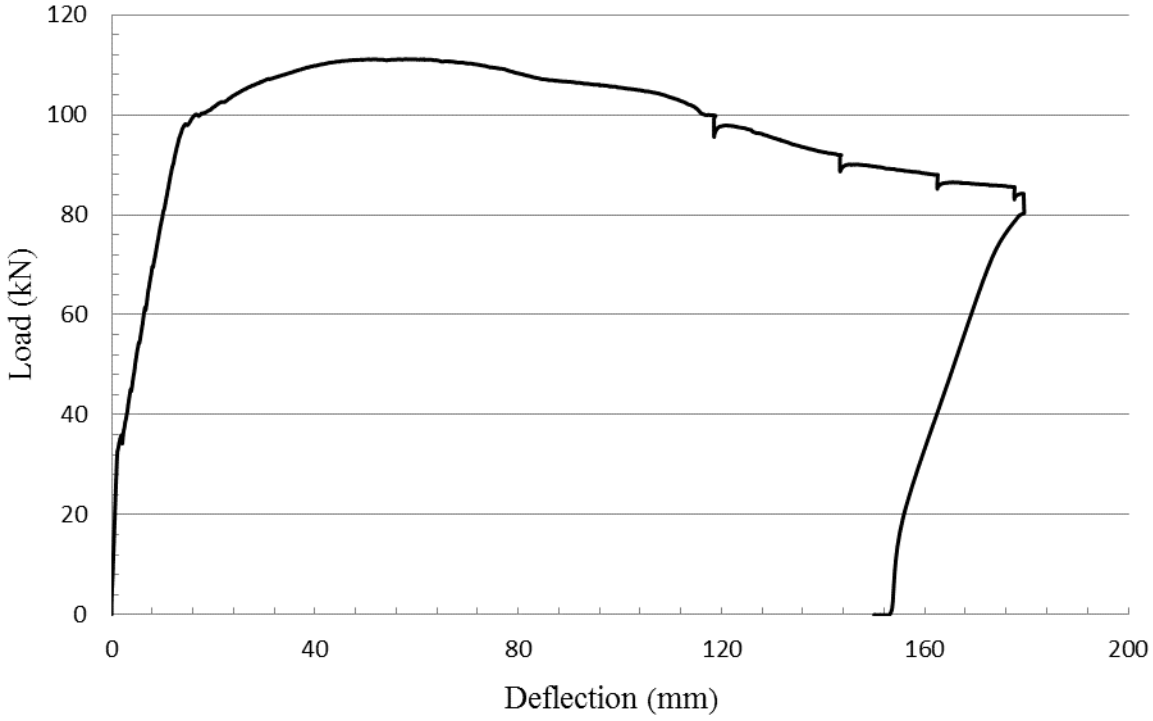

a – load versus mid span deflection

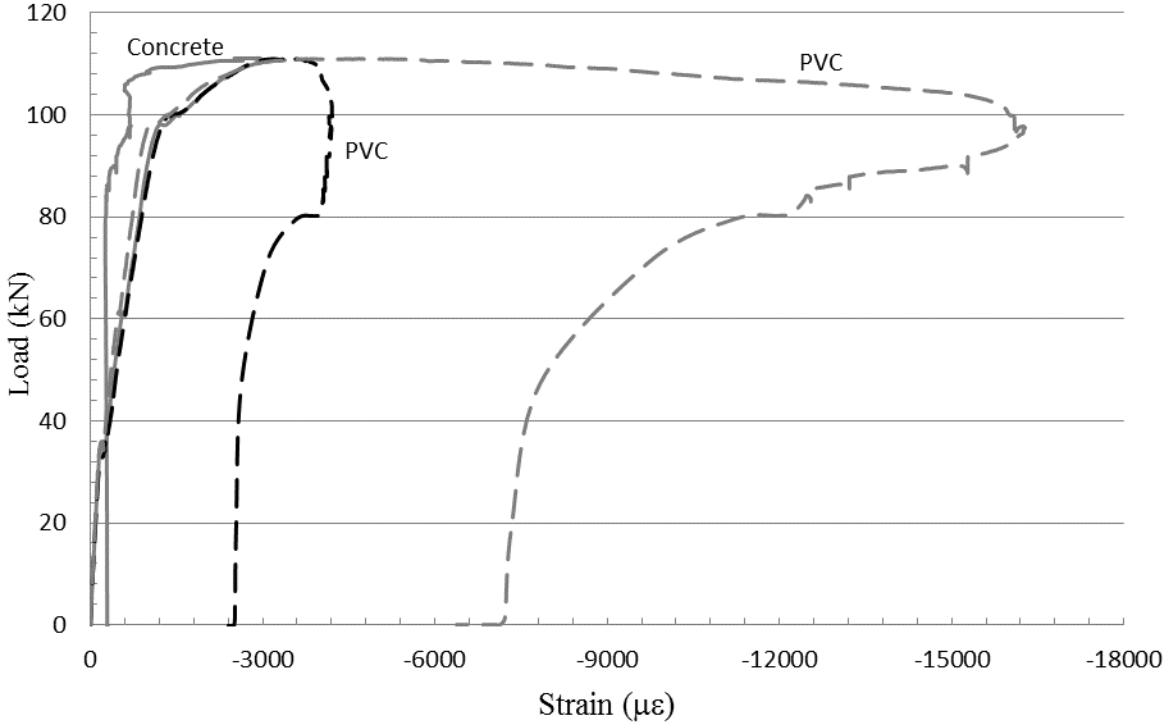

b – load versus compressive strain (Concrete and PVC panel)

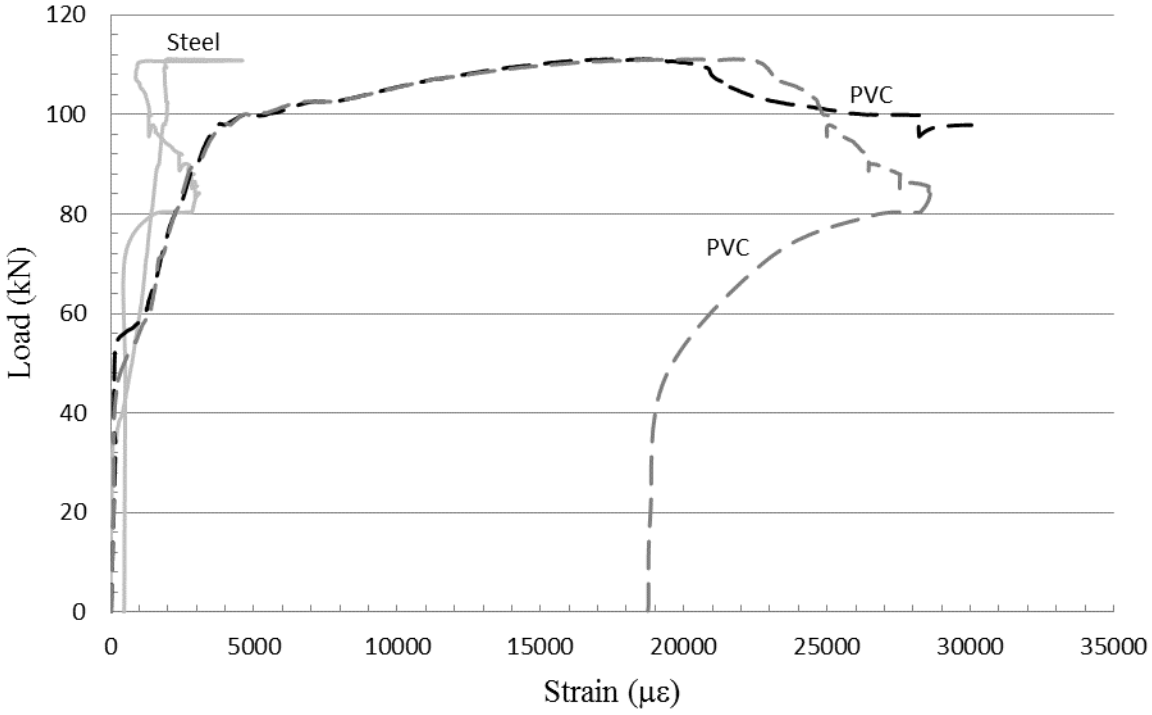

c – load versus tensile strain (steel and PVC panel)

Figure (A-4): Test Results for 7" thick wall reinforced with 3-15M bars

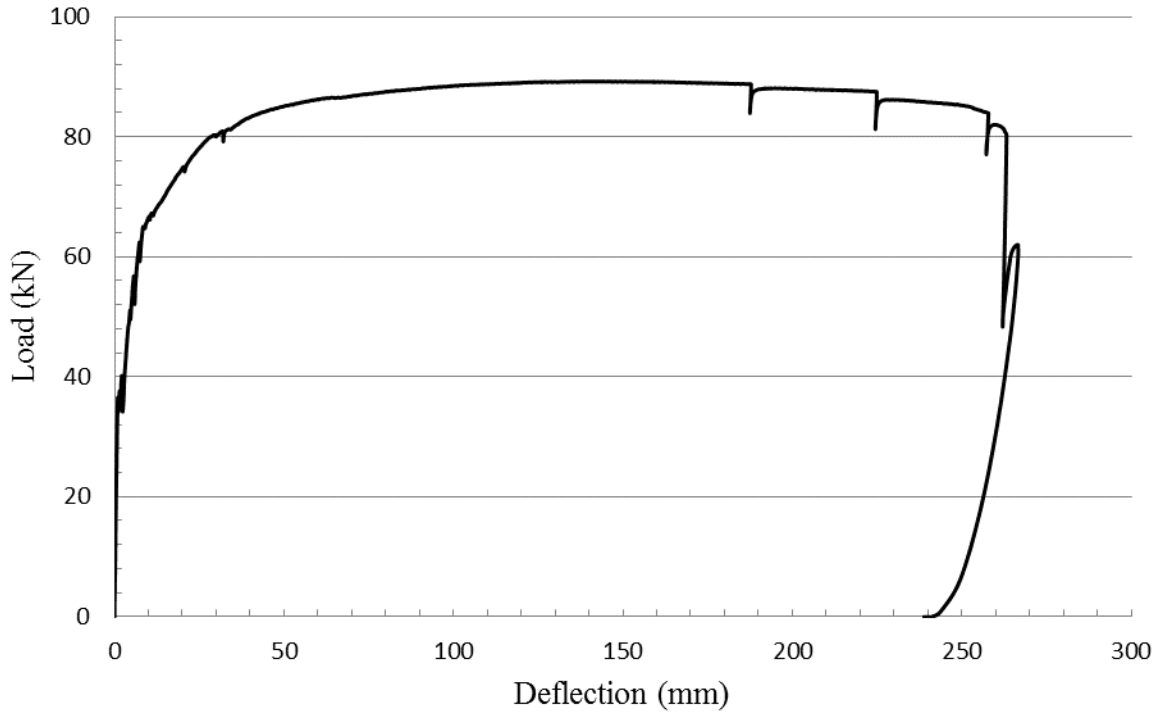

a – load versus mid span deflection

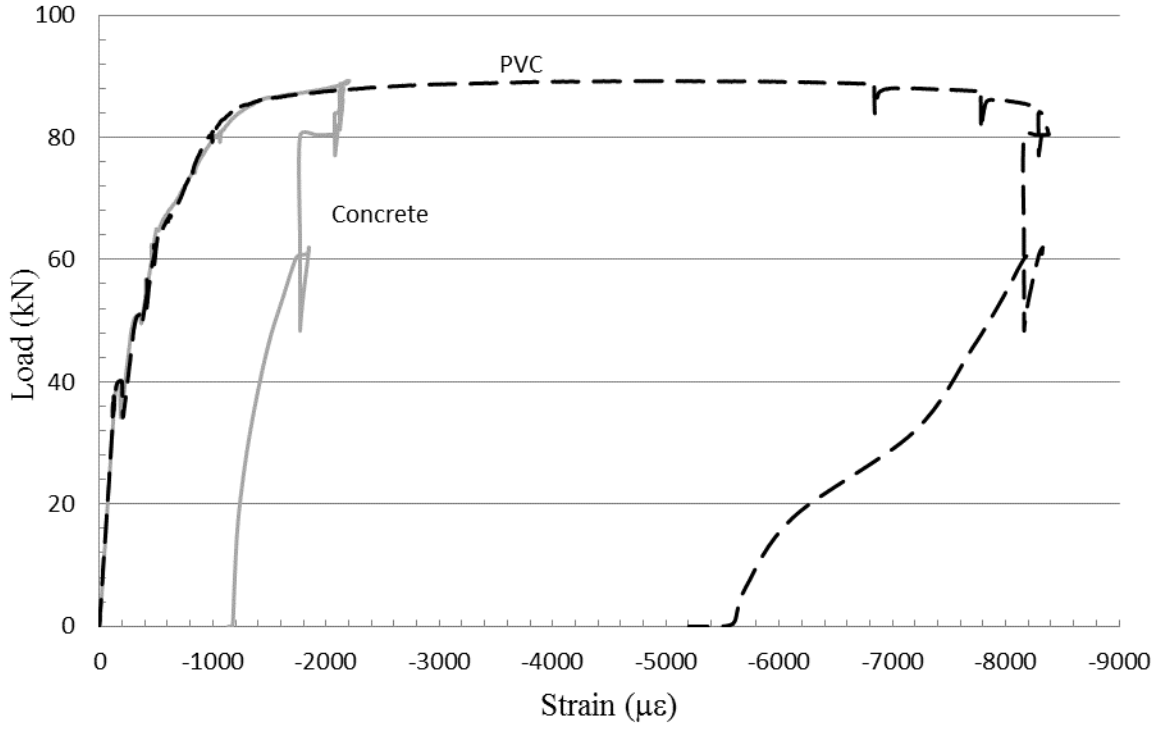

b – load versus compressive strain (Concrete and PVC Panel)

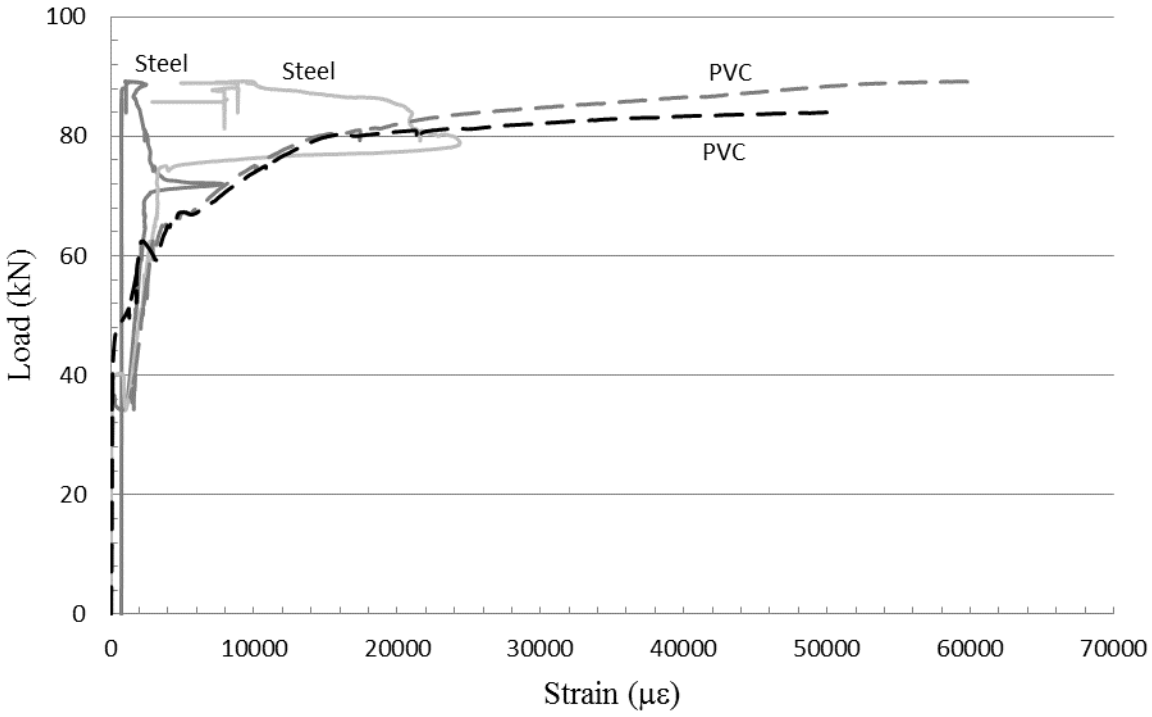

c – load versus tensile strain (steel and PVC panel)

Figure (A-5): Test results for 8" thick wall with 3-10M bars

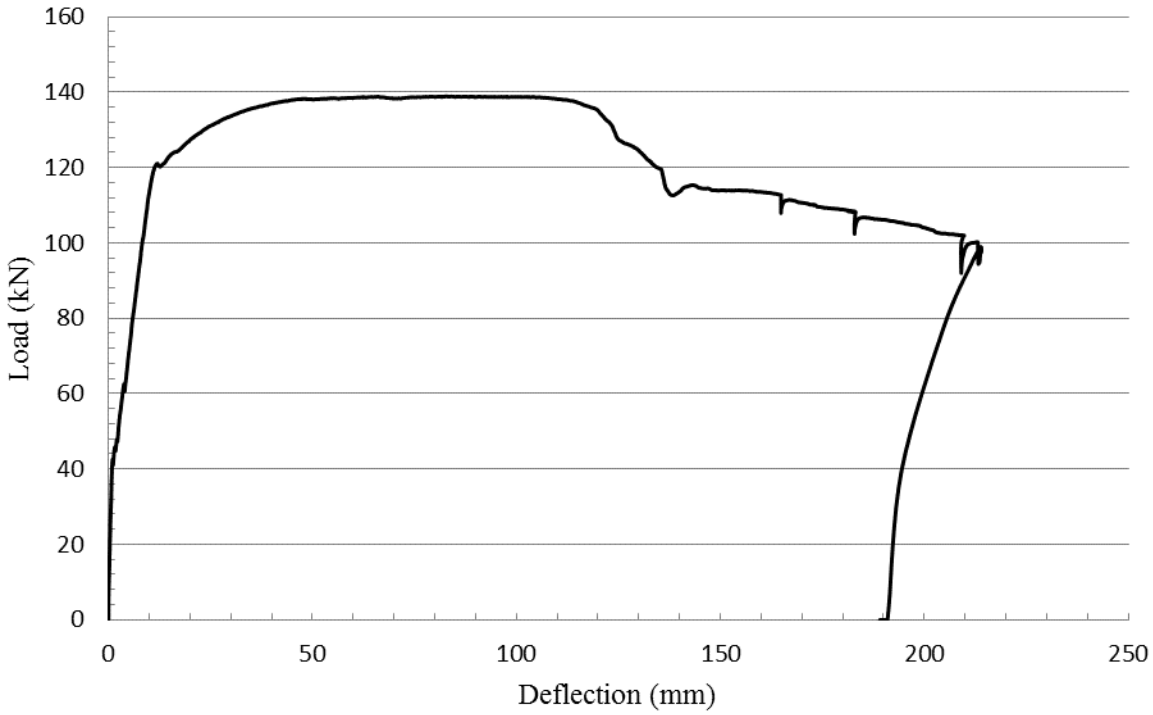

a – load versus mid span deflection

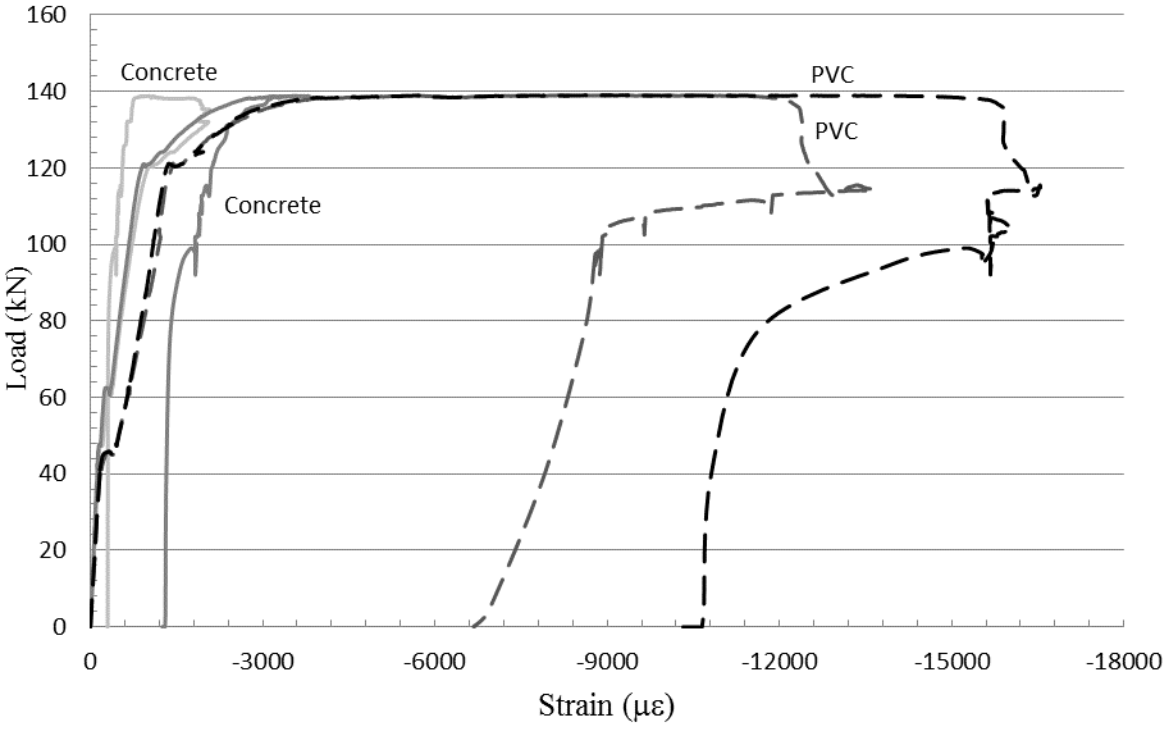

b – load versus compressive strain (concrete and PVC panel)

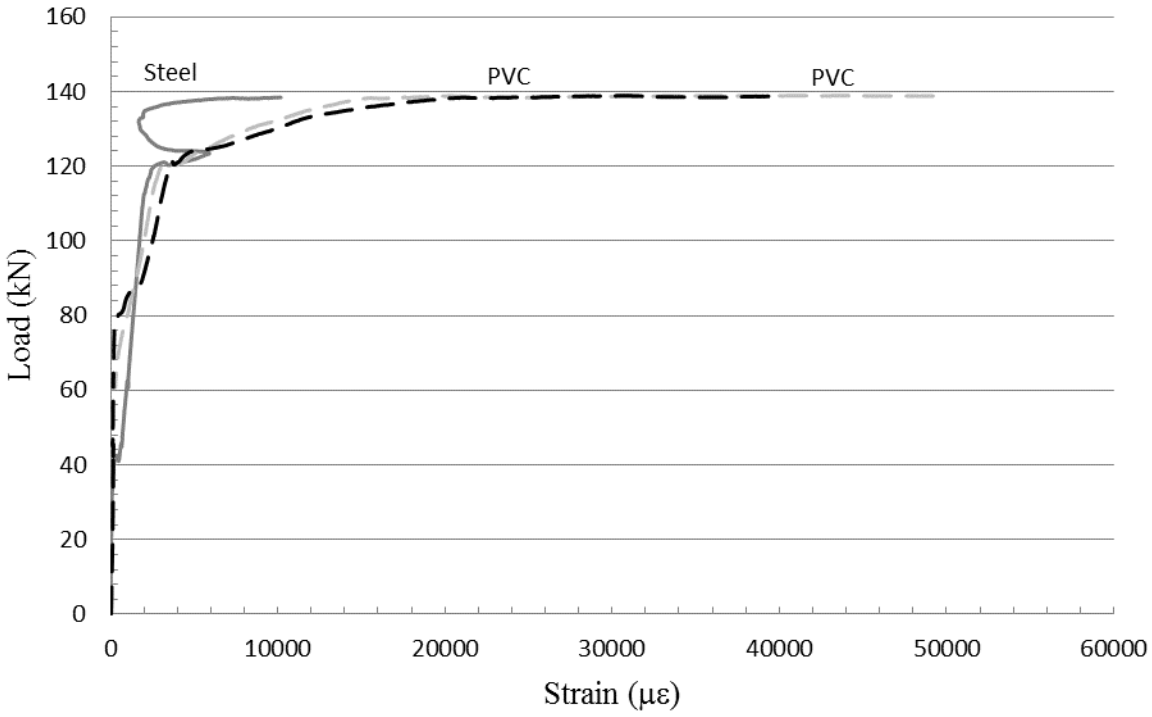

c – load versus tensile strain (steel and PVC panel)

Figure (A-6): Test results for 8" thick wall with 3-15M bars

Part B – Test Results for Hollow Panel Octaform Encased Specimens

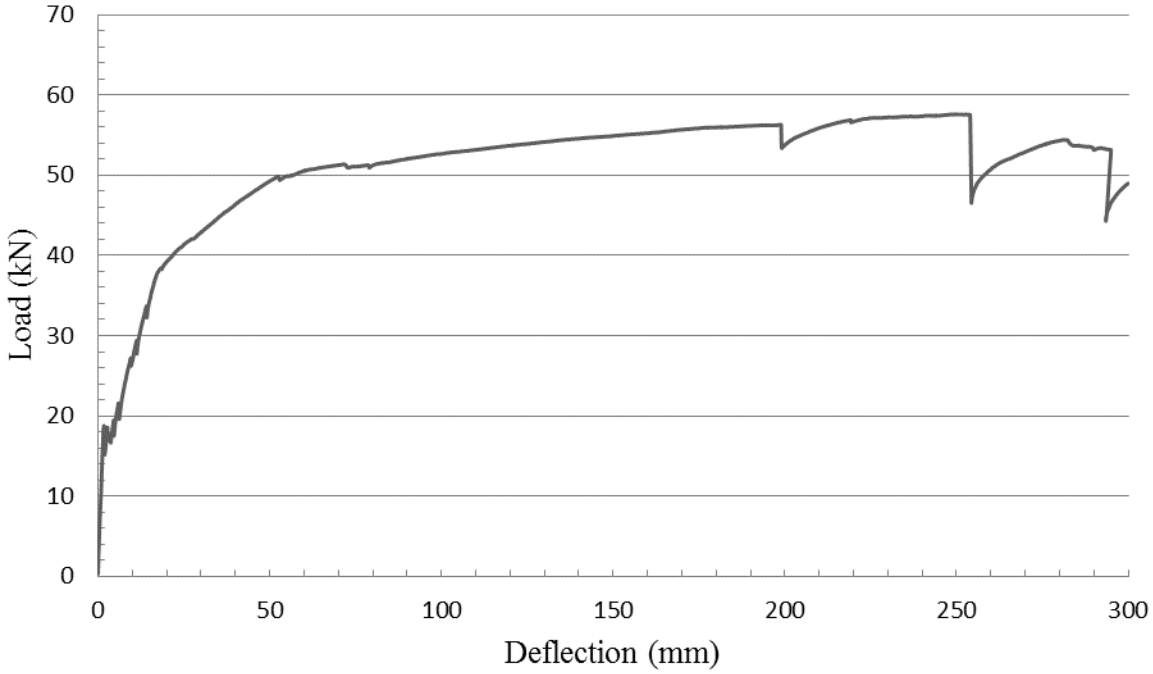

a – load versus mid span deflection

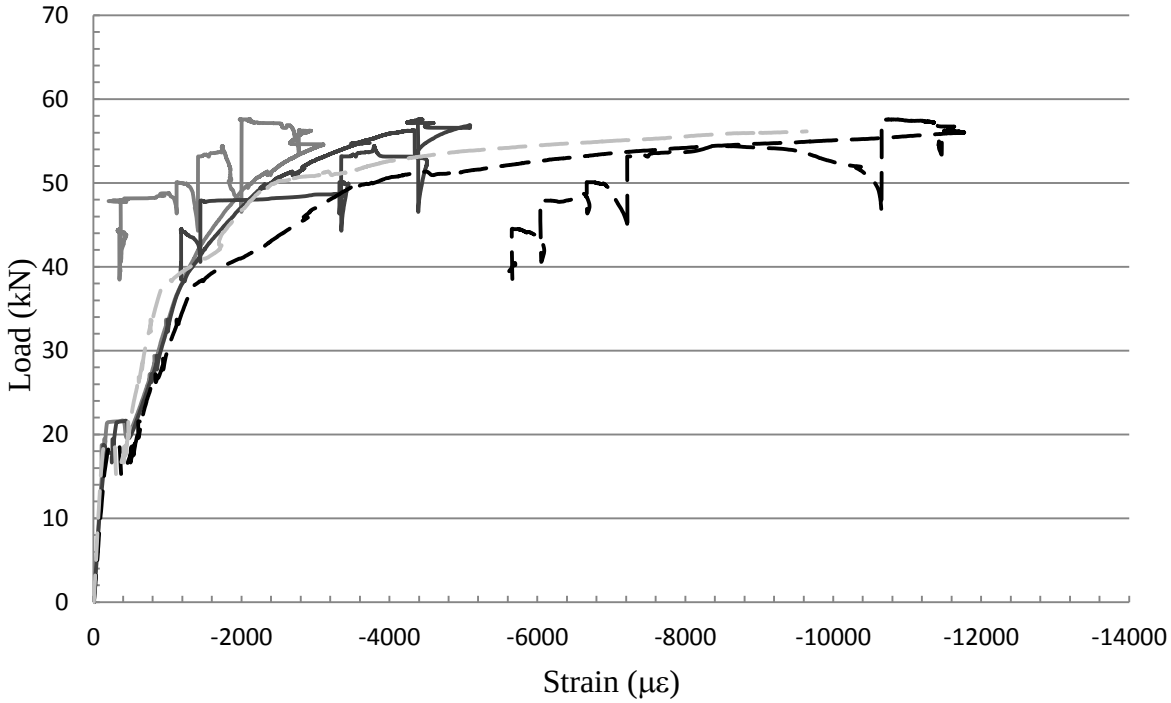

b – load versus compressive strain (concrete and PVC Panel)

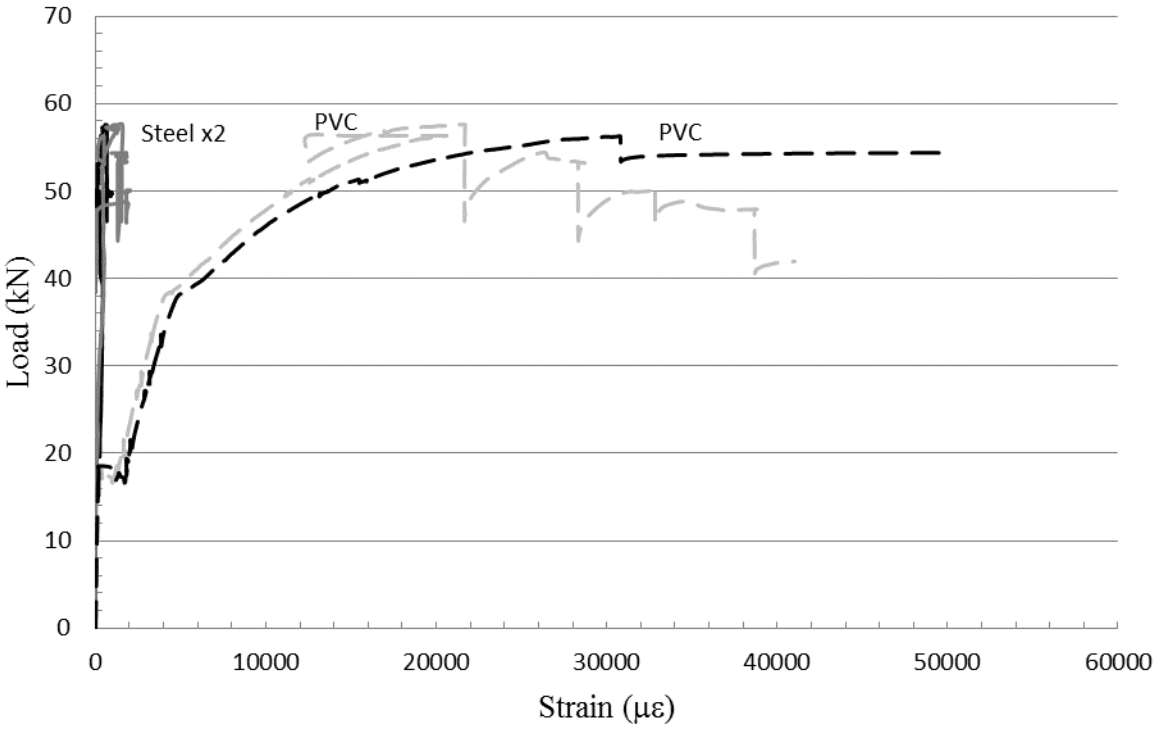

c – load versus tensile strain (steel and PVC panel)

Figure (B-1): Test results for 6" thick wall with 3-10M bars

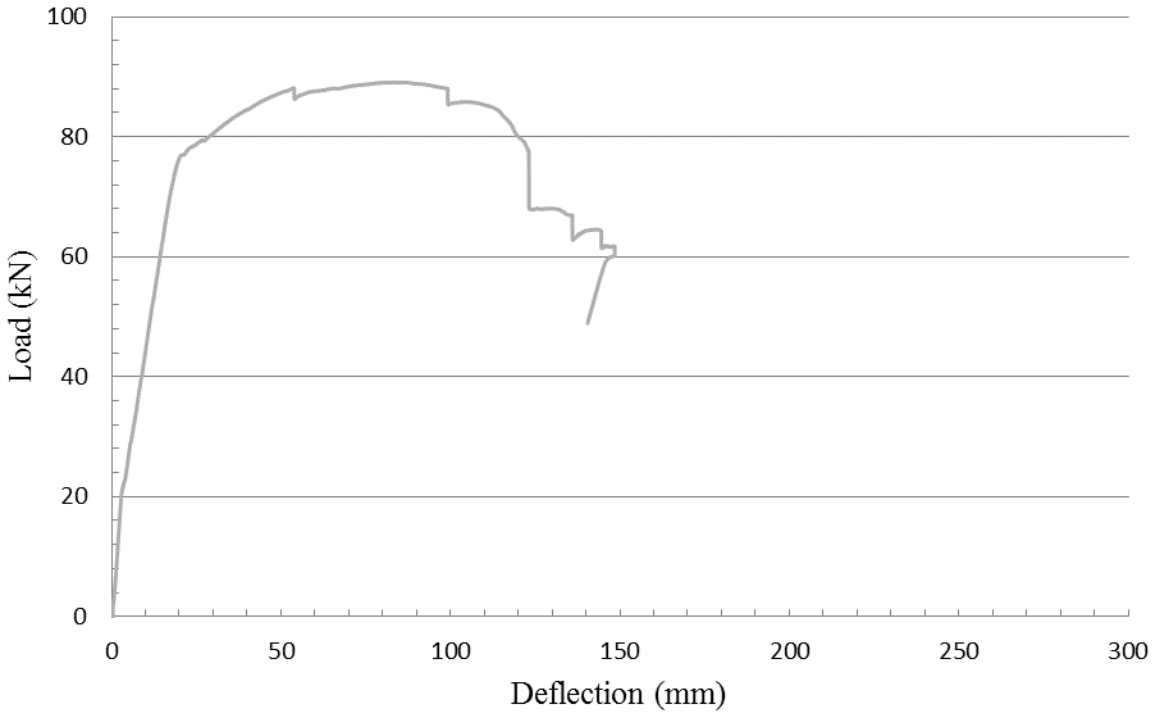

a – load versus mid span deflection

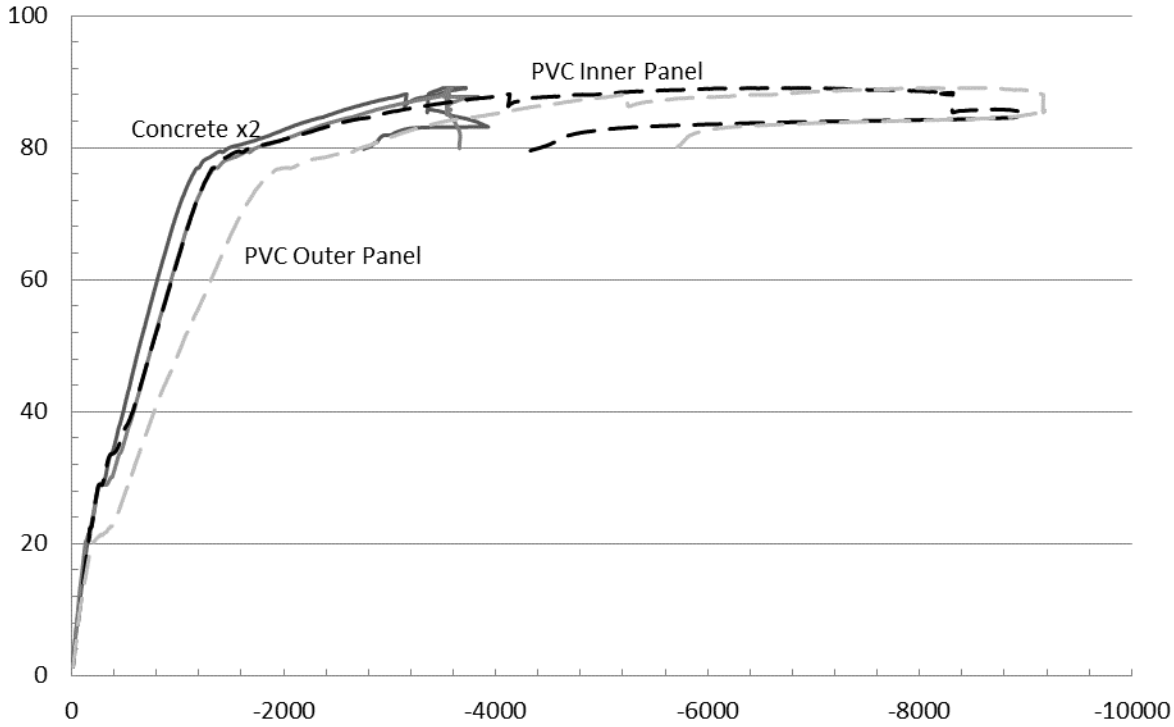

b – load versus compressive strain (concrete and PVC panel)

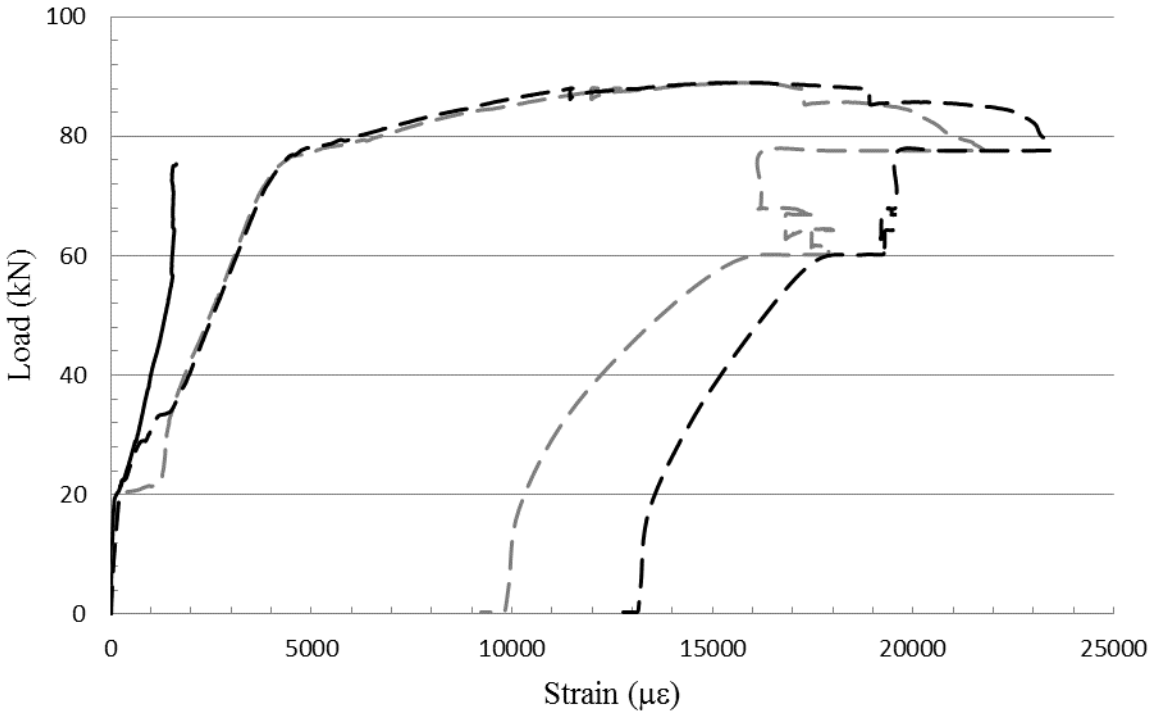

c – load versus tensile strain (steel and PVC panel)

Figure (B-2): Test results for 6" thick wall with 3-15M bars

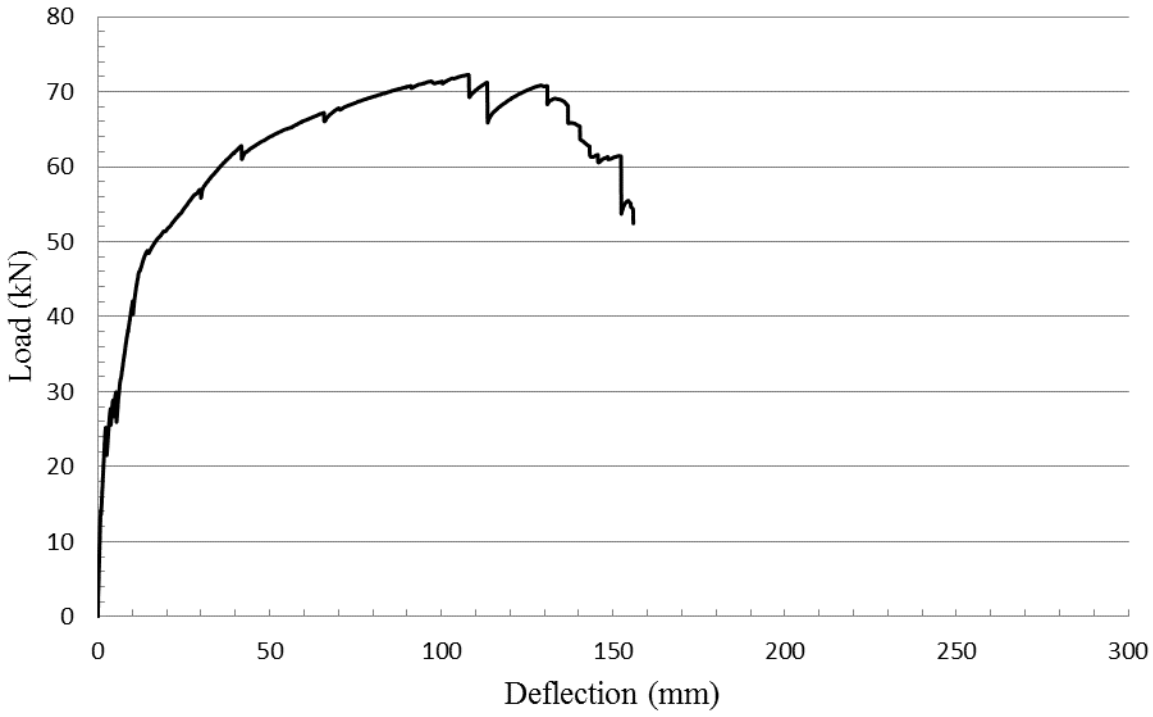

a – load versus mid span deflection

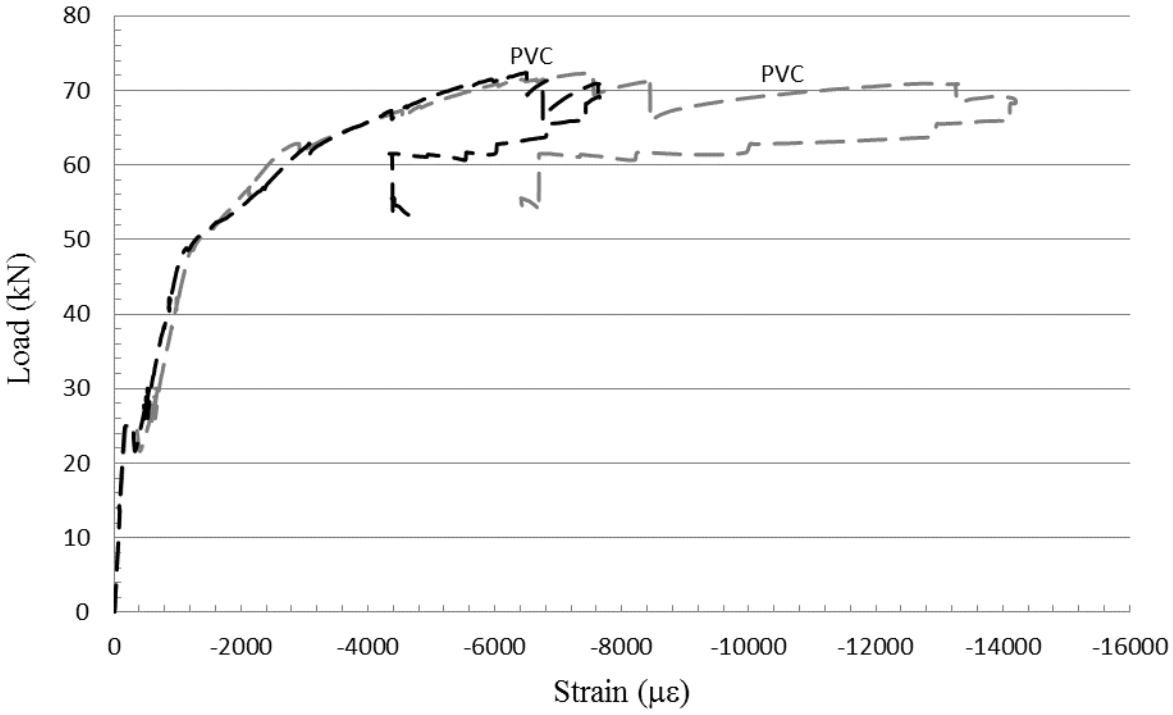

b – load versus compressive strain (PVC panel)

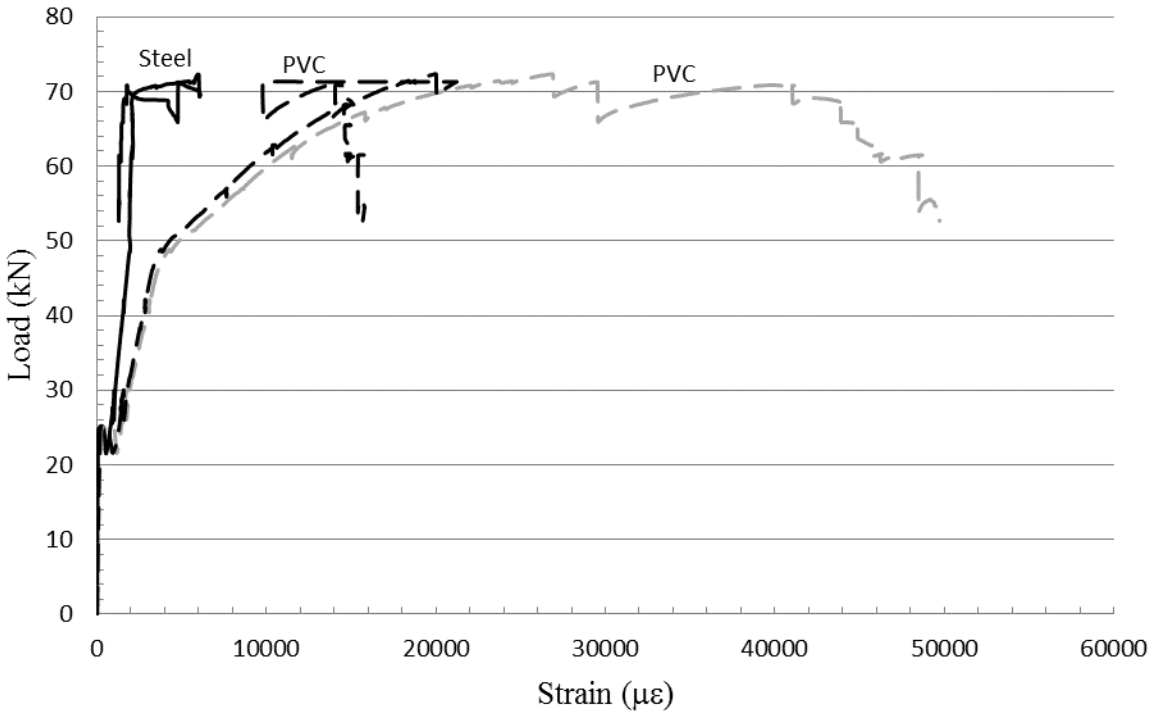

c – load versus tensile strain (steel and PVC Panel)

Figure (B-3): Test results for 7" thick wall with 3-10M bars

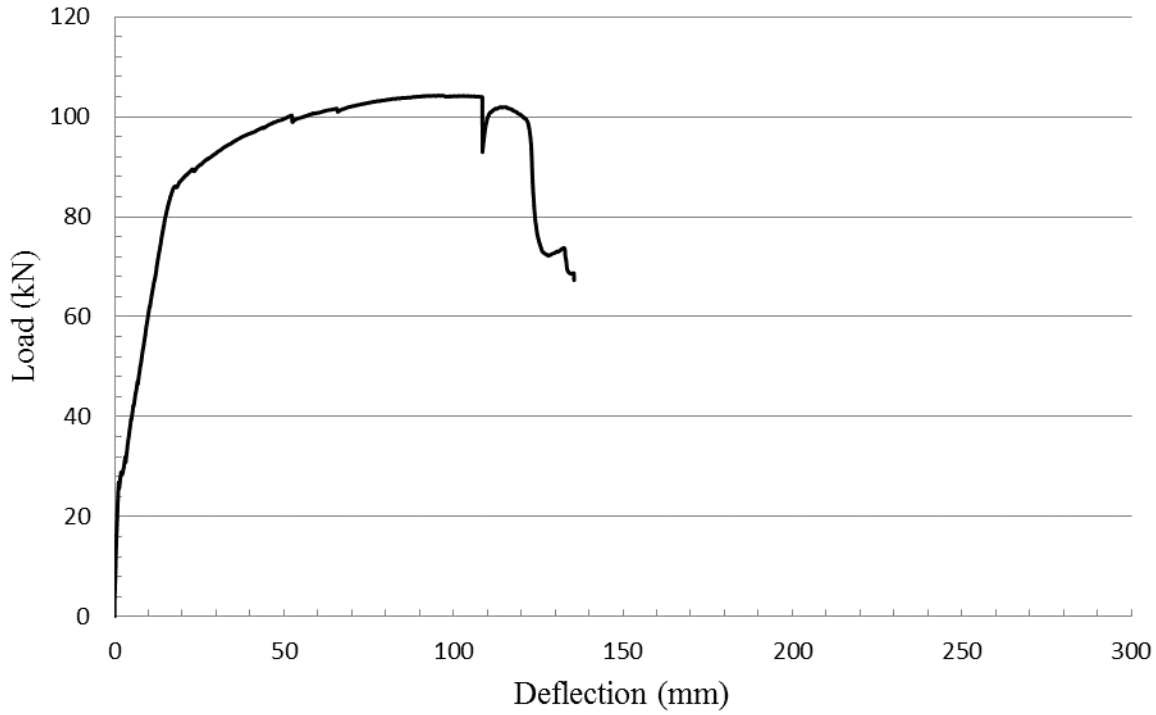

a – load versus mid span deflection

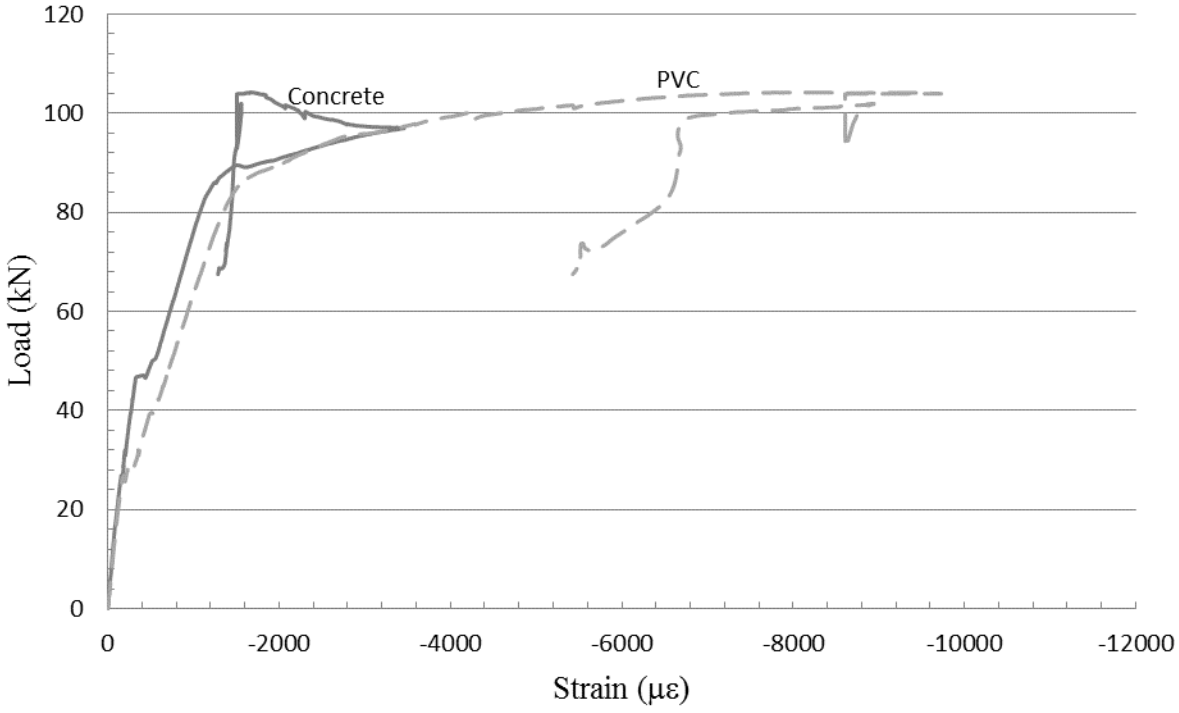

b – load versus compressive strain (concrete and PVC Panel)

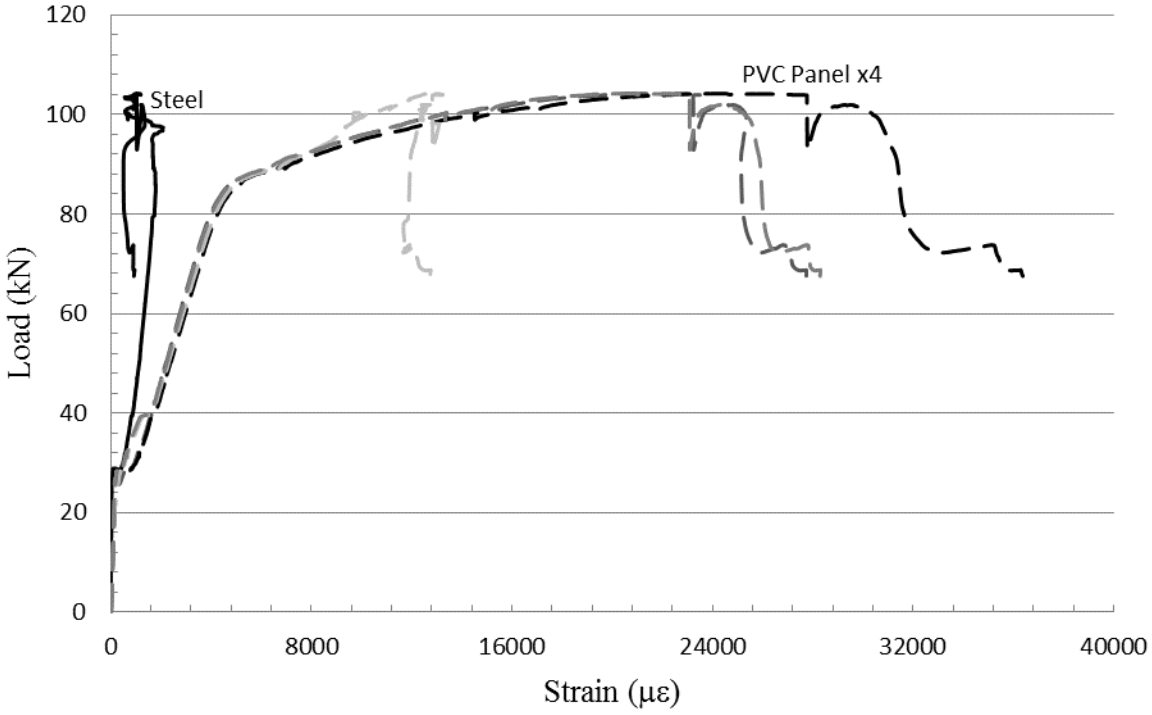

c – load versus tensile strain (steel and PVC panel)

Figure (B-4): Test results for 7" thick walls with 3-15M bars

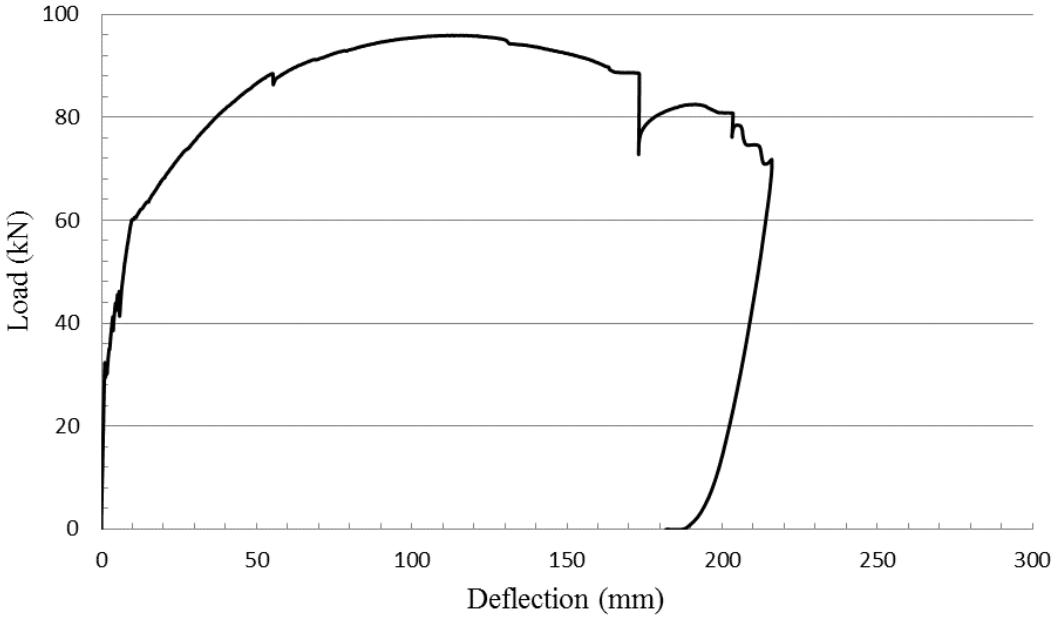

a – load versus mid span deflection

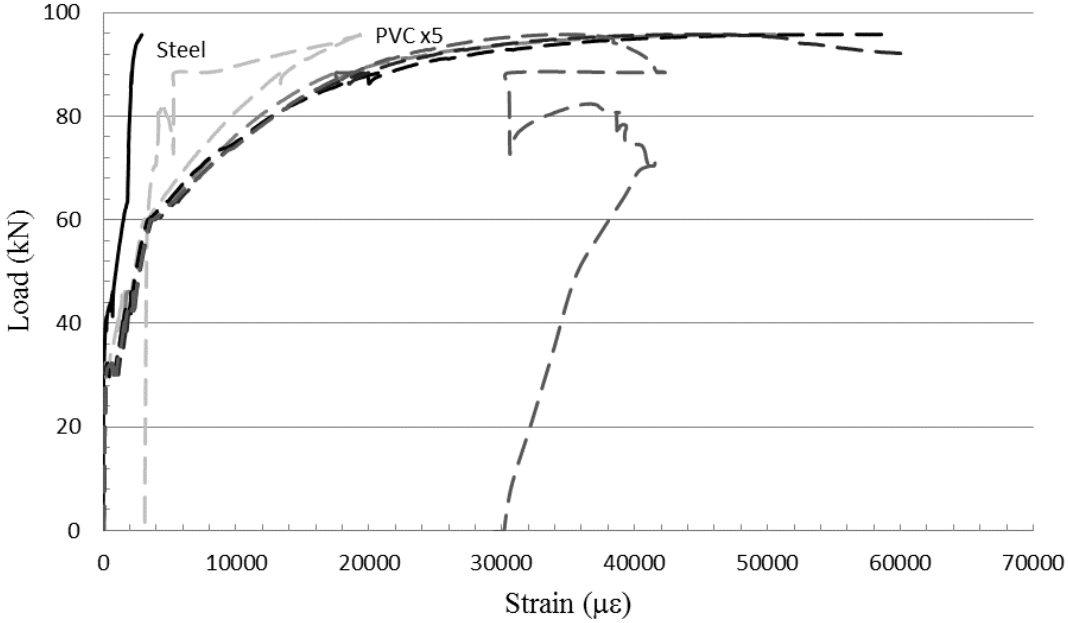

b – load versus tensile strain (steel and pvc)

*Figure (B-5): Test results for 8" thick wall reinforced with 3-10M bars**

*Load versus compressive strain data was ignored as strain gauges were placed too close to the loading points.

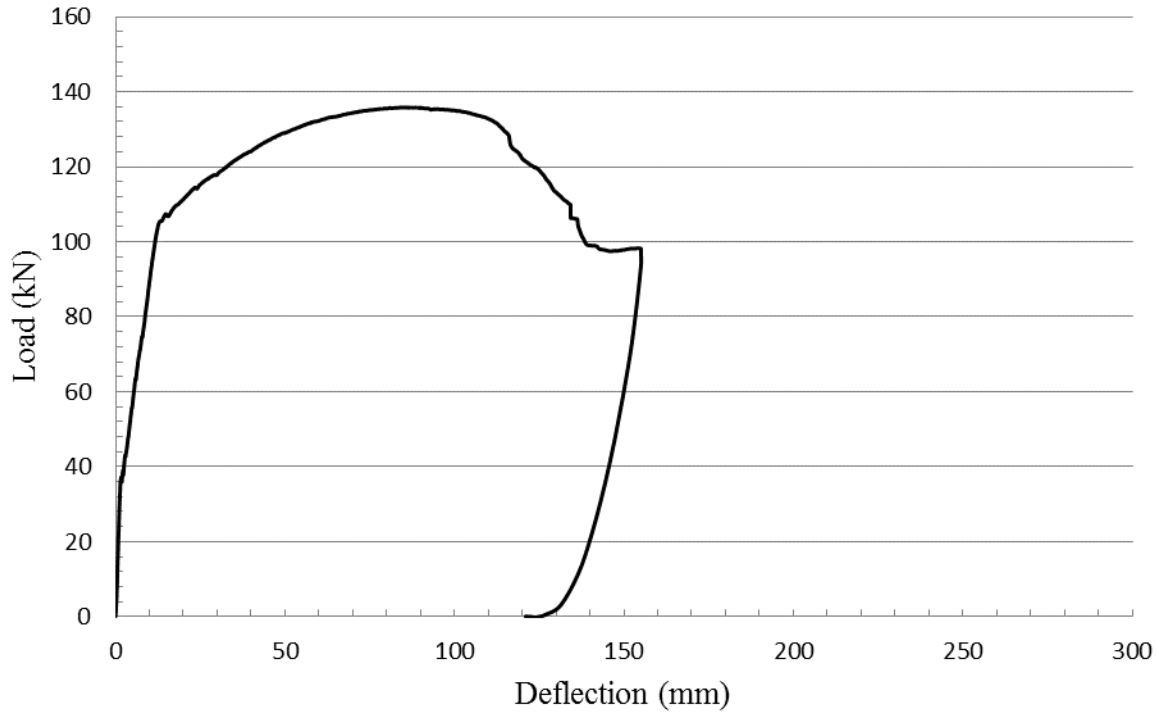

a – load versus mid span deflection

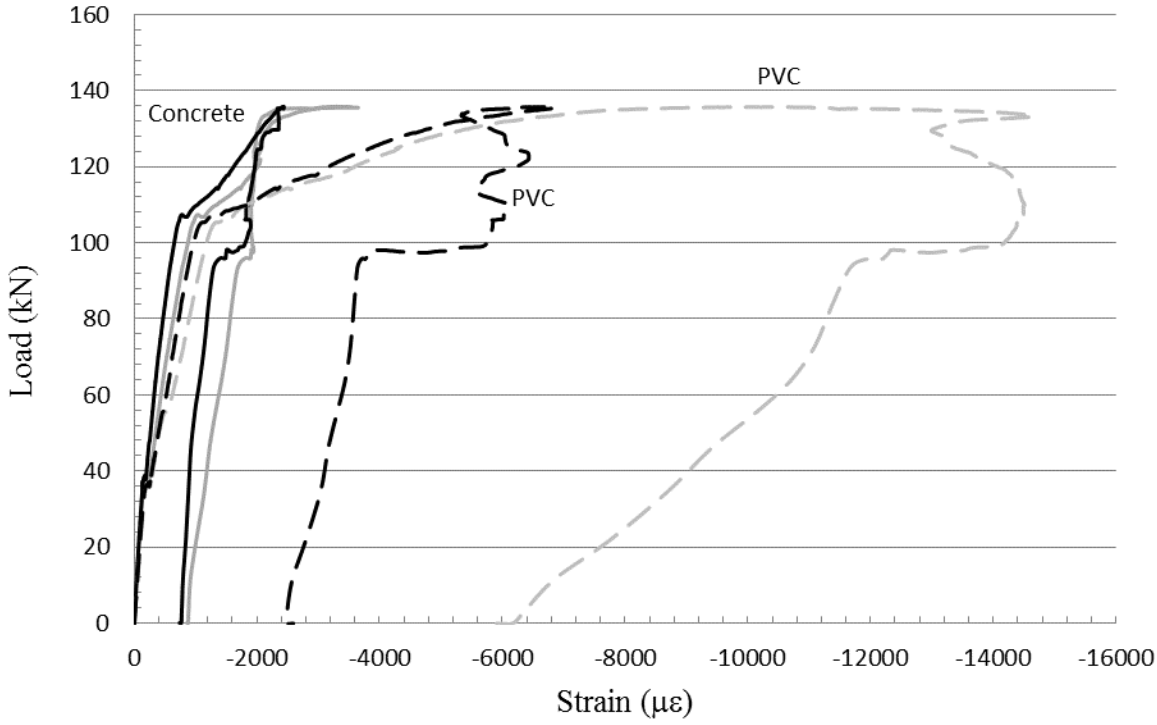

b – Load versus compressive strain (PVC panel and concrete)

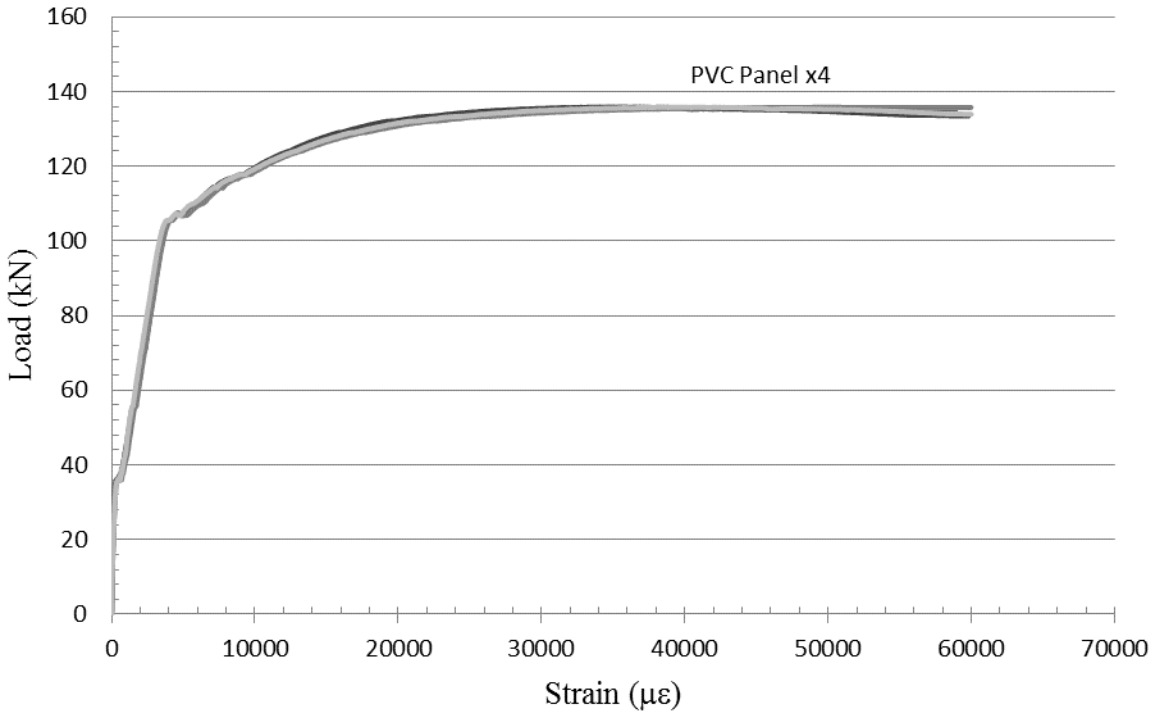

c – load versus tensile strain (steel and PVC panel)

Figure (B-6): Test results for 8" thick wall with 3-15M bars